# A System Dynamics Approach to Sediment Management at Small Hydropower Facilities

A Thesis Presented for the

Master of Science

Degree

The University of Tennessee, Knoxville

Sarah Ann Pierce Dowda

May 2020

## Acknowledgments

First, I would like to thank Dr. John Schwartz for coming to my aid when difficult circumstances arose, to help me finish my degree. I would also like to thank Dr. Thanos Papanicolaou for putting his faith in my abilities and constantly challenging me to think more critically. I am also deeply grateful to Dr. Benjamin Abban, an incredible teacher without whom this journey would not have been possible for me. I would like to thank Dr. Alejandro Caceres and my research group colleagues for their willingness to help me think through problems and share their knowledge. Lastly, I would like to thank my husband Charles, my parents, my sisters, and my friends. Your unfaltering support kept me going through the challenges and joys of this endeavor.

# Abstract

The sedimentation of reservoirs alters reservoir function and often leads to a reduction in power production at hydropower facilities. For low head structures with small reservoirs the effects of sedimentation can manifest quickly, reducing the efficiency and lifetime of projects. In order to optimize small hydropower power production this study offers a new approach to predict sedimentation at small dams. The first important component of this approach is the integration of upland sediment contributions with instream sediment dynamics. Accounting for temporal and spatial fluxes of sediment from the watershed can improve the precision with which sediment is managed at small impoundments. Important Instream components include mobilization flow thresholds, and account for the transport of distinct sediment size fractions. The second aspect of import is the application of systems level thinking to small hydropower production. It is proposed here that this approach can optimize power production by allowing decision makers to examine the tradeoffs of different design and management scenarios, making these smaller facilities more cost effective. A system dynamics model was therefore developed using Vensim software incorporating upland sediment contributions, impoundment hydraulics, fluxes of sediment out of the reservoir by means of a sediment passage, and power production. The model was used to evaluate a study site located on the South Umpqua River near Winston, OR. USGS flow data was used to simulate 25 years of hydraulics and sediment transport at the site. By running different scenarios of sediment management using a sediment passage, tradeoffs between sediment accumulation, water retention, and power production could be assessed to optimize energy generation. An optimized sediment management regime was able to reduce the dam's mean sediment trapping efficacy by approximately 15%. By the end of the 25-year model run, it increased annual energy production by 60%. Important factors to help guide optimal operation of the sediment module were found to be the depth of sediment in the impoundment, and the probability of sediment flux into the impoundment. Results show that incorporating this approach into the analysis of potential hydropower sites can give stake holders insight into long term power production and site management.

# Table of Contents

1. INTROUCTION ..... 1
1.1. Small hydropower, benefits and challenges ..... 1
1.2. Previous approaches to sediment management ..... 1
1.3. Objectives ..... 3
2. METHODS ..... 4
2.1. Study design ..... 4
2.2. Case study area ..... 4
2.3. Development of decision support tool: data needs and framework ..... 7
2.4. Model sensitivity analysis ..... 28
3. Results ..... 29
3.1. System model development outcomes ..... 29
3.3. Model sensitivity ..... 35
4. Discussion ..... 38
4.1. Analysis of system dynamics model development ..... 38
4.2. Interpreting system dynamics model output ..... 39
4.3. Evaluating model sensitivity ..... 40
4.4. Application on a broader scale ..... 40
4.5. Improvements to the system dynamics model for small hydropower facilities ..... 41
5. Conclusion ..... 42
Bibliography ..... 43
Appendices ..... 49
Appendix A: Results varying second and third sediment management parameters: probability of sediment influx into the impoundment and operations sluice gate height ..... 50
Appendix B. Hydraulic properties of head and flow rate for discrete events through the sediment passage and spillway modules ..... 51
Appendix C: The system dynamic model framework ..... 56
Vita ..... 80

# List of Tables

**Table 2.1**. Hydraulic Properties for a Range of Flow Discharge Values in the South Umpqua River near Winston, OR…… 7

**Table 2.2**. Sluice gate and spillway flow rate table for gate width of 6 m and gate height of 3 m…….. 14

**Table 2.3.** Instream sediment size fractions for coarse sediments…….…… 20

**Table 2.4**. Values at which each parameter was help constant during testing…….…….. 28

**Table 3.1.** Percent difference in net energy production and sediment trapping efficiency for control parameter values optimized for each variable respectively. …… 37

**Table B.1**. Hydraulic properties for gate opening of 6 x 1 m2 over a range of events…… 51

**Table B.2**. Hydraulic properties for gate opening of 6 x 3 m2 over a range of events…… 51

**Table B.3**. Hydraulic properties for gate opening of 6 x 7 m2 over a range of events…… 52

**Table B.4**. Hydraulic properties for gate opening of 18 x 1 m2 over a range of events…… 52

**Table B.5**. Hydraulic properties for gate opening of 18 x 3 m2 over a range of events…… 53

**Table B.6.** Hydraulic properties for gate opening of 18 x 7 m2 over a range of events…… 53

**Table B.7**. Hydraulic properties for gate opening of 30 x 1 m2 over a range of events…… 54

**Table B.8.** Hydraulic properties for gate opening of 30 x 3 m2 over a range of events…… 54

**Table B.9**. Hydraulic properties for gate opening of 30 x 7 m2 over a range of events…… 55

# List of Figures

**Figure 2.1.** Road map of study methodology showing the order in which system components were considered and incorporated into the model……5

**Figure 2.2.** Excerpt from model illustrating visual component of Vensim Software platform……..6

**Figure 2.3.** Location of the South Umpqua River watershed within (A) the United States, (B) the State of Oregon, and a plan view (C) of the potential hydropower Site……6

**Figure 2.4.** Instream sediment size distribution, data taken from Wallick et al. (2011)……9

**Figure 2.5.** Hydrograph for the South Umpqua River at Brockway used in model……..9

**Figure 2.6.** Diagram of modularized hydropower facility including, power, spillway, sediment passage, and environmental modules……10

**Figure 2.7.** Diagram of Kaplan turbine……11

**Figure 2.8.** Representation of flow configuration through the sluice gate and spillway modules (Gogus et al., 2006)……..14

**Figure 2.9.** Vensim format for a lookup variable……..15

**Figure 2.10.** The South Umpqua Watershed divided into 5 sub-watersheds and lowlands……17

**Figure 2.11.** Sediment delivery ratios for watersheds throughout the world with best-fit line for the United States. Figure modified from (Lu et al., 2005)……..17

**Figure 2.12.** Sediment rating curve for suspended fine sediment created using suspended sediment data from the USGS……19

**Figure 2.13.** Excerpt of interpolations used in model to calculate the shear stress in the impoundment at each time step……23

**Figure 2.14.** Relationship between the ratio of the particle settling velocity to the shear velocity, ws/u*, and the fraction of sediment being transported as bedload (Papanicolaou & Abban, 2016)……24

**Figure 2.15.** Two different cases of sediment distribution in the impoundment as modeled……..25

**Figure 2.16.** Excerpt from model of sediment dynamics in the impoundment……..27

**Figure 3.1.** Comparison of fine sediment contributions to the system as predicted using the RUSLE model and the sediment rating curve developed using TSS data from the USGS……30

**Figure 3.2.** A comparison of mean transport rates and mean monthly flow values for fine and coarse sediment throughout the year……31

**Figure 3.3.** Time averaged trapping efficiencies over the model run for coarse sediment, fine sediment and the sum of the two, total sediment trapping efficiency……32

**Figure 3.4.** A comparison of the hydraulic residence time of the impoundment for two runs……34

**Figure 3.5.** A comparison of the mean HRT calculated by the model and the HRT's of other small dams as measured by Skalak et al. (2009)……34

**Figure 3.6.** Net energy generation and trapped sediment volume over model run time with variations in the sediment volume threshold at which the sediment module is put into operation……35

**Figure 3.7.** Changes in final time step values of net energy generation and trapped sediment volume for a range of control parameter values modeled……36

**Figure A.1.** Impact of changes to the secondary management parameter, the probabilistic threshold of sediment influx into the impoundment……50

**Figure A.2.** Impact of changes to the third management parameter, the operational gate height of the sediment module……50

**Figure C.1.** Hourly hydrograph input……56

**Figure C.2.** Structural dimensions and sediment management parameters……57

**Figure C.3.** Subsystem calculating river conditions upstream of backwater effects……57

**Figure C.4.** Subsystem calculating water flow, storage, and depth in the impoundment when water depth < dam height……58

**Figure C.5.** Subsystem keeping track of the status of sediment in zone 1 as compared to the potential sediment that would be present if ramp were fully developed to dam face……58

**Figure C.6.** Subsystem keeping track of the length of zone 1 and 2 depending on the most recent gate opening height……59

**Figure C.7.** Subsystem keeping track of sediment trapping efficiency of the dam……59

**Figure C.8.** Subsystem keeping track of the movement of sediment through the impoundment……60

**Figure C.9.** System keeping track of the Hydraulic Residence Time (HRT) of the impoundment……61

**Figure C.10.** Subsystem calculating water elevation at the dam……61

**Figure C.11.** System calculating track of water available to each module……..62

**Figure C.12.** Subsystem keeping track of how each time step relates to modeled time……..62

**Figure C.13.** Subsystem calculating the hydraulics of the sluice gate……63

**Figure C.14.a.** Subsystem calculating bedload influx to the impoundment……..64

**Figure C.14.b.** Subsystem calculating bedload influx to the impoundment……..65

**Figure C.15.** Subsystem calculating suspended sediment flux into the impoundment……66

**Figure C.16.a.** Subsystem calculating resuspension of coarse sediment in impoundment……67

**Figure C.16.b.** Subsystem calculating resuspension of coarse sediment in impoundment……68

**Figure C.17.** Subsystem calculating net resuspended coarse sediment in impoundment for outflux……69

**Figure C.18.** Subsystem calculating transport potential of coarse sediment as bedload in the impoundment……69

**Figure C.19.** Subsystem calculating depth of water at dam……..70

**Figure C.20.a** Subsystem interpolating the flow through the sluice gate……71

**Figure C.20.b** Subsystem interpolating the flow through the sluice gate……72

**Figure C.21.** Subsystem supporting interpolations for flow through the sluice gate by setting boundary conditions……73

**Figure C.22.a** Subsystem interpolating water depth at dam when sluice gate is operational……74

**Figure C.22.b** Subsystem interpolating water depth at dam when sluice gate is operational……..75

**Figure C.23.a** Subsystem interpolating water gross head at dam when sluice gate is operational……76

**Figure C.23.b** System interpolating water gross head at dam when sluice gate is operational……77

**Figure C.24.** Subsystem interpolating water gross head at dam when sluice gate is operational……77

**Figure C.25.** Subsystem interpolating shear stress on sediment ramp when sluice gate is closed……78

**Figure C.26.** Subsystem calculating power production ……79

# 1. INTROUCTION

### 1.1. Small hydropower, benefits and challenges

A growing interest in small hydropower within the US and on a global scale is spurring the industry to examine the potential of these facilities more closely (e.g. Kao et l. 2014, Manzano-Agugliaro et al. 2017, Couto et al., 2018). The clean energy production and renewable nature of these projects makes them an attractive alternative energy source. While the definition of small hydropower varies throughout literature, this study adopts the definition of those projects having a capacity of 10 MW or less (Witt et al., 2017). Although small hydropower offers many benefits it also presents challenges. Similar to larger dams, a key issue facing these structures is the trapping of sediment. This issue impacts the financial feasibility of projects as well as posing environmental concerns.

Although a nationwide potential of 29 GW has been estimated for small hydropower generation in the US (Kao et al., 2014), the high costs of energy production for these projects as compared to other energy sources, due to a high operation and maintenance cost compared to income ratio, can deter investors. The trapping of sediment behind dams has the potential to disrupt power generation by reducing hydraulic head and impoundment storage capacity. In addition to reducing energy production, trapped sediment can shorten the life of hydropower projects, further reducing returns on investment. For projects already facing questionable economic feasibility, such problems have great significance.

From an environmental standpoint the introduction of a dam into a river is often associated with changes to sediment transport capacity along stream beds, impacting river geomorphology and habitat (e.g. Baxter, 1977, Ligon et al., 1995, Rollet et al., 2014). Although small dams have been shown to have less of an impact on river geomorphology than larger structures (e.g. Csiki & Rhoads 2014, Cheng & Granata 2007), these concerns need to be addressed in order for projects to have the full endorsement of all stake holders.

### 1.2. Previous approaches to sediment management

Sediment management solutions at hydropower sites to date include the mechanical removal of sediment through dredging operations and the use of sediment passages designed to allow sediment to be transported past a dam. Dredging operations tend to be expensive and can take a financial toll on the budgets of small hydropower operations (U.S. Army Corps of Engineers, 2015). Sediment passages add complexity to project planning as they differ from site to site depending on the types of sediment mobilized in the river and site configuration. For coarse sediments, sediment bypasses which transport sediment around the dam through a secondary channel or tunnel have been used (e.g. Morris & Fan 1998, Kondolf 2014, Sumi et al., 2004). Sediment sluice gates can also be used to pass coarse sediment along the riverbed, and flush fine sediment from behind dams (e.g. Morris & Fan 1998, Kondolf 2014). Passing dense clouds of fine sediment traveling as turbidity currents into reservoirs requires the use of a special sediment passage comprised of vents placed at the bottom of dams for this purpose. Each requires a different type of planning and management.

As a means to make small hydropower more cost effective, a new, modular design approach was put forward by U.S. Department of Energy (Smith et al., 2017, Witt et al., 2017). This approach seeks to reduce the cost of small hydropower projects by breaking structures into distinct components, or modules, in order to provide a more standardized approach to design and implementation. This design

includes a power module, a water passage module, a sediment passage module, an environmental module, and a recreational module. Sediment passage is incorporated as a key component of the system and is associated with site selection, as sites will have varying sediment composition and transport rates. Therefore, site specific operation of the sediment module is key to the optimization of power production at small hydropower facilities. Management needs to take into consideration the type of sediment being transported at the site, the timing of sediment fluxes and the complex feedbacks in the system between sediment, water, and power production.

An important component of this system which has gone unaddressed by many is the delivery of sediment from the uplands of a watershed to its river. The uplands are comprised of land surface areas surrounding head waters and can encompass the land that runs down directly to the potential hydropower site in instances of steep watersheds, or land that runs down to meet the low laying areas surrounding a river where sediment is often deposited due to the change in watershed slope. Uplands act as geomorphic controls within a watershed, connected to the river through the delivery of both water and sediment (e.g.Chen & Wang, 2019, Zhongbao et al., 2015). Sediments reaching the river from the uplands generally consisting of fine sediment (sand, silt, and clay) and modify the sediment size distribution and the timing of sediment fluxes through the system (e.g., Abban et al., 2016, Wilson et al., 2012). Upland sediment also has the potential to carry excess nutrients and pollutants into the system, which may become trapped behind the dam along with deposited sediments (e.g. Maavara et al., 2015, Evens, & Gottgens, 2007). For example, polycarbonate bisphenols (PCB's) and heavy metals are both known to attach to sediments and become concentrated behind dams (e.g. Ko & Baker, 2014, Quinton & Catt, 2007). Understanding the sourcing of such sediment can inform sediment management that may involve the harvesting of trapped sediment for nutrient recycling, or the intentional trapping of sediment to prevent the spread of contaminants (e.g. Sheehan et al., 2010, Sigua, 2009).

Sediment sources vary within the watershed. In addition to uplands sources from erosion, they can include headwaters and the river channel itself. In mountainous region of the US, headwaters can be a major generator of bedload sediment, supplying the larger size materials such as gravel and cobble (e.g. Robinson & Slingerland, 1998). In glaciated landscapes, headwaters are associated with moraines and supply rivers and stream with gravel. Studies have shown that bank and bed erosion of the stream channel can contribute up to 80% of the sediment transported, a process that can be exacerbated by dams (e.g. Simon and Rinaldi 2006, Schenk et al, 2010, Foucher et al., 2017). These sources come together to give rivers a unique sediment distribution that can adjust longitudinally along the river, and temporally through the seasons (e.g. Abban et al., 2016). Understanding the potential sources of sediment within a riverine system is critical to the location selection, decision making, and design approach for small modular hydropower facilities.

River hydraulics and sediment transport are complex physical processes that can be modeled, requiring skilled engineers and an extensive effort to complete a site assessment for potential use of a small hydropower facility. Such models included ConCEPTS, SAM, and others (Langendoen et al., 2001, Thomas et al., 2002). Although these models have many practical applications in the field, their uses are limited when it comes to hydraulics and sediment transport around structures such as dams. Other 3-dimensional models, such as FLOW- 3D have been used to study the transport of sediment through reservoirs (Castillo et al., 2014). However, these models tend to be costly and running multiple simulations for different management techniques is not a financially feasible method of analyzing potential site operations for many companies. Additionally, models such as those mentioned above do

not provide a platform for examining the tradeoffs between different components of the system from run to run.

### 1.3. Objectives

At the initial stages of site selection for small hydropower and the use of a sediment module, a decision support tool is needed to assess the feasibility of facility construction and to understand site specific, best-practice sediment management operations. A systems approach has the capability to address the numerous challenges discussed above. The objective of this study is to explore whether a new systems approach for understanding sediment transport and trapping at small hydropower is achievable and reliable taking the facilities' entire system into consideration, and individual modular components. An important component of this analysis and focus of this study is the incorporation of upland sediment contributions. Also incorporated is the impact of temporal fluxes of sediment through the system, and the behavior of distinct sediment size fractions. These components are brought together is a system dynamics model in which different scenarios and management approaches can be tested. It is proposed here that this approach can optimize power production by allowing decision makers to examine the tradeoffs of different design and management scenarios. This advantage of a systems-based decision support tool is to make small hydropower facilities more cost effective by reducing the engineering cost of site selection and facility design.

# 2. METHODS

## 2.1. Study design

This study consists of the development of a decision support tool using a systems approach to site and assess the feasibility of constructing a small modular hydropower facility and optimize its sediment management. The study will link system components for fine sediment source and total sediment load transport at a river site. The components driving the system and considered in this study can be broken into two major categories, those relating to the hydraulics of the system and those relating to sediment transport. Hydraulic components include: the river hydrograph, passage of water through the dam's modules, and water storage behind the dam. Sediment components include upland sediment contributions, instream sediment transport, trapping of sediment behind the structure, and passage of sediment through the sediment module and in suspension across the dam. Figure 2.1 provides the process by which components of the system are considered and brought into the model.

The system dynamics model used to develop the decision support tool was the Vensim PLE simulation software (Ventana Systems Inc., 2019), which provides a means to examine tradeoffs between different sediment management regimes at a hypothetical dam site. The Vensim platform allows users to construct models using different types of variables including levels, rates, and auxiliary variables. Relationships between these variables are represented visually in the model with arrows, i.e. when one variable has an arrow pointing to another, it signifies that it is being called by the equation of the second variable.

When a variable is first defined in the model, it appears without brackets. If it is used again elsewhere, it appears in brackets. A sample of the model's interface is shown in Figure 2.2. (Full model interface shown in Appendix C).

The model was comprised of 424 variables representing four main components: water, sediment, structure, and power. Each time step in the model represented one hour of time. Greater explanation of individual sub-system model development will be given for each in the section of decision support tool.

The model was built in stages starting with the system's hydrograph, flow requirements for each module, then incorporating the hydraulic properties of the impoundment, the sediment dynamics in the river and at the sediment passage module, and finally the power production system (Figure 2.1).

## 2.2. Case study area

The approach outlined herein was utilized in a case study to better demonstrate its potential applications. The hypothetical dam site selected for the case study is located on the South Umpqua River in Southwest Oregon near Brockway (Figure 2.3). Here, the river runs adjacent to a populated area providing easy access for dam construction and the potential for convenient distribution of hydropower. Also key for this study is the proximity of a USGS gauging station with flow records from the past 30 years, as well as suspended sediment records.

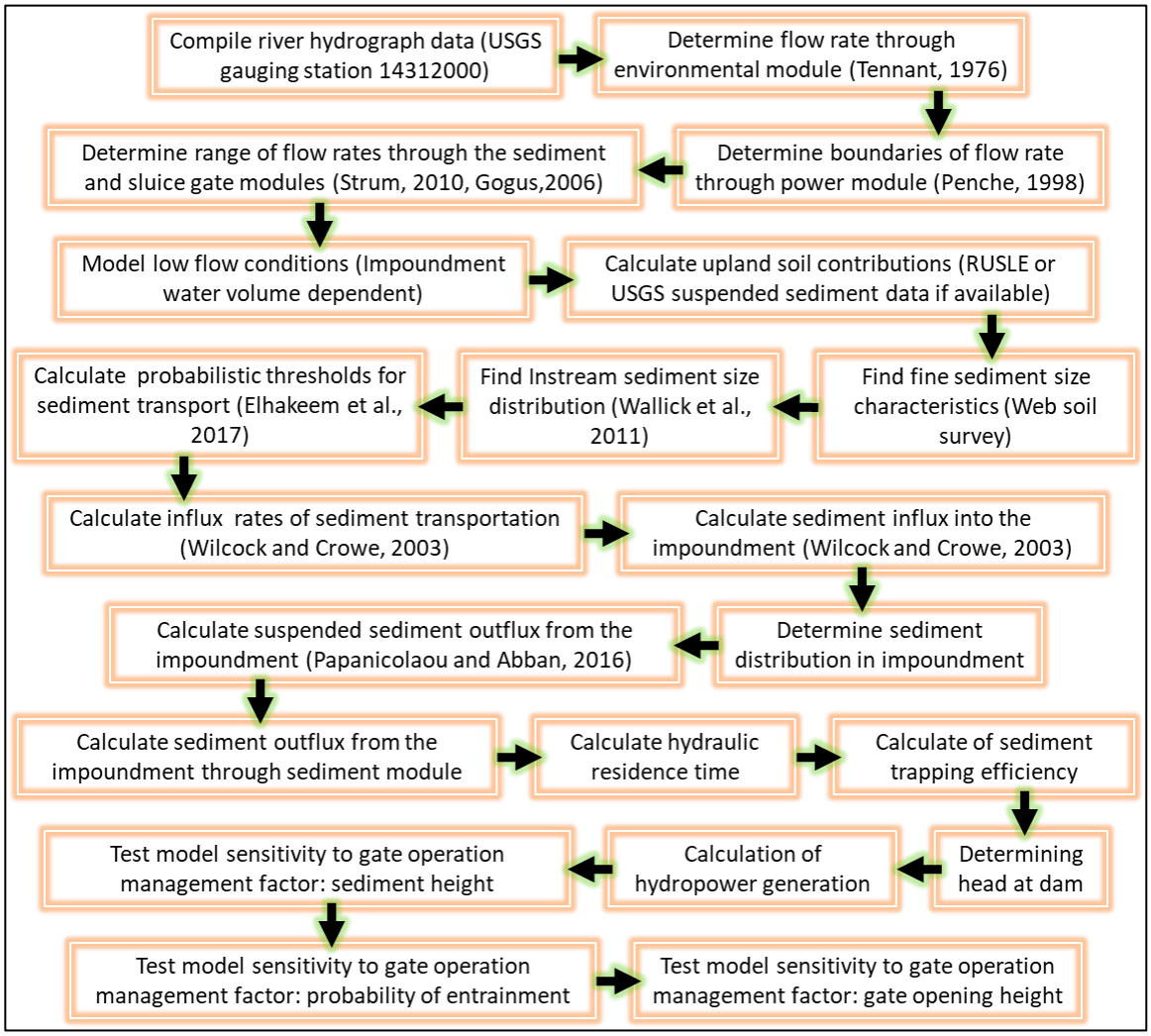



**Figure 2.1.** Road map of study methodology showing the order in which system components were considered and incorporated into the model.

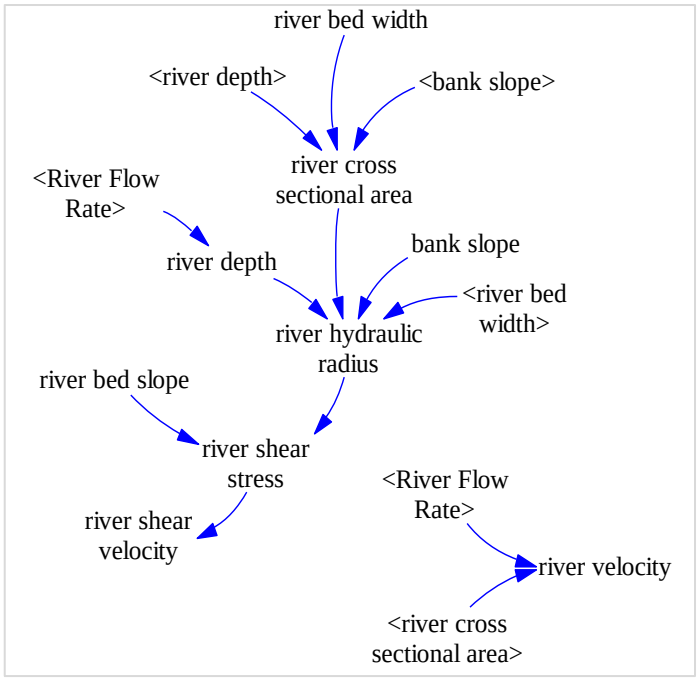



**Figure 2.2.** Excerpt from model illustrating visual component of Vensim Software platform.

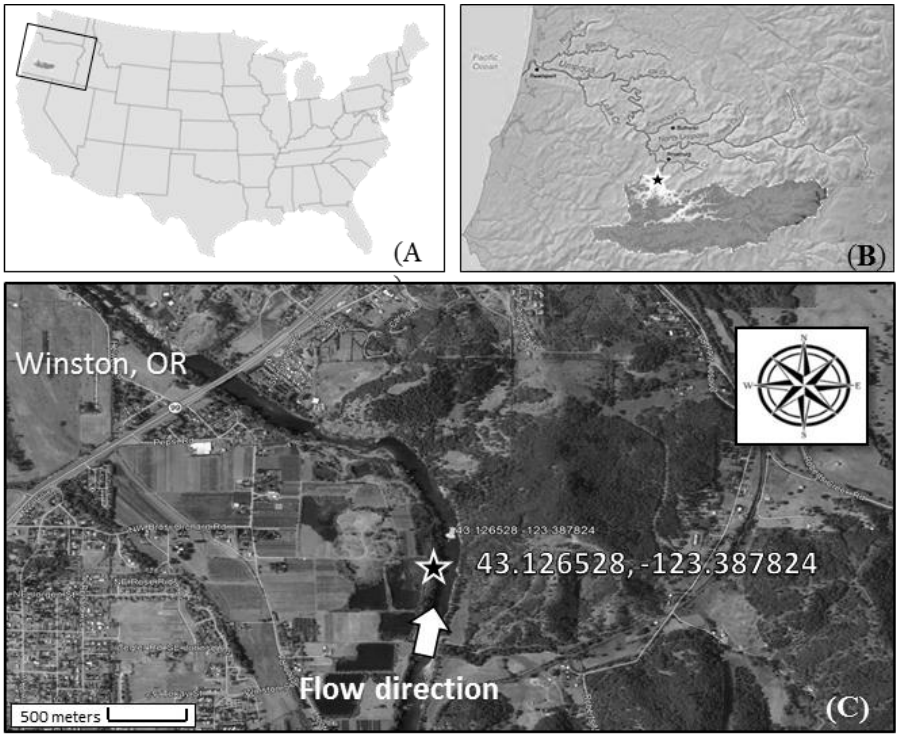



**Figure 2.3.** Location of the South Umpqua River watershed within (A) the United States, (B) the State of Oregon, and a plan view (C) of the site (indicated by star).

The site's drainage basin extends up into the Cascade Mountain range, resulting in a hydrology dependent not only on precipitation, but also on annual snow melts. The basin's 4325 $km^2$ area undergoes an 1,888 m change in elevation and experiences an average annual rainfall of 104 cm. The watershed is comprised of 75% forest and 22% pasture, with a small area of crop land (<1%) and development (<1%).

The river at this location has a slope of 0.00058 m/m. A range of hydraulic properties for the site are given in Table 2.1.

**Table 1.1** Hydraulic Properties for a Range of Flow Discharge Values in the South Umpqua River near Winston, OR. Variables in table are listed as follows: (1) flow discharge, Q; (2) river depth, H; (3) dimensionless shear stress defined as $\tau^* = \tau/(\gamma s-\gamma)d$, where $\tau$ is the bed shear stress, $\gamma s$ is the specific weight of the sediment, $\gamma$ is the specific weight of water , and d is the mean particle diameter; (4) $U_{bulk}$ is the bulk velocity defined as $U_{bulk} = Q/A$ where A is the cross-sectional area of flow; (5) the Froude number defined as $F=U_{bulk}/\sqrt{gH}$ ; (6) the Reynolds number defined as $Re = \rho R U_{bulk}/\mu$ where $\rho$ is the fluid density, R is the hydraulic radius, and $\mu$ is the fluid dynamic viscosity.

| Q ($m^3/s$) | H (m) | $\tau$ (Pa) | $\tau^*$ | $u_o$ (m/s) | Fr | Re |
|---|---|---|---|---|---|---|
| 2 | 0.5 | 2.8 | 0.005 | 0.06 | 0.03 | 2.37E+04 |
| 600 | 4.1 | 23.6 | 0.039 | 2.26 | 0.35 | 7.12E+06 |
| 1400 | 5.7 | 32.8 | 0.054 | 3.79 | 0.50 | 1.66E+07 |
| 2200 | 6.9 | 39.6 | 0.065 | 4.93 | 0.60 | 2.61E+07 |

The instream sediment size distribution was taken from the data of Wallick et al. (2011) (Figure 2.4). The site is reported to be predominantly gravel with 2% sand and a small percentage of small cobbles.

### 2.3. Development of decision support tool: data needs and framework

*System Hydraulics*

Watershed hydrology is the main driver of the system under consideration; thus, the river hydrograph was the first input built into the model. The hydrograph for this study was constructed using USGS flow data for station 14312000 consisting of 25 years of hourly data for the years 1994 through 2018. The

hourly hydrograph ranged from 2 $m^3/s$ to 2200 $m^3/s$. The upper range in this hydrograph represents a flow event with an eight-year return frequency. The hydrograph used is shown in Figure 2.5.

*Module Specifications*

A modularized dam structure was used in this study according to the designs proposed by Witt et al. (2017). The modules considered herein are the environmental module, where a fish passage can be incorporated and mandated environmental flow requirements can be passed downstream, a power module, which encompasses components necessary to generate hydropower, a sediment passage module, which allows for the passage of sediment passed the dam, and a spillway module, which passes surplus water downstream (Figure 2.6). Not considered at this time is the recreational module proposed

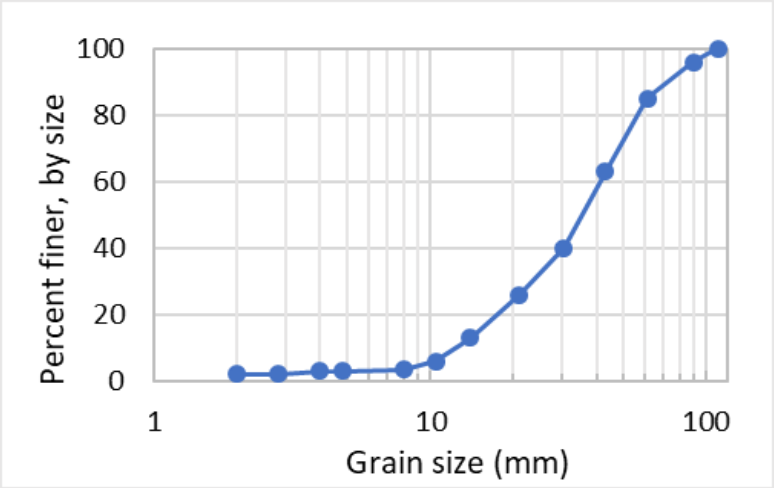



**Figure 2.4.** Instream sediment size distribution, data taken from Wallick et al. (2011).

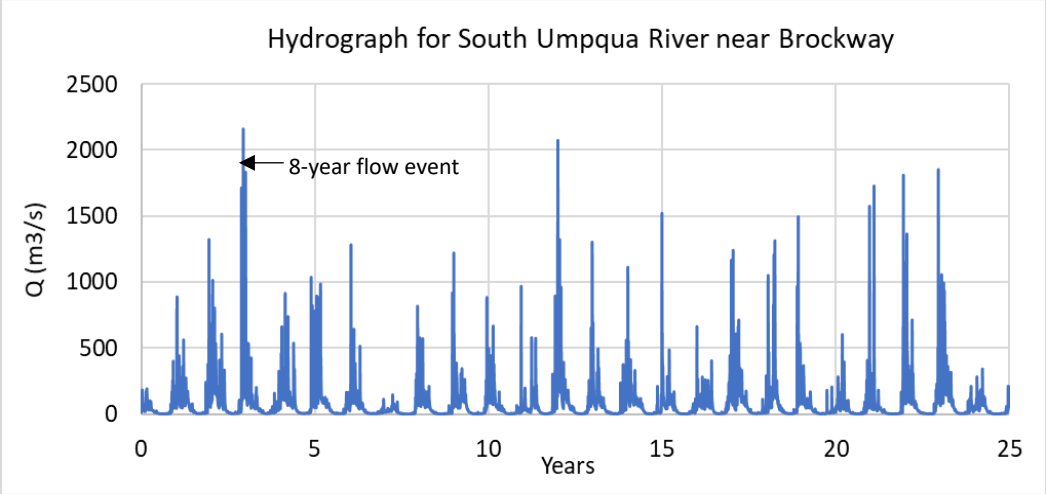



**Figure 2.5.** Hydrograph for the South Umpqua River at Brockway used in model.

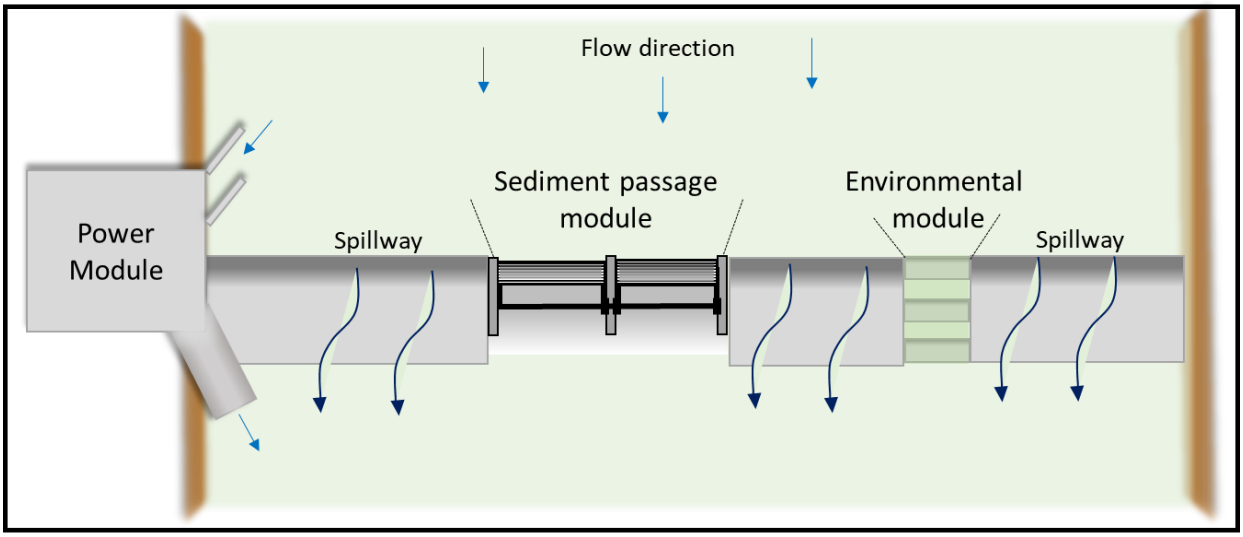



**Figure 2.6.** Diagram of modularized hydropower facility including, power, spillway, sediment passage, and environmental modules.

by Witt et al. (2017), designed for the passage of recreational boats (i.e. kayaks, canoes). Requirement's for such a module have not been set forth at this time and as such it has been left out of this study.

The amount of water passing through each module needed to be modeled at each time step. Tracking these flow values was important to ensure that minimal environmental flow requirements were being met, the power module was receiving flows within its design parameters, the head available for power generation could be calculated, and in order to track the amount of water being stored behind the dam. In order to accomplish this, the dimensions of each module had to be considered along with their flow

capacity if applicable, and the precedence with which water was directed through each.

*Environmental Flow Minimums*

The environmental module in the case study was assumed to be a passage of 2.5 meters in width. Beyond the width, which must be subtracted from the collective width of other modules, the design of this module is beyond the scope of this study. Water flowing through the environmental module was simply assumed to pass through, with no mechanism involved. There exists a good base of literature on the subject of environmental passage structure and design that should be considered for the actual design of this module. (e.g. Papanicolaou & Maxwell, 2000, Lee et al. 2008, Baki et al., 2016). This module took the highest order of flow precedence to ensure that environmental flow minimums were being met.

The environmental flow requirements for the site were calculated using the Tennant method (Tennant, 1976). This method sets the minimum environmental flow requirement to 10% of the mean annual flow. This minimum flow value took priority over other forms of abstraction in the model. This was accomplished by subtracting the environmental flow value from the hydrograph and modeling the remaining flow as being available for use though the power module, sediment module, etc. If the river

flow fell below the minimum environmental flow value, all river flow was diverted through the environmental flow module.

*Power Module*

The power module took second precedence and was placed to the side of the dam with water intake and outlets reaching into the river. The dimensions of these components were outside the scope of this study as they have to be mechanically engineered for optimum power production.

A Kaplan turbine was selected for modeling due to its ability to generate power at low flows (Figure 2.7). Many models have blades that adjust their angle based on the flow rate entering the turbine in order to optimize power generation.

Power generation was calculated using equation (2.1),

$$P = \eta\gamma QH \tag{2.1}$$

where η is the turbine efficiency, γ is the specific weight of water, $Q$ is the flow rate to the turbine, and $H$ is the hydraulic head.

A range of turbine efficiency for different flows was taken from IPCC (2012). Head losses were assumed to be 5% of the gross head (Penche, 1998), a value fixed throughout model runs. The gross head was calculated as the water elevation at the dam before abstraction to the power module.

The design flow for the turbine was determined using the guidelines of the European Small Hydropower Association (Penche, 1998). This entailed evaluating 20 years of USGS mean monthly discharge data and determining the mean flow. The environmental flow requirement was then subtracted from this value to

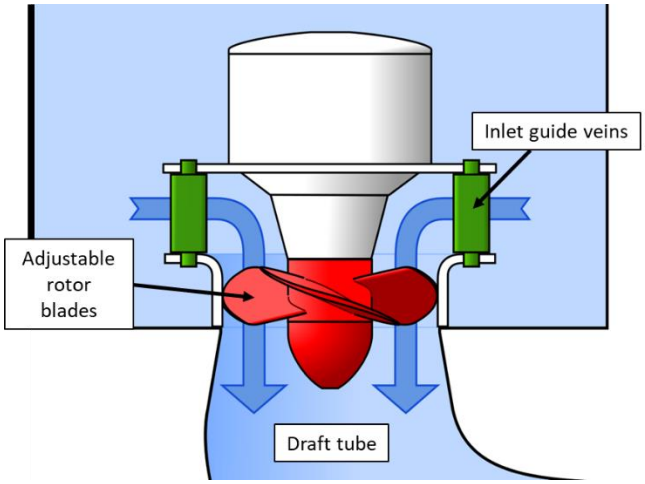



**Figure 2.7.** Diagram of Kaplan turbine

get the final design flow. The minimum and maximum allowable flows through the turbine where then taken as 30% and 110% of this value respectively.

Variables were created to track hourly power generation in kW, annual net kilowatt hour production, net kilowatt hour production, and to keep track of the percentage of time that power was being generated at the site.

*Sediment Passage Module*

A radial sluice gate was selected for the sediment passage module as they are a widely used gate for sediment passages in existing structures. Other types of gate could be substituted when considering other projects based on site conditions, budget, and desirable operation characteristics. The sluice gate can be opened and closed throughout the run of the model and as such, two scenarios needed to be modeled hydraulically, those where the gate was open, and those where the gate was shut. The modeling of water through the sediment passage module was linked with water passage over the adjacent spillways and thus the hydraulics for the two modules are laid out together below.

A spillway of 3.32 meters in height was tested for the hypothetical study site. This height was used as per the requests of the Department of Energy research team based out of Oak Ridge National Laboratory. For cases where the impoundment water elevation rose above 3.32 m, the dam was assumed to behave as a run of the river dam, with water influx set equal to water outflux. When the water elevation fell below 3.32 m, this assumption was no longer valid and water storage was calculated as a mass balance, comparing the rates of flow entering and exiting the reservoir.

*Modeling hydraulics of closed sluice gate*

When the sluice gate was not in operation, the rate of water being transmitted out of the impoundment via the spillway was the river flow rate, minus the values of flow through the environmental and power modules. Head on the spillway was calculated using the equation for flow over a spillway (Strum, 2010):

$$Q_{spill} = CLH_e^{1.5} \tag{2.2}$$

where *C* is the spillway discharge coefficient, *L* is the net effective crest length of the spillway, and $H_e$ is the total head on the spillway. The value of C depends upon the specific design of the spillway with a range of 3.0 to 4.0 and will change from project site to project site. Because this study is focused upon setting forth a methodology focused on sediment management instead of optimizing structural design of each component, a set value of 3.5 was used.

*Modeling hydraulics of open sluice gate*

Because reservoir water elevation is dependent upon the flux of water past the dam, and flux over the spillways and through the sediment module is likewise dependent upon the reservoir water elevation, a system of tables relating these values had to be incorporated into the model to prevent circular equations that prevent the model from running.

Due to the assumption of a run-of-river operation, the tables were able to relate water elevation and flow through the modules based on incoming flow rates. The tables were constructed as follows.

Nine tables were constructed each assuming a different sluice gate width and opening height. A range of water depths were established upon which each table was built. Based on these depths the flow rate through the sluice gate could be calculated. For depths where the sluice gate opening was submerged, flow rates through the sluice gate were calculated using an equation for flow through the orifice of a radial sluice gate (Strum, 2010),

$$Q_G = C_d L w \sqrt{2gH} \tag{2.3}$$

where $Q_G$ is the flow through the gate, $C_d$ is the discharge coefficient, $L$ is the crest length of the gate bay, $w$ is the gate opening distance, g is the gravitational constant, and $H$ is the hydraulic head measured from the water surface to the center of the gate opening. The discharge coefficient, $C_d$, ranges from a value of 0.68 to 0.73 (Strum, 2010). For the reasons stated above relating to the value of C selected for modeling, a set value of $C_d = 0.7$ was used to generate the tables.

The corresponding flow over the spillway was calculated using the assumed water depth minus the spillway height to get the spillway head, $H_e$, and using Equation 2.2. This head was used to calculate flow over the spillway when the gate was in operation. Flows through all modules were then added and set equal to the river flow rate to create the sought-after relationships.

For water depths where flow through the sluice gate had a free surface, i.e. the water surface was below the bottom lip of the radial sluice gate, the relationships between water depth and flow rate through the sediment and spillway modules were calculated using the equations of Gogus et al. (2006). These equations treat the sluice gate opening and adjacent spillways as a compound weir, as depicted in Figure 2.8.

The equation for flow conditions as shown in Figure 2.8A are:

$$Q = \frac{2}{3} b \left(\frac{2}{3} g\right)^{1/2} H_1^{3/2} \tag{2.4}$$

where Q is the flow rate through the gate and adjacent spillways (not in use for this case), b is the width of the gate, g is gravitational acceleration and $H_1$ is the hydraulic head above the gate. For instances when the adjacent spillways are passing water (Figure 2.8B), the equation becomes:

$$Q = \left(\frac{g}{B_{up}}\right)^{1/2} \left[bz + B_{up}\left(\frac{2}{3}H_1 - \frac{bz}{3B_{up}} - \frac{2z}{3}\right)\right]^{3/2} \tag{2.5}$$

Where $B_{up}$ is the width of the gate and adjacent spillways, and z is the height of the gate.

Equations 2.1 –2.5 were brought together to create the tables, an example of which is shown below in table 2.2. (Full set of tables shown in Appendix B).

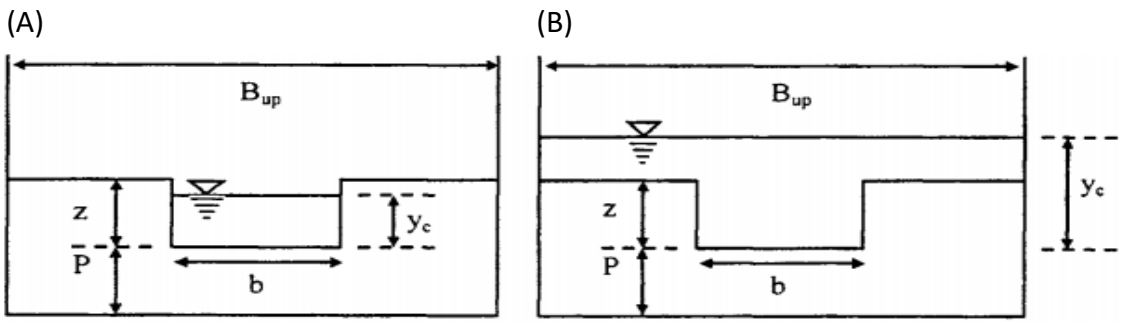



**Figure 2.8.** Representation of flow configuration through the sluice gate and spillway modules. (A) represents cases where water elevation is below the spillways. (B) represents cases where flow is passing both through the sluice gate and over the spillways (Gogus et al., 2006).

**Table 2.2**. Sluice gate and spillway flow rate table for gate width of 6 m and gate height of 3 m. Q total is the total flow being transmitted past the gate, H is the head controlling flow through the sluice gate, $Q_G$ is the flow rate throught the sluice gate, $Q_{spill}$ if the flow rate over the spillway, y from bed is the total water depth, and $H_e$ if the head over the spillway, and Q/b is the unit flow rate.

| H (m) | $Q_G$ ($m^3/s$) | $Q_{spill}$ ($m^3/s$) | Q total ($m^3/s$) | y from bed (m) | $H_e$ (m) | Q/b |
|---|---|---|---|---|---|---|
| 2.0 | 73 | 17 | 90 | 3.5 | 0.2 | 15 |
| 3.0 | 90 | 177 | 267 | 4.5 | 1.2 | 44 |
| 3.5 | 97 | 296 | 393 | 5.0 | 1.7 | 65 |
| 4.5 | 110 | 611 | 721 | 6.0 | 2.7 | 120 |
| 5.5 | 122 | 970 | 1091 | 7.0 | 3.7 | 182 |
| 6.5 | 132 | 1388 | 1520 | 8.0 | 4.7 | 253 |
| 7.5 | 142 | 1857 | 1999 | 9.0 | 5.7 | 333 |
| 8.0 | 147 | 2377 | 2523 | 10 | 6.7 | 421 |

These tables were incorporated into the model in the form of lookup variables with an input of total river flow rate minus flow through the environmental and power modules (since a run of river flow regime was assumed) and an output of hydraulic head at the dam.

An example of one of these lookup variables as it exists in the model is shown below in Figure 2.9.

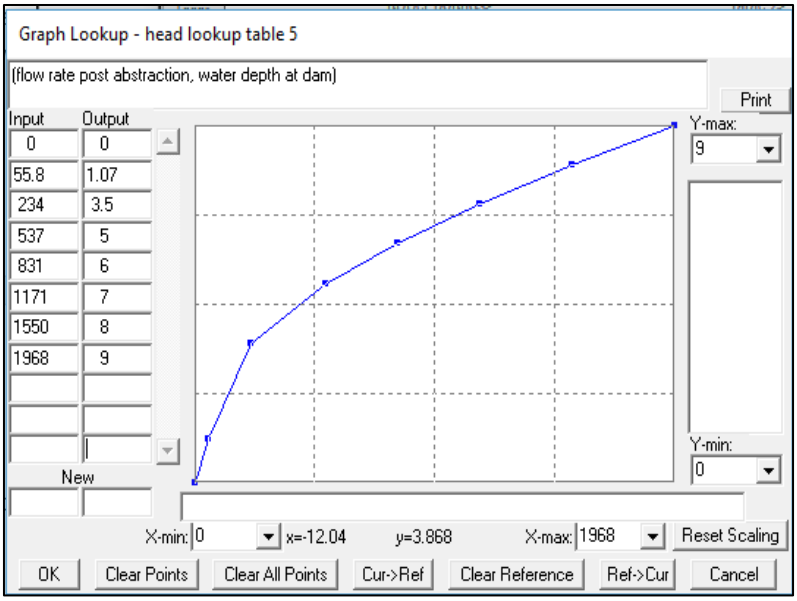



**Figure 2.9**. Vensim format for a lookup variable.

*Modeling low flow conditions*

In the case of low flow conditions, instances where the water surface elevation is lower than the spillway elevation, the dam is no longer considered to be functioning as a run of river structure, since water can be stored behind the dam. Calculations for the water elevation at the dam become dependent on the water volume in the impoundment. A mass balance of water in and water out is used along with the approximated dimensions of the hypothetical impoundment. A water volume to depth relation was developed for discrete intervals in a spreadsheet. These relations were inserted into the model as a lookup variable to interpolate the water depth at each time step.

*Estimation of Upland Sources: Fine Sediment Contributions*

Analyzing sediment transport conditions for the study site began with a watershed scale approach. The processes of erosion and delivery of upland fine sediments to a river reach are an important component of instream sediment transport dynamics. Although the case study site used had suspended sediment data available to model the flux of fine sediment through the system, it can be assumed that many potential dam sites will not have such information readily available. As such, estimates of fine sediment transport in the river must be made using models that can predict the delivery of fine sediment from the uplands to the river. This was therefore incorporated into the methodology of this study, and then compared to the USGS suspended sediment measurements to test accuracy.

Upland erosion rates were calculated using the watershed erosion model RUSLE, the equation for which is shown below:

$$A = RKLSCP \tag{2.6}$$

where A is the average watershed soil loss in tons/acre, R is the rainfall/runoff factor, K is the soil erodibility factor, L is the slope length factor, S is the slope steepness factor, C is the cover and management factor, and P is the conservation practice factor (USDA, 1997). Watershed characteristics such as drainage area, slope, slope length, and land use composition ratios were determined through GIS analysis of regional DEM's and data from the Multi-Resolution Land Characteristic Consortium.

To account for temporal variability in erosion, the rainfall factor was broken into monthly values, and the erosion rates for each month were calculated separately. To account for spatial variability in erosion, the upland area of the watershed was broken into 5 sections (Figure 2.10), delineated using local topography and drainage patterns. Erosion rates were calculated for each area seperatly to improve the accuracy of total watershed erosion estimates. The lowlands were not included in these calculations as they tend to be areas of deposition rather than erosion. Erosion rates for each area were kept separate for application of the sediment delivery ratio, and then summed to find total upland sediment contributions.

*Sediment delivery ratio*

The ongoing process of erosion and deposition along the hillslopes and lowlands of a watershed leads to a discrepancy between the total volume of sediment that is eroded in the watershed and the volume of sediment that is delivered into the river. To calculate the percentage of total eroded material that made its way into the river, a sediment delivery ratio was applied to each of the sub-watershed results from the RUSLE model.

An appropriate sediment delivery ratio for the site was approximated using Figure 2.11. below taken from Lu et al. (2005). This figure relates a watershed's area to its sediment delivery ratio. Lines pertaining to the United States were used to create a best fit line. This was done because no sediment delivery ratio was available in the literature for this region. If such information is available for other sites under consideration, a more locally specific ratio would be preferable.

This line was used to estimate what portion of the eroded soil volume from each section of the South Umpqua River's uplands was delivered to the river, and the sediment yield volume from each was then summed to get a total sediment yield for the watershed.

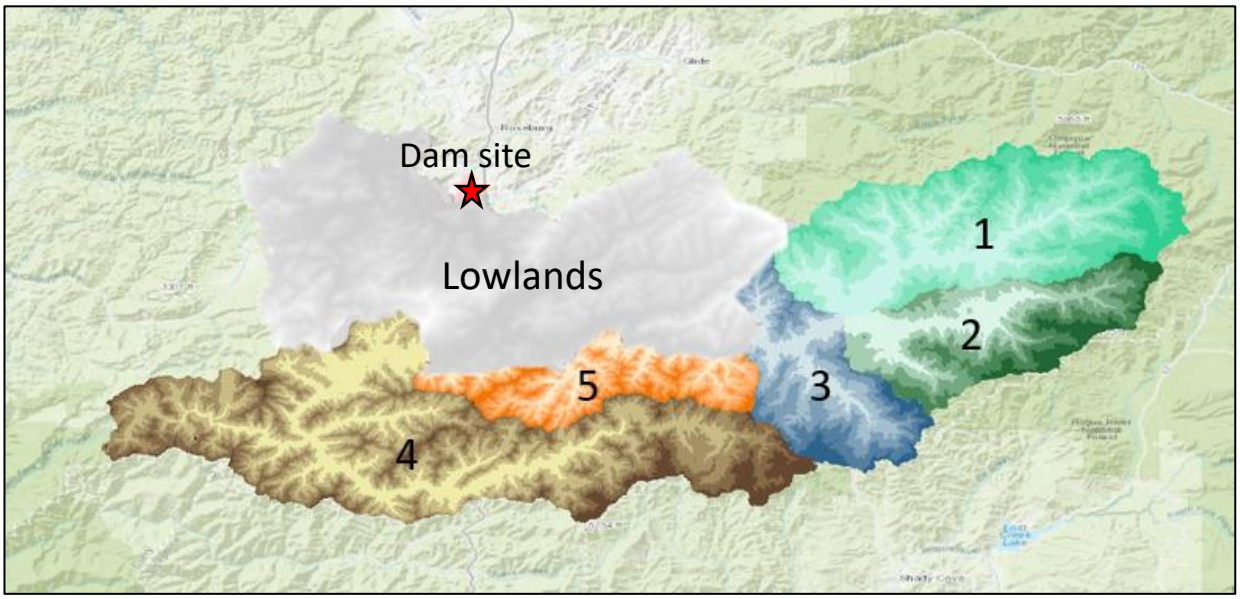



**Figure 2.10.** The South Umpqua Watershed divided into 5 sub-watersheds and lowlands.

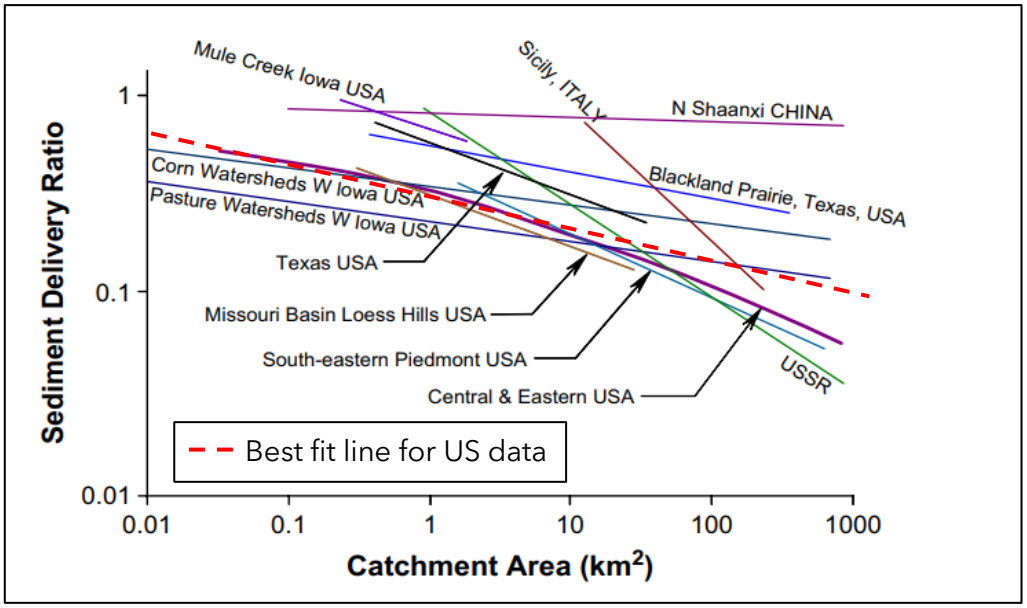



**Figure 2.11**. Sediment delivery ratios for watersheds throughout the world with best-fit line for the United States. Figure modified from (Lu et al., 2005).

Because USGS suspended sediment data was available for the study site, a sediment rating curve was built for the purpose of comparing measured values of fine sediment in the river to predictions made using the method outlined above. The sediment rating curve was developed using data from gaging station 14312000, South Umpqua near Brockway, OR (Figure 2.12).

The fine sediment rating curve developed using the USGS data was broken into two separate curves, one for flow rates over 90 $m^3/s$ and one for flow rates under 90 $m^3/s$. These distinct trends are representative of the hysteresis inherent in the transport of suspended sediments passing through natural river systems.

The exponential equations taken from the curves were used in the model to predict the influx of fine sediment into the system using the river flow rate as an input.

*Fine sediment characteristics*

Because most fine sediment transported in the South Umpqua River can be assumed to have originated in the uplands, the size characteristics of fine sediment traveling in suspension were based off of upland fine soil composition. Upland soil composition was investigated using the Web Soil Survey. This tool was used to find the ratio of sand to silt to clay, and these ratios were used to take a weighted average of the diameter of the fine material. The diameters used for the sand, silt, and clay were simply the median particle size of each class, 0.375, 0.0235, and 0.0003 mm respectively.

*Coarse sediment characteristics*

The sediment size distribution for instream coarse material was taken from the study of Wallick et al. (2011). While the presence of a sediment size distribution in existing literature was convenient for this study, it is likely that many potential hydropower sites will need to have a sediment size distribution generated by other means. This can be accomplished either by collecting sediment on site using a pebble count (e.g. Bevenger & Rud, 1995) or be analyzed by other means such as imagery (e.g. Buscombe & Warrick, 2010).

*Sediment Entrainment Thresholds*

Understanding the flow conditions under which sediment is being transported is important for accurate operation of the sediment passage module. Using a probabilistic approach to calculate transport thresholds in the river has the advantage of reducing the error involved with such predictions, incorporating the effects of turbulence on sediment entrainment along the riverbed. The probabilistic model developed by Elhakeem et al. (2017) incorporates the role of turbulence as well as bed irregularities in the physical processes of sediment transport.

Sediment transport conditions for the site were calculated using this model, for which the probability of sediment entrainment, P, is defined as:

$$P = [1 + exp(-0.07056m^3 - 1.5976)]^{-1} - [1 + \exp(-0.07056m_c^3 - 1.5976m_c)]^{-1} \qquad (2.7)$$

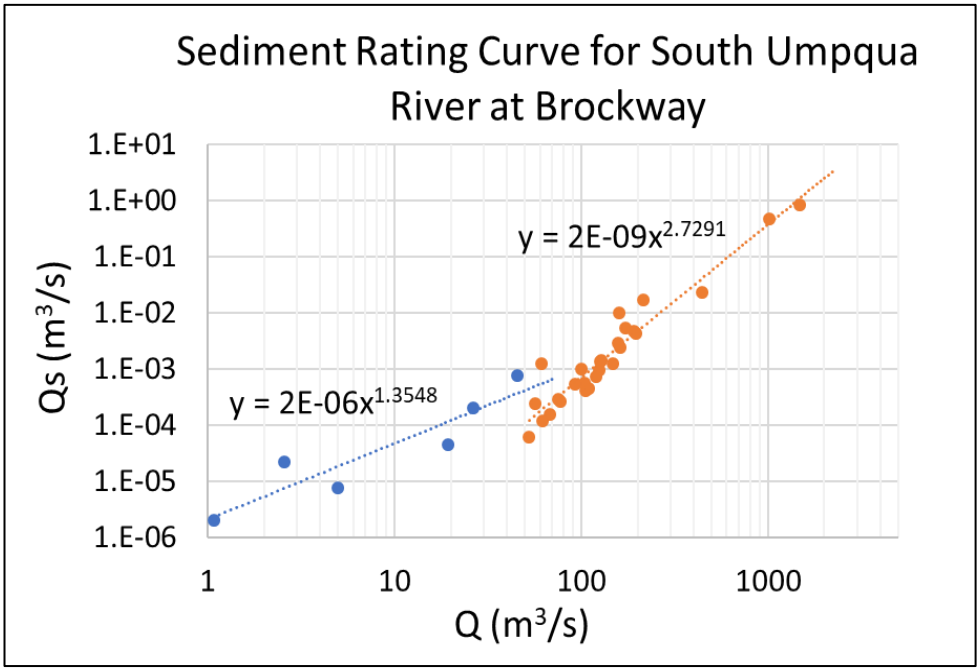



**Figure 2.12**. Sediment rating curve for suspended fine sediment created using suspended sediment data from the USGS.

where $m = (X - \bar{X})/\sigma_x$, $m_c = (X_c - \bar{X})/\sigma_x$ . The variable $X = \ln \tau_*$, where $\tau_*$ is the dimensionless shear stress, $\bar{X}$ is the mean of $X$, $\sigma_x$ is the standard deviation of $X$, and $X_c = \ln \tau_{*c}$. $\tau_{*c}$ is the critical dimensionless shear stress, the lowest shear stress value at which sediment on the river bed can be entrained.

The critical dimensionless shear stress was calculated using equation 2.8 below, which compares the hydrodynamic forces that are exerted on a particle at the moment of incipient motion (e.g., Papanicolaou et al., 2002, Choi & Kwak, 2001),

$$\tau_{*c} = \frac{\cos S}{0.75(r_m C_D + C_L) f^2} \tag{2.8}$$

Where $S$ is the mean bed slope, $r_m = \sqrt{3(R_r + 1)^2 - 4}$, which calculates the ratio of the drag force to lift force moment arms and $R_r$ is the relative roughness, $C_D$ is the drag coefficient, $C_L$ is the lift coefficient and $f = u_b/u_*$, the ratio of the time averaged velocity approaching the particle to shear velocity.

The model produced a curve relating probability of entrainment to the dimensionless shear stress along the riverbed. The dimensionless shear stress was then related to flow discharge, so that the probability of sediment entrainment could be calculated for a range of discharge conditions selected from the site's natural hydrograph.

*Modeling bedload*

The volume of bed load sediment moving through the system was predicted using the equation of Wilcock and Crowe (2003) for sediment transport.

In order to more accurately predict the transport of sediment in the river, the river's sediment size distribution was broken into six size fractions that were used throughout the study whenever the transport of sediment was involved. These size fractions are shown in Table 2.3.

**Table 2.3**. Instream sediment size fractions for coarse sediments

| Sediment size (mm) | Fraction of sediment composition |
|---|---|
| 0.0028 | 0.02 |
| 0.0080 | 0.02 |
| 0.0170 | 0.09 |
| 0.0300 | 0.27 |
| 0.0710 | 0.45 |
| 0.1100 | 0.15 |

The mobilizing conditions for each size fraction present at the site were calculated to understand event-based transport volumes as well as temporal variations in deposition and entrainment.

The Wilcock and Crowe equation was developed for gravel bed rivers where sand is present and can be used with multiple size fractions for improved accuracy. The equation is as follows:

$$q_{bi} = W_i^* F_i u_*^3 / ((s-1)g) \tag{2.9}$$

where $q_{bi}$ is the volumetric sediment transport rate of size fraction $i$, $W_i^* = f(\tau / \tau_{ri})$, $\tau$ and $\tau_{ri}$ are the shear stress and the reference shear stress of the system respectively, $F_i$ is the percentage of sand in the substrate, $s$ is the ratio of sediment density to water density, and g is the gravitational constant. The variable $W_i^*$ is referred to as the transport function and was plotted for all size fractions in the Wilcock and Crow experiments in order to find trends in the data. The lines observed there were,

$$W_i^* = \begin{cases} 0.002\phi^{7.5} & \text{for } \phi < 1.35 \\ 14\left(1 - \dfrac{0.894}{\phi^{0.5}}\right)^{4.5} & \text{for } \phi \geq 1.35 \end{cases} \tag{2.10}$$

where $\phi = \tau/\tau_{ri}$. $\tau_{ri,}$ the reference shear stress, was measured by Wilcock and Crowe when $W_i^*$ took the value 0.002 and was likewise plotted to find the equation,

$$\tau_{rm} = \frac{0.021 + 0.015\, exp[-20F_s]}{(s-1)\rho g D_{sm}} \tag{2.11}$$

Where $F_s$ is the percent sand on the bed surface, ρ is the density of water, and $D_{sm}$ is the mean surface grain size.

It was assumed that the system acted as a transport limited system, in which as much sediment as the system was able to transport was available to be transported. Thus, this equation was utilized to predict all influx of bedload into the reservoir.

*Fine Suspended Sediment*

The influx of suspended fine sediment into the impoundment was calculated using the sediment rating curve developed using the USGS suspended sediment data for the site. The volume of sediment using this approach is dependent upon the volume of water entering the impoundment.

*Impoundment Sediment Dynamics*

Sediment entering the reservoir is assumed by the model to deposit in the shape of a wedge, or ramp, with its apex against the face of the dam.

Coarse and fine sediment entering the system from upstream constitute the total sediment influx. At each time step, the volume of all incoming bedload, and the volume of fine sediment that falls out of suspension, calculations for which are described below, is added to the volume of the ramp.

To calculate the rate at which sediment is moving through the impoundment the bed shear stress needed to be calculated for a range of sediment storage and flow conditions. To accomplish this, a series of water surface profiles were developed for a set of flow conditions modeled at the site. Each flow rate was used for two separate water surface profiles, the first assuming no sediment deposition in the reservoir, and the second assuming a fully formed sediment ramp. These profiles were developed using the standard step method (Chow 1959), which calculates the energy slope, $S_E$, and water depth, H, along the length of the reservoir. These were used to calculate the shear stress using the basic equation for bed shear stress, $\tau_o = \gamma H S_E$, where γ = the specific weight of water. Because shear stress is not distributed evenly along the ramp, impoundment shear stress was calculated for three separate, longitudinal sections of the ramp before it was averaged for use in the model.

The shear stress values calculated from the water surface profiles were used to create a system of lookup variables that were used to interpolate the shear stress and water depth on the ramp based on the conditions in the impoundment such as the height of trapped sediment and the operational status of the sluice gate (open or closed). An excerpt from the model illustrating the layout of the interpolation process is shown in Figure 2.13.

This interpolated shear stress was used to calculate the rate at which bedload was transported through the reservoir using the Wilcock and Crowe equations (2003).

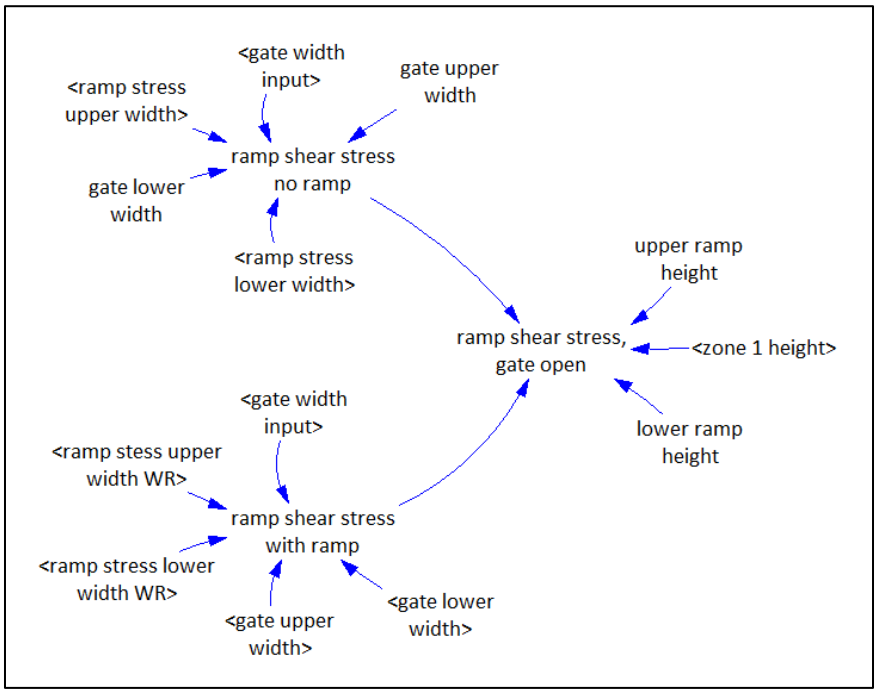



**Figure 2.13.** Excerpt of interpolations used in model to calculate the shear stress in the impoundment at each time step

*Fine sediment trapping*

The shear stress calculated for the impoundment was used to calculate what percentage of fine suspended sediment fell out of suspension and was trapped in the impoundment at each time step. The shear stress was first transformed into shear velocity, $u_*$, where $u_* = (\tau/\rho)^{0.5}$, and ρ is the density of water. This form of shear stress is used in what is known as the Rouse Criterion, the ratio of a particle's settling velocity to the shear velocity, which dictates its state of suspension. The particle settling velocity was calculated using the equation of Tan (2018),

$$w_{s_i} = \sqrt{\left(13.95\frac{\upsilon}{d_i}\right)^2 + 1.09\Delta g d_i} - 13.95\frac{\upsilon}{d_i} \quad (2.12)$$

where, v is the kinematic viscosity of water, and $d_i$ is the particle diameter of each size fraction, *i*.

The ratio of these terms is used to determine what percentage of incoming suspended sediment is washed through the impoundment and what percentage settles and forms part of the sediment ramp. Figure 2.14

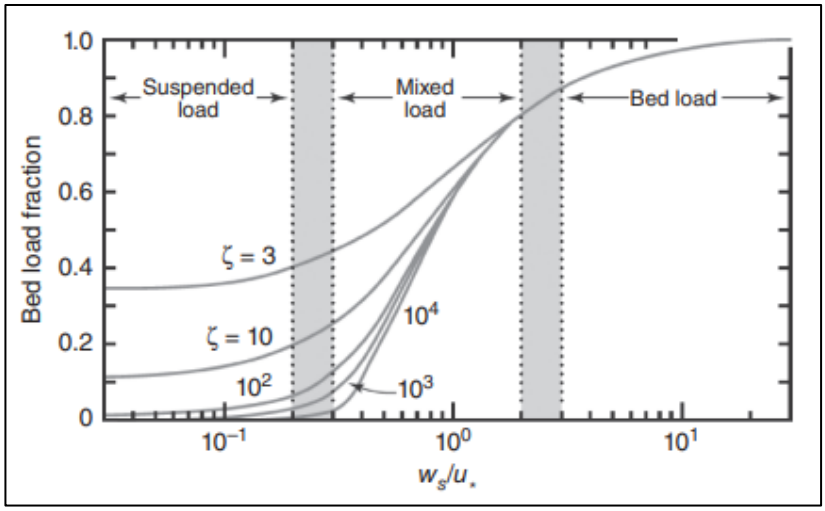



**Figure 2.14.** Relationship between the ratio of the particle settling velocity to the shear velocity, $w_s/u_*$, and the fraction of sediment being transported as bedload (Papanicolaou & Abban, 2016).

was used to evaluate these percentages. Sediment traveling as bed load was assumed to contribute to the ramp.

*Coarse sediment outflux*

Coarse sediment traveling as bed load traveled passed the dam only when the sediment passage module was in operation. This was largely dependent on the distribution of sediment, which is outlined below in detail.

Coarse sediment being transported to the front of the impoundment was analyzed for its potential to become suspended using the same Rouse criterion outlined above. If any of the coarse sediment size fractions were found to be traveling in suspension, it was transported out of the impoundment regardless of whether the sediment passage module was in operation or not. The same held true for fine sediment that had deposited in the impoundment. If impoundment shear stress rose to a level that resuspended the fine sediment size fraction, this sediment was subtracted from the volume of trapped sediment behind the dam.

*Modeling impoundment sediment distribution*

In order for the model to track the effects of sluice gate operation on the distribution and evacuation of sediment from the impoundment, trapped sediment is modeled in two separate zones. When the sluice gate is opened, high flow rates through the gate lead to an increase in local shear stress, causing all sediment within range to be evacuated through the gate. This range is represented in the model as Zone 2, with a length of four times the height of the sediment gate opening. Sediment outside of this range

continues to be transported according to the shear stress imposed by reservoir conditions and is represented in the model as Zone 1.

The management of these zones is further broken into two cases, reflecting two different behaviors of sediment accumulation. In the first, Zone 2 is filled relative to Zone 1, i.e. the sediment ramp is fully formed

up to the face of the dam. At this point, the sediment behaves as a single ramp. This is addressed in the model by combining the volume of Zone 2 and Zone 1 into a single volume tracked by Zone 1, which for this condition extends the full length of the reservoir (Figure 2.15A).
When the sluice gate is opened, case 2 is activated. Zone 2 is reinstated, and the sediment volume that spans its length is fully evacuated. This volume is simultaneously subtracted from Zone 1, whose length is shortened to a distance outside of the range of increased shear stress. As sediment is transported towards the dam, it is transported from Zone 1 to Zone 2. When the gate closes again, the volume of sediment refilling Zone 2 is monitored (Figure 2.15B). If it reaches a volume that constitutes a fully developed ramp, the model reverts back to case 1.

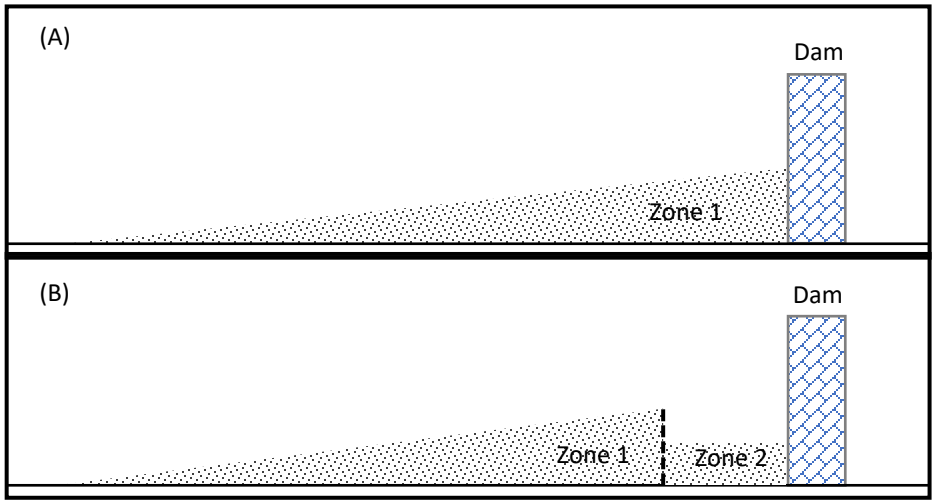



**Figure 2.15.** Two different cases of sediment distribution in the impoundment as modeled

An excerpt from this portion of the model is shown in Figure 2.16.

With the major hydraulic and sediment components in place, other routines were put in place to monitor measurements which can be used to compare one dam site to another, making it easier to understand the behavior of an impoundment in context. These measurements are the hydraulic residence time, and the dam trapping efficiency. Both are discussed below.

*Hydraulic Residence Time*

The hydraulic residence time (HRT) of a reservoir represents how much time on average water spends in an impoundment. Because the amount of time water spends behind a dam directly relates to its ability to hold sediment in suspension, it is a good indicator for how well a dam will trap fine sediment (Morris & Fan, 1998). The HRT was calculated in the model by dividing the volume of stored water in the reservoir, $V_{trapped}$, with the river discharge, $Q_{river}$, entering the reservoir at each time step:

$$HRT = \frac{V_{trapped}}{Q_{river}} \tag{2.13}$$

The mean HRT for the dam without the use of the sediment passage module was found and compared the HRT from other existing dam sites as a way to check model performance.

*Dam trapping efficiency*

A good measure of the efficiency with which a dam traps total sediment, including coarse and fine, can be gained by comparing the amount of sediment entering the reservoir to the amount of sediment trapped in the reservoir. This value is known as a dam's trapping efficiency. It is expressed as a ratio between the rate of sediment influx and the rate at which sediment is accumulating behind the dam.

$$TE = \frac{sediment\ influx - sediment\ outflux}{sediment\ influx} \tag{2.14}$$

Where TE is the trapping efficiency and the sediment influx and outflux are rates of transport calculated in $m^3/s$. The time averaged trapping efficiency for each model run was tracked by summing the trapping efficiency for each time step and dividing by the number of time steps.

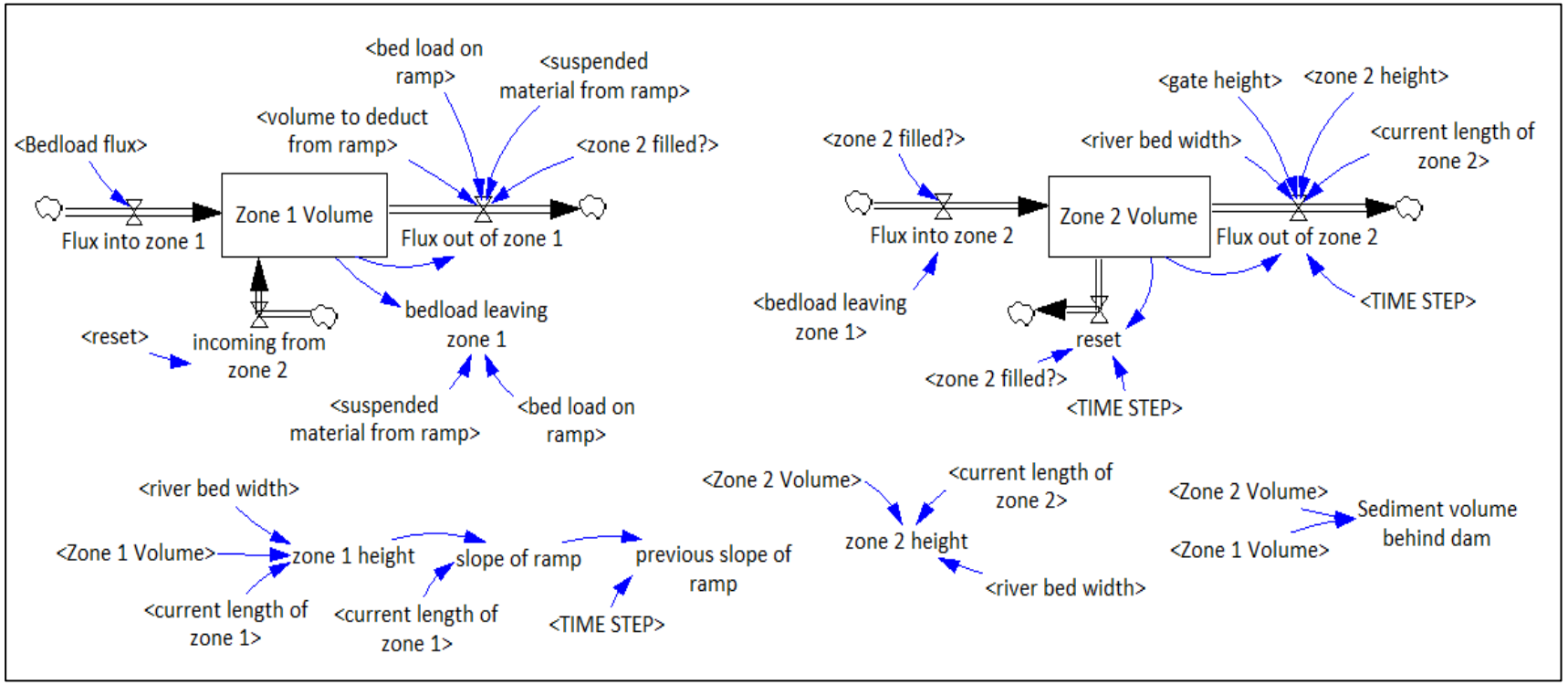



**Figure 2.16.** Excerpt from model of sediment dynamics in the impoundment.

*Subroutines*

While the main routines making up the model have been outlined above, several subroutines were also built into the model to serve two different purposes. Those that give further information with which to evaluate different model runs include routines keeping track of the percentage of time that the sluice gate is open, the percent of time that power is being produced, annual net power generation and to help organize output, a routine for keeping track of the month of the year based on the hourly time step of the model. Other sub routines that were put into place simply to make sure that the model was generating measurements that made physical sense, include a routine for tracking the bulk velocity and shear stress of the river, and the flow velocity through the sediment passage module.

### 2.4. Model sensitivity analysis

Model sensitivity to three different parameters controlling the operation of the sediment sluice gate were tested in order to qualitatively understand the impact that different sediment management decisions would have on power production, sediment volume accumulation, and trapping efficiency of the dam. The first order control parameter for gate operation is the height of sediment trapped in the reservoir. This height is measured as a percentage of the sluice gate height. Once the selected threshold height has been reached, the sluice gate is brought into operation during appropriate flow events.

The second order control parameter for gate operation is the probability of sediment transport into the reservoir. Once a threshold of probability has been reached upstream, the gate is brought into operation, given the first control condition has been met. A range of probability thresholds were tested that reflected the site characteristics, including its natural hydrograph.

Lastly, a third order control parameter, operational gate height, was evaluated. Gate height effects the transport of sediment across the dam and also the hydraulic head available for power production. This variable was measured as a percentage of dam height.

While testing each parameter, the other two were held constant. The values at which each was held during testing is shown in Table 2.4. These values were selected because they were shown not to push the results of sediment trapping and power production to extremes in either direction but represented a middle ground.

**Table 2.4.** Values at which each parameter was help constant during testing.

| Critical sediment volume as percentage of reservoir capacity | Probability of entrainment | Gate height as percentage of dam height |
|---|---|---|
| 20% | 0.01 | 75% |

# 3. Results

### 3.1. System model development outcomes

The finished model was comprised of both hydraulic and sediment components of the system. Hydraulic routines included the river hydrograph, which gave an incoming flow rate at each time step, the flow through the environmental module, which was subtracted from flow available to other modules, flow through the power module, which had an upper and lower boundary, and flow through the sediment passage module and spillway module. These last two were broken into routines for cases where the gate was closed, the gate was open with water passing only through the gate, and the gate was open with water moving through the gate and over the spillway. The last two were further broken into cases where the gate was open high enough that it allowed free surface flow through the sediment module, and cases where the sediment module was submerged.

Sediment components consisted of upland sediment contributions, introduced into the system as fine sediment in suspension, the influx of coarse sediment from the river, the outflux of both suspended and bedload sediment, and sediment trapping in the impoundment.

These components were brought together to calculate the hydraulic residence time of the impoundment and the dam sediment trapping efficiency for both fine, coarse and total sediment.

Lastly, the impact of different sediment management regimes on power production and sediment trapping was examined. Management variables that were manipulated all impacted the operation of the sediment sluice gate. Gate operation was dependent upon the depth of trapped sediment in the impoundment, transport thresholds for sediment influx into the impoundment, and the height to which the sluice gate was opened when in operation.

*Design Flows for Environmental Module*

The environmental flow requirement for the site, estimated using the Tennant method (1976) set the environmental flow minimums to be 10% of the mean annual flow. This was calculated to be 7 $m^3/s$. The river hydrograph was less than or equal to this value 27% of the time at which point, all river flow was diverted through the environmental module.

*Design Flows for Power Module*

When calculating the design flow of the turbine, the environmental flow minimum was subtracted from the mean annual flow rate for the site of 77 $m^3/s$ to result in a design flow of 70 $m^3/s$. However, this flow value was greater than the upper flow boundary for a Kaplan turbine (50 $m^3/s$). The design flow was therefore lowered to 45 $m^3/s$ which meets the boundaries for the Kaplan turbine, and also allows maximum flow, which is 110% of the design flow, to pass through the turbine. The lower boundary of flow allowable for the turbine operation, 30% of the design flow, was calculated to be 12.9 $m^3/s$. The upper boundary was calculated to be 49.5 $m^3/s$. The amount of flow passing through the power module was dependent upon the management regime in place for that run, and so differed from run to run.

*Water Storage*

The impoundment storage volume potential was estimated to be 423,000 $m^3$. The actual water storage behind the dam was dependent upon the flow conditions at the site and the amount of trapped sediment in the impoundment.

*Upland Contributions*

The RUSLE model predicted an upland erosion rate of 4.6 million tonnes of soil per year, equivalent to a mean loss of 0.54 mm annually. Erosion rates varied throughout the year, with the lowest rates occurring in July and the highest rates occurring in October. Applying the sediment delivery ratio, taken from the data of Lu et al. (2005, Figure 2.11), to this rate of erosion resulted in a prediction of approximately 0.45 million tonnes of sediment being delivered to the river annually.

In order to draw a comparison, the fine sediment influx calculated using the sediment rating curve for each of the 12 months was averaged over the course of the 25-year simulation. This average value is compared to the monthly sediment yield predicted using the RUSLE model in Figure 3.1. The percent difference in these values from month to month range from 16% to 200% with a mean percent difference of 166%.

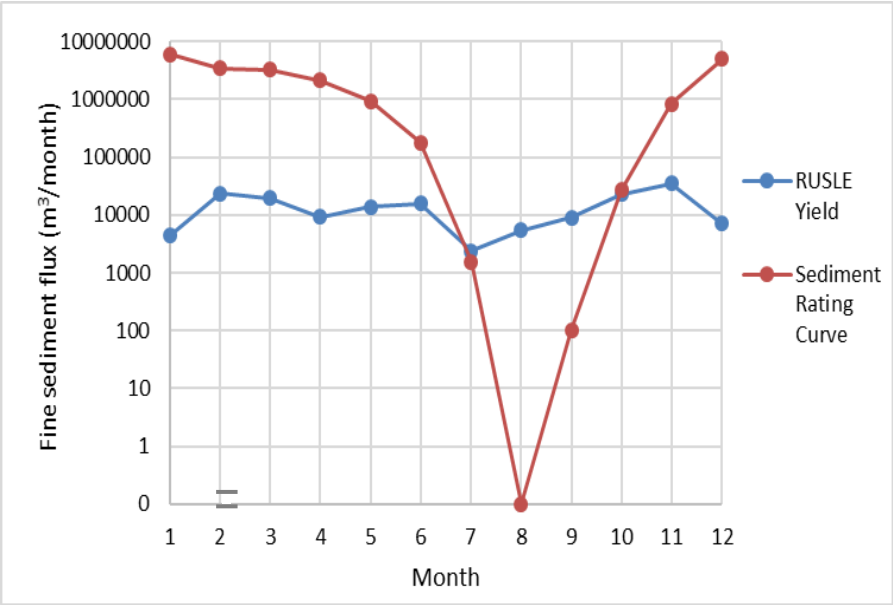



**Figure 3.1**. Comparison of fine sediment contributions to the system as predicted using the RUSLE model and the sediment rating curve developed using TSS data from the USGS.

*Sediment Entrainment*

For the 25-year simulation for the South Umpqua study site, the probability of entrainment as calculated using the methods of Elhakeem et al. (2017) ranged from P = 0% during the dry season, to P = 15% for the largest flow event present in the hydrograph of 2200 $m^3/s$, meaning a particle is likely to be in motion 15% of the time. These values were used at each time step in the model to make sediment management decisions by tying the operation of the sediment sluice gate to the probability that sediment was entering the system. A threshold was set for the probability for different runs at which the gate was opened. Once the probability fell below the selected value, the gate was once again closed.

For volumetric sediment transport conditions, the upper range was calculated to be 1.1E-02 $m^3/s$ for coarse sediment traveling as bedload, and a maximum fine sediment transport rate of 2.6 $m^3/s$, while levels dropped to approximately 0 $m^3/s$ during low flow events.

For months with high mean flow rates, fine sediment constituted the majority of the sediment volume being transported into the impoundment. This trend was reversed for dryer months, although rates of transport during these months were very low making the difference in transport rates insignificant to the buildup of sediment in the reservoir (Figure 3.2).

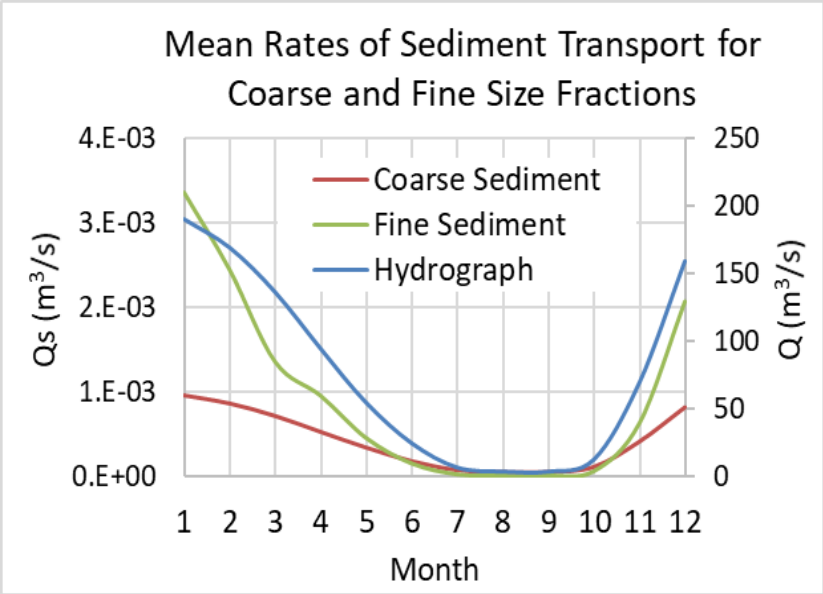



**Figure 3.2.** A comparison of mean transport rates and mean monthly flow values for fine and coarse sediment throughout the year.

### 3.2. System dynamics model output

The system dynamics model was not calibrated for this study although all the output for appropriate variables were checked during initial runs to make sure they made physical sense. Calibration will require data from an existing site comprised of time dependent sediment trapping. This study instead focuses on the construction of the model and the components of the system taken into consideration.

*Trapping Efficiency*

Trapping efficiency at the site was dominated by the flux of coarse sediment through the system. The time averaged coarse trapping efficiency ranged from 86% to 99% for different model runs, as compare to a range of 53% to 56% for time averaged fine sediment trapping efficiency. This difference in spread emphasizes the impact of the sediment module on the trapping of coarse sediment. Total time averaged trapping efficiency for the dam ranged from 86% to 89%, values closer to those for coarse sediment despite the higher volume of fine sediment moving through the system.

Although the excessive buildup of sediment in the reservoir had a negative impact on the fine sediment trapping efficiency, it can be seen in Figure 3.3B that a small amount of sediment in the impoundment actually lowers the trapping of fine sediment as compared to scenarios with no trapped sediment volume in the reservoir.

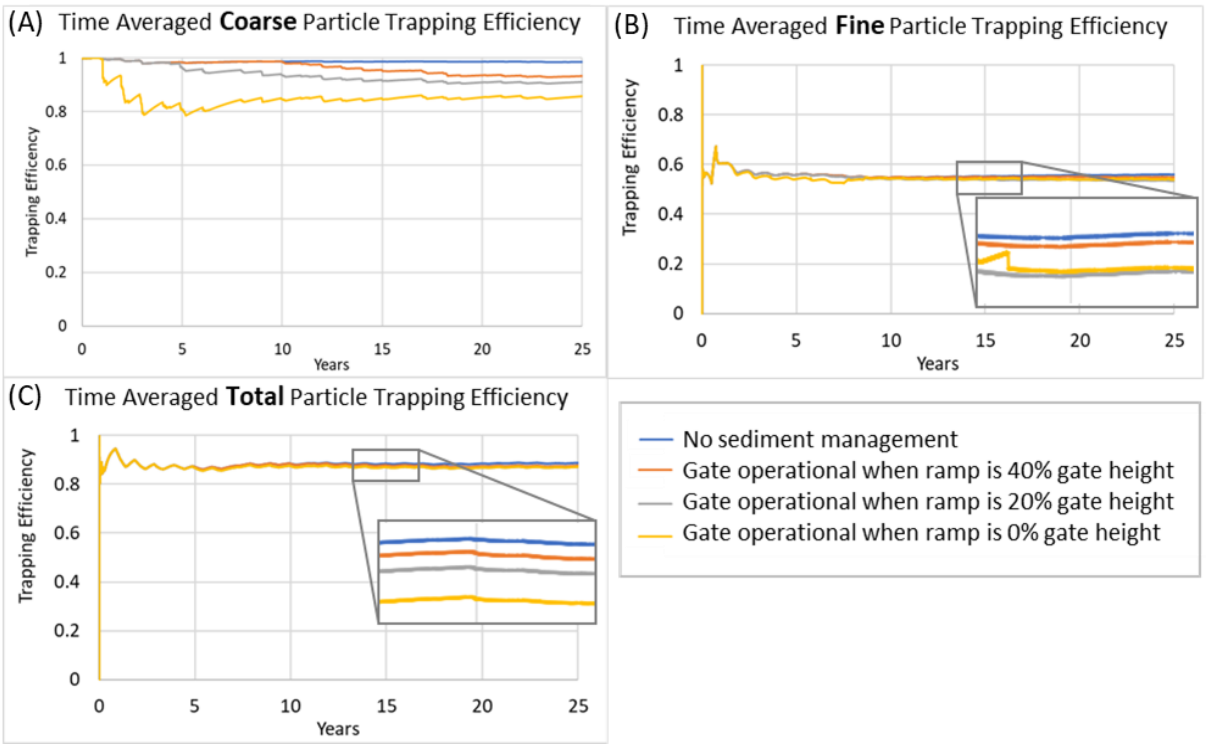



**Figure 3.3.** Time averaged trapping efficiencies over the model run for coarse sediment, fine sediment and the sum of the two, total sediment trapping efficiency

*Hydraulic Residence Time*

The hydraulic residence time (HRT) ranged from 3.8 days during very low flow events to 0.005 days during high flow events, meaning it took this many days for the water in the impoundment to turn over. A comparison of the HRT for the scenario with no sediment management, i.e. the sediment sluice gate was not put into operation, and scenarios with effective sediment management, revealed the impact that sediment management has on an impoundment's HRT. While the HRTs from both runs remained similar for the first 6 years, from approximately years 7 through 16, the scenario with sediment management had lower HRTs during months of low flow by up to 0.3 days. At year 17 to 25 however, the HRT for the run without sediment management was lower during all seasons by as much as 1.6 days.

Two runs are compared in Figure 3.4, one with no sediment management, and the second with what was determined to be an optimized sediment management regime, discussed below.

The mean HRT for the impoundment without any sediment management was calculated to be 0.38 days, while the mean HRT for an optimized management regime was 0.45 days. When compared to the HRT's measured in a study by Skalak et al. (2009) (figure 3.5), this output seemed appropriate, falling within the same magnitude of order as dams of a similar height. The comparison is shown in Figure 3.5 (note that four dams with heights of 11.3, 14.3, 19.8, and 57.0 m included in the study of Skalak et al., 2009 were not considered in figure 3.5 as their heights were not within the same magnitude of order as the dam tested in this study).

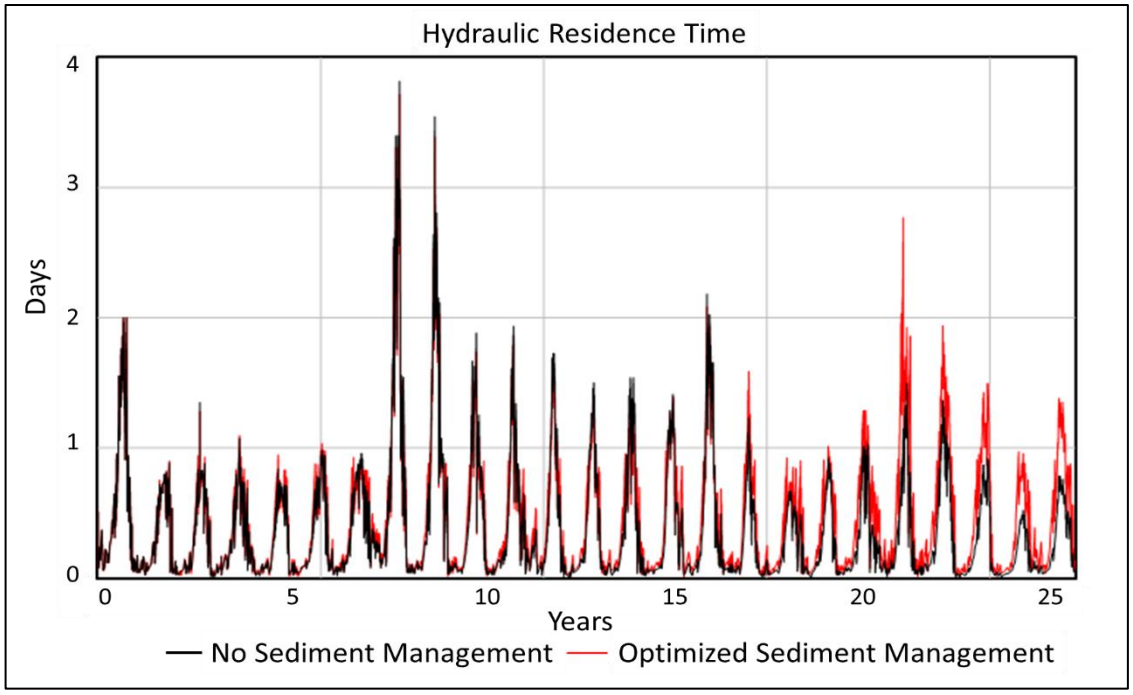



**Figure 3.4.** A comparison of the hydraulic residence time of the impoundment for two runs.

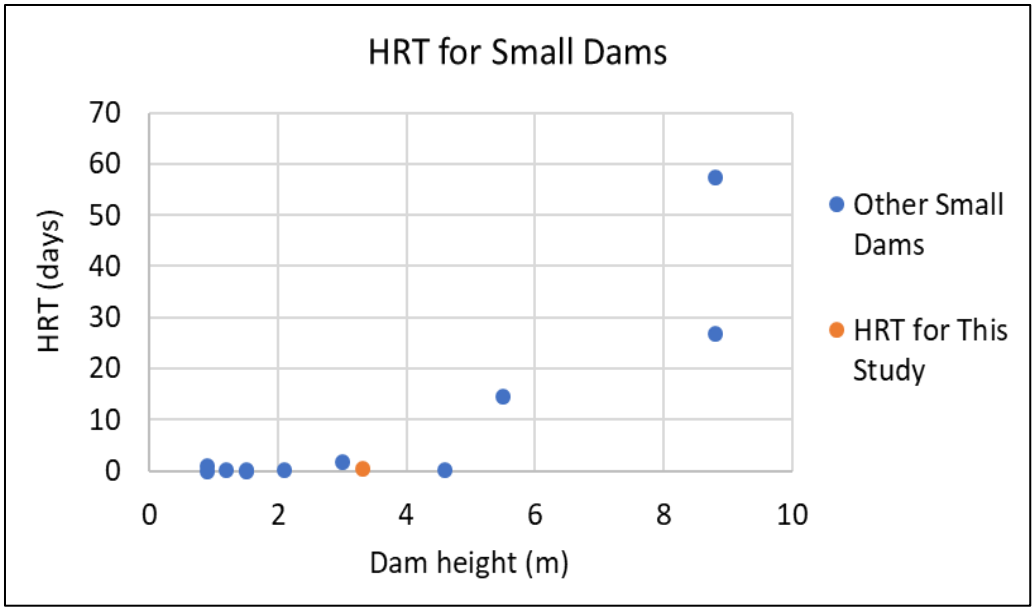



**Figure 3.5.** A comparison of the mean HRT calculated by the model and the 's of other small dams as measured by Skalak et al. (2009).

### 3.3. Model sensitivity

*Impact of Control Parameters Over Time*

Due to the dynamic nature of the system, sensitivity of net energy production and trapped sediment volume to control parameters changed over the course of model runs. For example, Figure 3.6 shows the impact of three different values for the first control parameter, which restricts gate operation based upon the sediment height in the impoundment. It shows that for the first 5 years of power production modeled for this site, sediment management has little impact on power generation. Gradually over the next 20 years simulated, a divergence in net energy production occurs, with an inverse relationship between trapped sediment and net energy production. The trapped sediment volume reaches a quasi-steady state for each control parameter value at which the sediment module first becomes operational at approximately 1 year, 5 years, and 10 years as the sediment height reaches the threshold of 0%, 20% and 40% of the gate height respectively

When the second condition for gate operation, the probability of sediment influx into the impoundment, is set to a high threshold, the volume of sediment in the impoundment becomes independent of the first control parameter, as does the net energy generation as the probability of entrainment in the river dictates when the gate first becomes operational. For these cases, steady state for sediment volume is not reached during the simulated 25 years. Figures for this scenario are shown in Appendix A.

Values for trapped sediment and energy production show little sensitivity to operational gate height over time. Instead, they follow the same trend as those produced by a gate operation for the value set for the first two parameters (Figure shown in Appendix A).

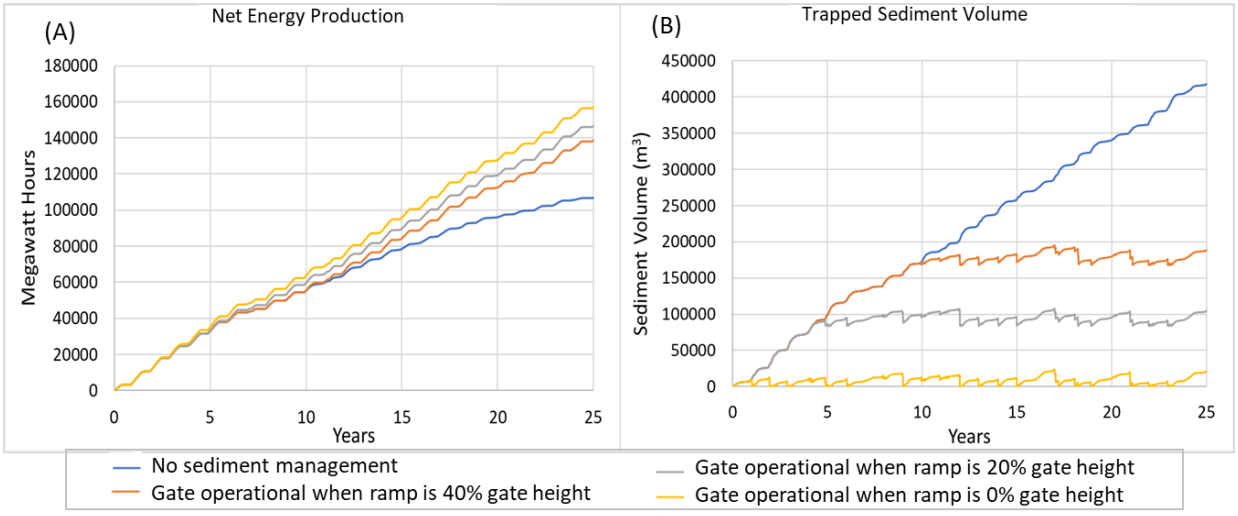



**Figure 3.6.** Net energy generation and trapped sediment volume over model run time with variations in the sediment volume threshold at which the sediment module is put into operation.

*Evaluation of Model Sensitivity Long Term*

Model sensitivity to the three control parameters varied for values of net energy production and trapped sediment volumes as measured at the end of each simulation (Figure 3.7). Changes made to gate operation based on the sediment height in the reservoir resulted in an almost linear impact on net power production and trapped sediment volume, with optimization of both energy production and sediment trapping prevention occurring when gate operation took place at sediment height equal to 0% gate height. The sediment trapping efficiency for this parameter increased by 3% as tested values were increased to 100% gate height, while energy production fell by 32%.

While the model displayed sensitivity to the second control parameter, probability of sediment influx into the impoundment, optimization for sediment trapping and energy production did not coincide for a single value of P. Rather energy production was optimized for gate operation at P = 0.005, declining as this value was increased or decreased. Trapped sediment volume was lowest for P = 0 rising steadily until P reached a value of 0.15, the highest P value experienced during the model simulation. Trapping efficiency increased by 9% for this range, and the net energy production fell by 30% from optimal gate operation for power production of P = 0.005 to lowest production at P = 0.15.

The model showed the least sensitivity to changes made to the operational gate height. This control parameter changed the sediment trapped efficiency by less than 0.001% in the reservoir. Increasing the

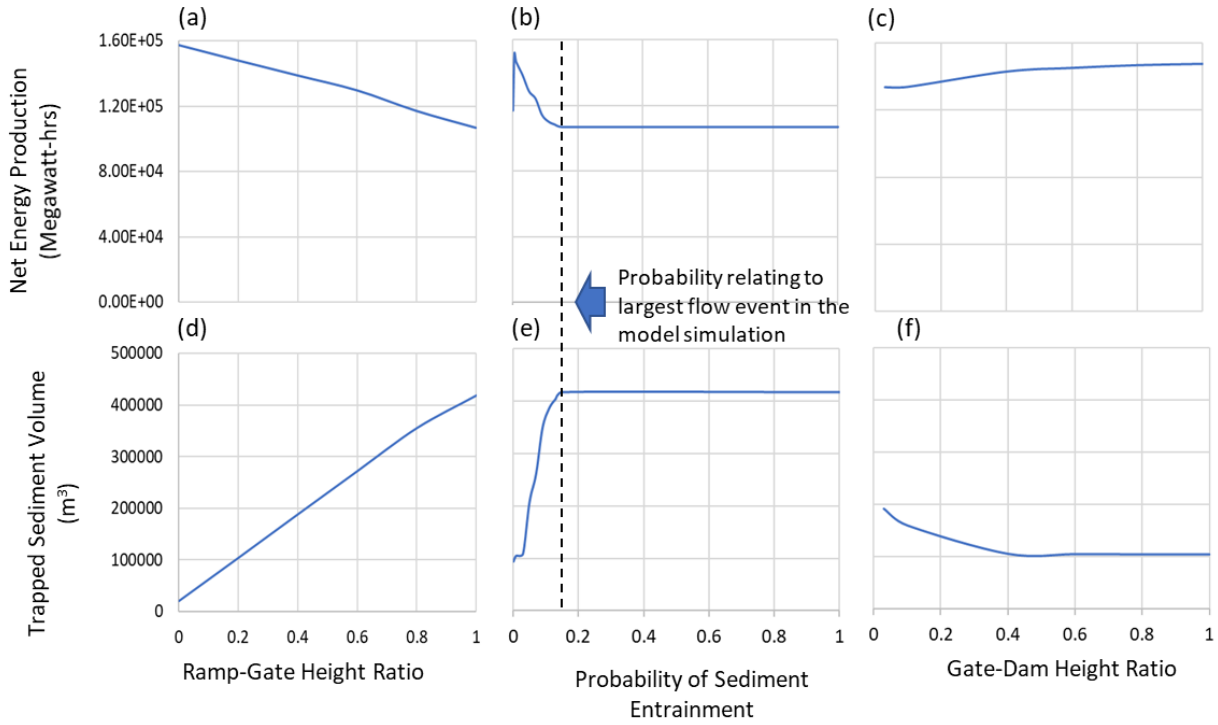



**Figure 3.7.** Changes in final time step values of net energy generation and trapped sediment volume for a range of control parameter values modeled.

gate height from 10% of the dam height to 100% of the dam height resulted in a decrease in net energy

production by less than 0.001%. Table 3.1 shows the percent changes in net energy generation and trapping efficiency over the range of control parameter values.

**Table 3.1.** Percent difference in net energy production and sediment trapping efficiency for control parameter values optimized for each variable respectively.

| Control Parameter for Gate Operation | Percent decrease in net energy production | Percent increase in trapping efficiency |
|---|---|---|
| Sediment ramp height | 32% | 3% |
| Probability of entrainment | 30% | 9% |
| Gate opening height | 0% | <0.001% |

# 4. Discussion

### 4.1. Analysis of system dynamics model development

Flows through the environmental and power module were straight forward variables to build into the system dynamics model, simply being subtracted from the river hydrograph or stored water as available. In contrast, the process of modeling flow through the sediment passage and spillway modules was much more involved, requiring the use of multiple spreadsheets to generate input for the lookup variables called upon by the model to determine flow and hydraulic head at each time step. Continuity from time step to time step in these variables was important regardless of the change in equations which governed them. As different conditions of gate operation and flow arose in the model, the transition between the equations and routines that determine the head at the dam and flow rates through these modules performed well, without any unexpected jumps in water height or flow rate.

*Upland Contributions*

The upland erosion rates for the study site as predicted by RUSLE fall within reported ranges for mountain ranges of the west coast (Montgomery & Brandon, 2002). However, a study performed by Reneau and Dietrich (1991) examining erosion at a site within the same mountain range as the study site found erosion rates to be less than those predicted in this paper by an order of magnitude. Their study measured 0.05-0.08 mm of erosion as compared to this study's predicted 0.5 mm. The source of such a discrepancy could generate from a number of factors. According to a recent review on USLE type erosion models conducted by Alewell et al. (2019), data from studies measuring erosion rates in the field are biased by factors such as their time scale, the area covered by the study, and the heterogeneous nature of upland erosion itself. It is equally likely that the problem stems from RUSLE calculations, as this model has the tendency to over-estimate erosion rates for systems with low annual erosion rates (Kinnell, 2010), which due to its extensive undeveloped area, this watershed can be assumed to have.

When comparing the RUSLE results to the sediment rating curve developed using suspended sediment data from the USGS, the RUSLE results under-predicted the delivery of fine sediment to the river for most of the year, the exception being in the months of low flow events, June – September. This could stem from the fact that the river lacks the power necessary to transport delivered sediment during these low flow months. The sediment delivery ratio applied is unlikely to be an important source of error, although it may account for some. This is because even before the sediment delivery ratio is applied, the values of fine sediment being transported through the system as predicted using the sediment rating curve are higher than gross erosion values predicted by RUSLE.

Perhaps the most important potential source of error stems from the fact that fine sediment being added to the system as a result of bank erosion was not added to the RUSLE output. Bank erosion can constitute a large percentage of a river's fine sediment and the discrepancy between the sediment rating curve and the RUSLE data could in large part be the due to this missing component in the study. In order to use upland models to predict fine sediment delivery to the system moving forward, bank erosion will have to be incorporated into these calculations.

Regardless of the source of error, these differences show that the estimation of sediment from the uplands using the RUSLE model should be executed carefully for use in the system dynamics model, making sure to use appropriate factors for the site being considered to reduce model error which can compound problems listed above.

### 4.2. Interpreting system dynamics model output

Output from the system dynamics model was able to make the tradeoffs between variables clear for different sediment management regimes, as well as supporting the overall benefits of sediment management to optimal small hydropower generation. Structuring the model in order to produce these results is the first step in being able to accurately predict best management practices for potential small hydropower sites. Tracking such variables as trapping efficiency and hydraulic residence time gives information about the impacts a small dam may have on a riverine system.

*Trapping Efficiency*

As expected, the trapping efficiency (TE) for coarse particles was greater than that for fine particles, the latter being mostly transported though the impoundment in suspension. Interestingly, an increase in coarse particle TE was seen to reduce fine particle TE. The accumulation of sediment behind the dam was able to reduce the volume of water being stored just enough that it impacted the ability of fine particles to flow passed the dam without settling.

Although trapping efficiency for coarse particles neared 100% for scenarios with no sediment management, the dam was not able to trap all coarse materials. During larger flow events, smaller size fractions became suspended briefly, allowing some coarse material to exit the system even for scenarios where the gate was not operational. A study by Pearson and Pizzuto (2015) found that during large enough flow events, the sediment behind small dams can be completely flushed over the dam. Although the 8-year flow event that marked the greatest flow modeled in this study did not have the capacity to remove all sediment from behind the dam, the removal of smaller size fractions during this event does indicate that the model has the capability of replicating such behavior if larger flow events were modeled.

*Hydraulic Residence Time*

The changes seen over time in the site's hydraulic residence time (HRT) is a trend supported by literature (e.g. Morris & Fan, 1998). As a reservoir fills with sediment, its water storage volume becomes smaller, while its incoming flow tends to remain the same. Thus, the ratio of water storage to incoming flow grows smaller with the passage of time. Because of this, dams tend to trap less incoming fine sediment over time. This is because the amount of time water spends behind a dam is related to the amount of time that fine sediment has to fall out of suspension.

The small size of the structure being modeled herein promoted the passage of fine sediment in suspension, while larger structures that increase the hydraulic residence time can trap greater amounts of fine sediment. The model could be used to help determine the tradeoffs between dams of different heights at a potential site.

The agreement between the modeled HRT of this study's hypothetical impoundment and the HRT's measured by Skalak et al. (2009) is the closest the author was able to get to a comparison of modeled sediment trapping efficiency to data currently present in literature. Although many one-time measurements of trapped sediment behind small dams are available in literature, time dependent sediment trapping data for small dams appears to be absent. One-time measurements represent the whole of a dam's history, including large events which may diminish the amount of sediment trapped. As a result, it is difficult to compare these measurements with the model's output as the data to recreate

such a history would need to be available to replicate the data. A way to accomplish such a thing needs to be designed in order for the model to be properly calibrated but is beyond the scope of this study.

### 4.3. Evaluating model sensitivity

Results from the system dynamics model show a buffer of 5 years during which accumulating sediment had minimal impact on power production. The duration of this lag, however, is invariably linked to the hydrograph. Thus, instead of putting importance on the amount of time it took for power production to start diminishing, it should be put upon the volume of trapped sediment that starts having negative impacts on the system. Large events can wash great amounts of sediment into an impoundment quickly, reducing the efficiency of a facility's power generation, while consecutive years of low flow could stretch this period of build up for years.

Long term, for this system, the benefits of sediment management are pronounced. While gate operation has an immediate and dramatic effect on trapped sediment volume, as can be seen in Figure 3.6 B, its benefits to energy production are manifested gradually, but with increasing returns. This demonstrates that for small hydropower facilities, both short- and long-term sediment management goals should be set.

The management parameters tested in this study could help decision makers understand how best to reach such goals. The two most important management parameters in this study were found to be gate operation based on the height of trapped sediment at the gate, and the probability of sediment transport into the impoundment. The model showed greatest sensitivity to these parameters, indicating selecting the most appropriate, site-specific thresholds for each is important

The minimal impact of operational gate height on both power production and sediment trapping is not unexpected. This is because coarse sediment moves along the bed, and flows at which the gate is operational tend to be high, reducing the impact of water loss through the gate on hydraulic head. However, it is likely that if the dimensions of the sluice gate were increased the response of these variables would become more pronounced. A dam height of 3.32 m and a gate width of 6 m as used in this model provide only a small range for varying gate opening area, resulting in a small range of water passage through the gate and area of heightened shear stress in the impoundment.

### 4.4. Application on a broader scale

This model was built to simulate a gravel bed river system and is applicable for use on rivers with this type of bed only. For this system dynamics model to be applicable on a nation-wide scale, the model needs to be able to properly model both gravel and sand bed rivers, and cohesive sediment systems. For sand bed rivers, this could be accomplished by adding a second sediment transport equation to the model that is appropriate for sand bed. The model could then be programed to use one or the other based upon sediment size distribution entered. Incorporating a routine for cohesive sediments will be much more involved, as the behavior of these sediments is quite complex.

Other areas need to be addressed as well, as this model continues to be developed moving forward. One such area is the prediction of fine sediment contributions to the river. As stated previously, the sediment originating from bank erosion is not considered in this model. This need to be addressed in order to more accurately predict the amount of fine sediment moving through the system.

As mentioned above, while this paper examines the structure and sensitivity of a system dynamics model, in order for such a model to implemented by those designing small hydropower facilities, the model discussed herein needs to be validated using data from existing dam sites. While sediment data from large reservoirs are ubiquitous, sediment data for small dams is less common often originating in studies performed for dam removal projects. While finding appropriate data to validate the model may be challenging, this step is crucial to the real-world application of this model.

### 4.5. Improvements to the system dynamics model for small hydropower facilities

Although the system dynamics model developed here can be used to predict the behavior of a small hydropower system, there is need for improvement moving forward.

One such improvement is the need to analyze the impact of the sediment passage module width on sediment distribution within the impoundment. Although the hydrological framework for varying the sediment passage width has been built into the model, the impact of gate width on sediment transport has not yet been incorporated. The width of the sediment passage impacts the area of heightened shear stress and thereby the volume of sediment that is evacuated from the impoundment while the gate is operational.

Incorporating calculations for the virtual velocity of sediment being transported through the impoundment could also improve the accuracy of sediment accumulation in the impoundment and passage through the sediment module. Virtual velocity is the concept of tracking a particles velocity by dividing the overall distance it has moved by the amount of time it took to move that distance, thus incorporating the particles resting time in predicting how long it takes to be transported downriver (e.g. Parsons et al., 2018, Brenna & Mao, 2019). Predicting how long it takes sediment to move through the impoundment could help improve sediment passage module management.

The Vensim PLE platform used is the most basic version of the model available. There are more advanced versions, Vensim Pro and Vensim DSS, which can interface with other models. Connecting the model to an uplands model such as WEPP (the Water Erosion Prediction Project) (e.g. Flanagan et al. 2007) has the potential to greatly improve upland soil. This same approach could provide an option for incorporating bank erosion by linking the system dynamics model to a computational bank erosion model such as CONCEPTS (CONservational Channel Evolution and Pollutant Transport System) (Langendoen et al., 2001).

# 5. Conclusion

This study presented a new system dynamics framework for approaching sediment management planning at new and repurposed small hydropower facilities. A system dynamics model was built using Vensim software in order to facilitate this approach. Output from the model successfully showed trends in power production and sediment trapping as a result of different sediment management scenarios.

Model output also showed the operation of the sediment sluice gate is most sensitive to management parameters linking gate operation to the height of sediment buildup in the impoundment, and the probability of sediment influx into the impoundment, while gate opening height in the case study had minimal impact on power generation and trapped sediment volume.

This study is the first step in model development to create a decision support tool which can be used to assess the feasibility of facility construction and predict site specific, best-practice sediment management operations. Future work will need to focus on calibrating and validation of the model.

## Bibliography

Abban, B., A.N. Papanicolaou, M.K. Cowles, C.G Wilson, O. Abaci, K. Wacha, K. Schilling, and D. Schnoebelen. (2016). An enhanced Bayesian fingerprinting framework for studying sediment source dynamics in intensively managed landscapes. Water Resources Research, 52, DOI:10.1002/2015WR018030.

Alewell, C., Borrelli, P., Meusburger, K., & Panagos, P. (2019). Using the USLE: Chances, challenges and limitations of soil erosion modelling. International Soil and Water Conservation Research, 7(3), 203–225.

Baki, Abul Basar M. B, David Z. Z. Zhu, and Nallamuthu Rajaratnam. (2016). Flow Simulation in a Rock-ramp Fish Pass." Journal of Hydraulic Engineering 142.10.

Baxter, R. M., Glaude, Pierre, and Canada Department of Fisheries Oceans. (1980) Environmental Effects of Dams and Impoundments in Canada: Experience and Prospects. Ottawa: Dept. of Fisheries and Oceans. Print. Canadian Bulletin of Fisheries and Aquatic Sciences ; 205.

Bevenger, Gregory S., and Rudy M. King. (1995) A Pebble Count Procedure for Assessing Watershed Cumulative Effects. Fort Collins, Colo. (240 W. Prospect Rd., Fort Collins 80526): U.S. Dept. of Agriculture, Forest Service, Rocky Mountain Forest and Range Experiment Station

Brenna, A., Surian, N., & Mao, L. (2019). Virtual Velocity Approach for Estimating Bed Material Transport in Gravel-Bed Rivers: Key Factors and Significance. Water Resources Research, 55(2), 1651–1674. https://doi.org/10.1029/2018WR023556

Buscombe, D., Rubin, D., & Warrick, J. (2010). A universal approximation of grain size from images of noncohesive sediment. Journal of Geophysical Research: Earth Surface, 115(F2), n/a–n/a. https://doi.org/10.1029/2009JF001477

Castillo , L. G., Álvarez , M. A., Carrillo J. M. (2014) Numerical modeling of sedimentation and flushing at the Paute-Cardenillo Reservoir. ASCE-EWRI. International Perspective on Water Resources and Environment Quito, January 8-10, 2014

Chen, Y., & Wang, Y. (2019). Variations in Basin Sediment Yield and Channel Sediment Transport in the Upper Yangtze River and Influencing Factors. Journal of Hydrologic Engineering, 24(7), 05019016.

Cheng, F., and T. Granata (2007), Sediment transport and channel adjustments associated with dam removal: field observations. Water Resources Research 43, W03444, doi:10.1029/2005WR004271.

Choi, S.U., & Kwak, S.(2001).Theoretical and probabilistic analyses of incipient motion of sediment particles. Korean Journal Civil Engineering, 5(1), 59–65.

Couto, Thiago BA, and Julian D Olden. (2018) "Global Proliferation of Small Hydropower Plants – Science and Policy." Frontiers in Ecology and the Environment 16.2: 91-100.

Csiki, S.J., and B.L. Rhoads, (2014), Influence of four run-of-river dams on channel morphology and sediment characteristics in Illinois, USA. Geomorphology 206, 215–229

Dredging and Dredged Material Management**,** U.S. Army Corps of Engineers**,** Washington, DC. (2015). **pp. 5-20 – 5-21.**

Elhakeem, Papanicolaou, & Tsakiris. (2017). A probabilistic model for sediment entrainment: The role of bed irregularity. International Journal of Sediment Research, 32(2), 137-148.

Evens, James E., Gottgens, Johan F. (2007) Contaminant Stratigraphy of the Ballville Reservoir, Sandusky River, NW Ohio: Implications for Dam Removal. Journal of Great Lakes Research, 33, 182–193. https://doi.org/10.3394/0380-1330(2007)33[182:CSOTBR]2.0.CO

Flanagan, D. C., Gilley, J. E., & Franti, T. G. (2007). Water Erosion Prediction Project (WEPP): Development History, Model Capabilities, and Future Enhancements. Transactions of the ASABE, 50(5), 1603–1612. https://doi.org/10.13031/2013.23968

Foucher, A., Salvador-Blanes, S., Vandromme, R., Cerdan, O., & Desmet, M. (2017). Quantification of bank erosion in a drained agricultural lowland catchment. Hydrological Processes, 31(6), 1424–1437. https://doi.org/10.1002/hyp.11117

Gartina Falls & Water Supply Creek hydroelectric projects, (2011) Inside Passage Electric Cooperative, Anchorage.

Göğüş, M., Defne, Z., & Özkandemir, V. (2006). Broad-crested weirs with rectangular compound cross sections. Journal of Irrigation and Drainage Engineering, 132(3), 272-280.

IPCC—Intergovernmental Panel on Climate Change. (2012). Renewable Energy Sources and Climate Change Mitigation: Special Report of the Intergovernmental Panel on Climate Change— Chapter 5, Hydropower, Cambridge University Press, New York, NY, USA.

Kao, S. C., R.A. McManamay, K.M. Stewart, N.M. Samu, B. Hadjerioua, S.T. DeNeale, D. Yeasmin, M.F.K. Pasha, A.A. Oubeidillah, and B.T. Smith (2014), New Stream-reach Development: A Comprehensive Assessment of Hydropower Energy Potential in the United States, GPO DOE/EE1063, Washington, DC: Wind and Water Power Program, U.S. Department of Energy.

Kinnell, P. (2010). Event soil loss, runoff and the Universal Soil Loss Equation family of models: A review. Journal of Hydrology, 385(1-4), 384–397. https://doi.org/10.1016/j.jhydrol.2010.01.024

Ko, F., & Baker, J. (2004). Seasonal and annual loads of hydrophobic organic contaminants from the Susquehanna River basin to the Chesapeake Bay. Marine Pollution Bulletin, 48(9-10), 840–851. https://doi.org/10.1016/j.marpolbul.2003.10.014

Kondolf, G. Mathias, Gao, Yongxuan, Annandale, George W., Morris, Gregory L., Jiang, Enhui, Zhang, Junhua, . . . Yang, Chih Ted. (2014). Sustainable sediment management in reservoirs and regulated rivers: Experiences from five continents. Earth's Future, 2(5), 256-280.

Langendoen et al. (2001). CONCEPTS – A process-based modeling tool to evaluate stream-corridor restoration design. Wetlands Engineering & River Restoration Conference, Reston, VA, August 27-31.

Lee, Haegyun, Ching-Long Lin, and Larry J. Weber. (2008) Application of a Nonhydrostatic Model to Flow in a Free Surface Fish Passage Facility." Journal Of Hydraulic Engineering-Asce 134.7: 993-99. Web.

Ligon, F.K, W.E Dietrich, and W.J Trush. (1995). Downstream Ecological Effects of Dams: A Geomorphic Perspective." Bioscience 45.3 : 183-192. Web.

Lu, Hua, C.J Moran, and Ian P Prosser. "Modelling Sediment Delivery Ratio over the Murray Darling Basin." Environmental Modelling and Software 21.9 (2006): 1297-308. Web.

Maavara, T., Parsons, C., Ridenour, C., Stojanovic, S., Dürr, H., Powley, H., & Van Cappellen, P. (2015). Global phosphorus retention by river damming. 15603 – 15608. Retrieved from http://www.escholarship.org/uc/item/8r44v648

Manzano-Agugliaro, F., Taher, M., Zapata-Sierra, A., Juaidi, A., & Montoya, F. (2017). An overview of research and energy evolution for small hydropower in Europe. Renewable and Sustainable Energy Reviews, 75, 476–489. https://doi.org/10.1016/j.rser.2016.11.013

Montgomery, David R, and Mark T Brandon. (2002) Topographic Controls on Erosion Rates in Tectonically Active Mountain Ranges." Earth and Planetary Science Letters 201.3-4: 481–489. Web.

Morris, G., & Fan, J. (1998). Reservoir sedimentation handbook: design and management of dams, reservoirs, and watersheds for sustainable use . New York: McGraw-Hill.

Papanicolaou, A. N., and B. K. Abban. (2016) Channel Erosion and Sediment Transport" Chapter 65 in Handbook of Applied Hydrology, 2nd ed. V. P. Singh, ed., McGraw-Hill. ISBN-13:978-0071835091.

Papanicolaou, A.N., Diplas, P., Evaggelopoulos, N., & Fotopoulos, S.(2002). A stochastic incipient motion criterion for spheres under various bed packing conditions. Journal of Hydraulic Engineering, 128(4), 369–380.

Papanicolaou, A.N., and A. Maxwell. (2000). Hydraulic performance of fish bypass-pools for irrigation diversion channels. Journal of Irrigation and Drainage Engineering. 126(5):314-321.

Pearson, A., & Pizzuto, J. (2015). Bedload transport over run-of-river dams, Delaware, U.S.A. Geomorphology, 248, 382–395. https://doi.org/10.1016/j.geomorph.2015.07.025

Penche, Celso. (1998) Layman's Guidebook on How to Develop a Small Hydro Site. 2nd ed., European Small Hydropower Association.

Parsons, A., Cooper, J., Wainwright, J., & Sekiguchi, T. (2018). Virtual velocity of sand transport in water. Earth Surface Processes and Landforms, 43(3), 755–761. https://doi.org/10.1002/esp.4262

Quinton, J., & Catt, J. (2007). Enrichment of heavy metals in sediment resulting from soil erosion on agricultural fields. Environmental Science & Technology, ES & T, 41(10), 3495–3500. https://doi.org/10.1021/es062147h

Reneau, Steven L., and William E. Dietrich. (1991). Erosion Rates in the Southern Oregon Coast Range: Evidence for an Equilibrium Between Hillslope Erosion and Sediment Yield. Earth Surface Processes and Landforms 16.4: 307–322. Web.

Robinson, R., & Slingerland, R. (1998). Origin of fluvial grain-size trends in a foreland basin; the Pocono Formation on the central Appalachian Basin. Journal of Sedimentary Research, 68(3), 473–486. https://doi.org/10.2110/jsr.68.473

Rollet, Piégay, Dufour, Bornette, and Persat. (2014) Assessment of Consequences of Sediment Deficit on a Gravel River Bed Downstream of Dams in Restoration Perspectives: Application of A Multicriteria, Hierarchical and Spatially Explicit Diagnosis. River Research and Applications 30.8 : 939-53. Web.

Schenk, C., Hupp, C., Richter J., and Kroes D. (2010). Bank erosion, mass wasting, water clarity, bathymetry, and a sediment budget along the dam-regulated lower Roanoke River, Norht Carolina. Reston, Va: U.S. Dept. of the Interior, U.S. Geological Survey.

Sheehan, C., Harrington, J., & Murphy, J. (2010). A technical assessment of topsoil production from dredged material. Resources, Conservation & Recycling, 54(12), 1377–1385. https://doi.org/10.1016/j.resconrec.2010.05.012

Sigua, C. G., & Revues Inra, I. (2009). Recycling biosolids and lake-dredged materials to pasture-based animal agriculture: alternative nutrient sources for forage productivity and sustainability. A review. Agronomy for Sustainable Development, 29(1), 143–160. https://doi.org/10.1051/agro:2008037

Skalak, Katherine, James Pizzuto, and David D. Hart. (2009). Influence of Small Dams on Downstream Channel Characteristics in Pennsylvania and Maryland: Implications for the Long-Term Geomorphic Effects of Dam Removal 1. JAWRA Journal of the American Water Resources Association 45.1: 97-109. Web.

Smith, B.T., A. Witt, K.M. Stewart, K. Lee, S. DeNeale, M. Bevelhimer et al., (2017). A multi-year plan for research, development, and prototype testing of standard modular hydropower technology. R1, ORNL/TM-2016/102. Oak Ridge National Laboratory. Oak Ridge, TN

Sturm, Terry W. Open Channel Hydraulics. Boston: McGraw-Hill, (2001). Print

Sumi, T., M. Okano, and Y. Takata (2004), Reservoir sedimentation management with bypass tunnels in Japan, in Proceedings of 9th International Symposium on River Sedimentation, ii, pp. 1036–1043, Yichang, China

Tan, G., Fang, H., Dey, S., & Wu, W. (2018). Rui-Jin Zhang's Research on Sediment Transport. Journal of Hydraulic Engineering, 144(6), 02518002.

Tennant, D.L. 1976. Instream flow regimens for fish, wildlife, recreation and related environmental resources. Fisheries 1: 6-10.

Thomas, W. A., Copeland, R.R. McComas, D. N (2002). SAM Hydraulic Design Package for Channels. US Army Corps of Engineers. Coastal and Hydraulics Laboratory.

USDA Agricultural Research Service Handbook 703. (1997) Predicting Soil Erosion by Water: A guide to Conservation Planning With the Revised Universal Soil Loss Equation (RUSLE)

Wallick, R. J., O'Connor, J. E., Anderson, S., Keith, M., Cannon, C., Risley, J. C. (2011) Channel Change and Bed-Material Transport in the Umpqua River Basin, Oregon. Scientific Investigation Report 2011-5041, U.S. Geological Survey, Reston, Virginia.

Wilcock, Peter R., & Crowe, Joanna C. (2003). Surface-based transport model for mixed-size sediment. Journal of Hydraulic Engineering, 129(2), 120-128.

Wilson, C., Papanicolaou, A., & Denn, K. (2012). Partitioning fine sediment loads in a headwater system with intensive agriculture. Journal of Soils and Sediments, 12(6), 966–981. https://doi.org/10.1007/s11368-012-0504-2

Witt A., B. Smith, M. Bevelhimer, A. Fernandez and N. Bishop, Jr. (2017). Making small hydro development affordable and acceptable. Hydro Review. 36(7)

Witt, A., B.T. Smith, A. Tsakiris, T. Papanicolaou, K. Lee, K. M. Stewart, et al. (2017). Exemplary design envelope specification for standard modular hydropower technology. R1, ORNL/TM-2016/298. Oak Ridge National Laboratory. Oak Ridge, TN

Ventana Systems inc. (2019) Vensim PLE. Retrieved from https://vensim.com/docs/

Zhongbao, X., Bofu, Y., & Yuguo, H. (2015). Spatiotemporal Variations in Annual Sediment Yield from the Middle Yellow River, China, 1950-2010. Journal of Hydrologic Engineering, 20(8).

# Appendices

**Appendix A: Results varying second and third sediment management parameters: probability of sediment influx into the impoundment and operations sluice gate height**

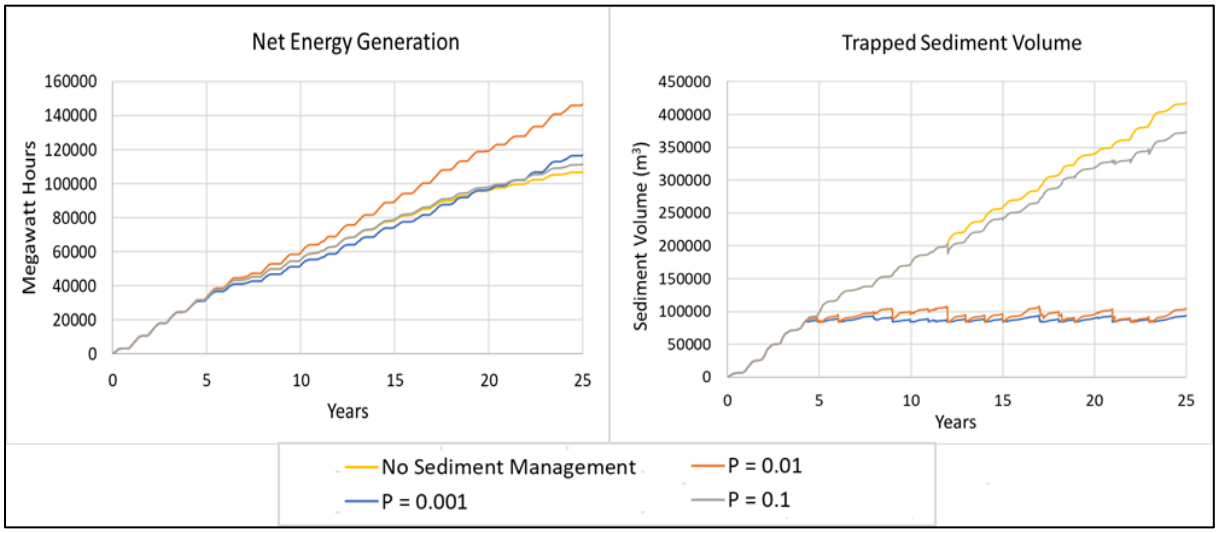



**Figure A.1.** Impact of changes to the secondary management parameter, the probabilistic threshold of sediment influx into the impoundment.

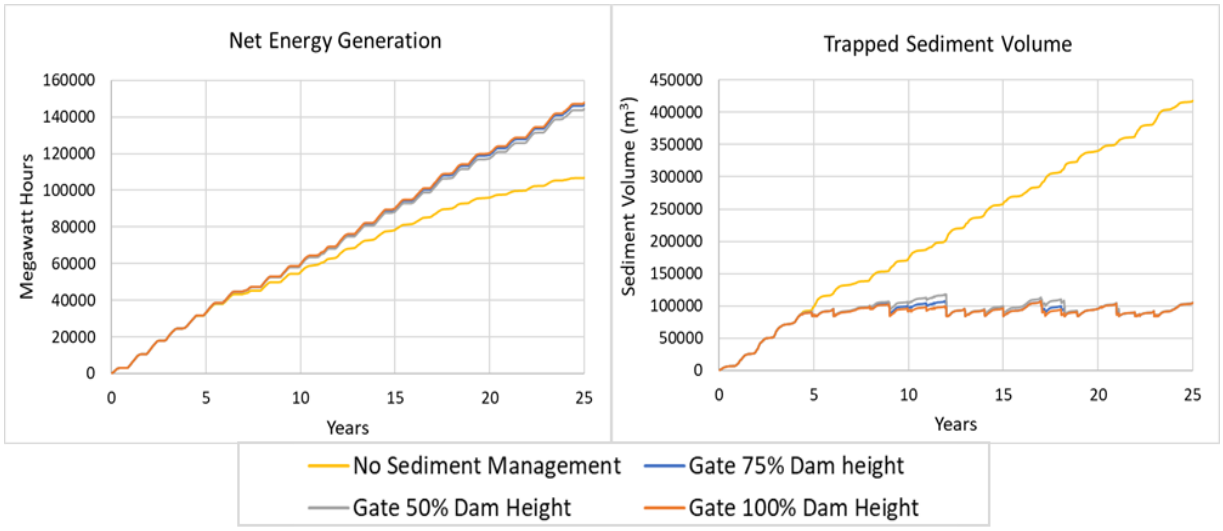



**Figure A.2.** Impact of changes to the third management parameter, the operational gate height of the sediment module.

**Appendix B. Hydraulic properties of head and flow rate for discrete events through the sediment passage and spillway modules**

**Table B.1**. Hydraulic properties for gate opening of 6 x 1 $m^2$ over a range of events

| Gate width: 6 m<br>Gate opening height: 1 m | | | gate opening area 6 $m^2$ | | | |
|---|---|---|---|---|---|---|
| Q orifice + Q spill ($m^3/s$) | Head (m) | Q orifice ($m^3/s$) | Q spill (m3/s) | y from bed (m) | y from spill way (m) | Q/b |
| 46.7 | 3.0 | 29.9 | 16.8 | 3.5 | 0.2 | 7.8 |
| 211.4 | 4.0 | 34.5 | 176.9 | 4.5 | 1.2 | 35.2 |
| 479.1 | 5.0 | 38.6 | 440.5 | 5.5 | 2.2 | 79.8 |
| 849.9 | 6.0 | 42.3 | 807.6 | 6.5 | 3.2 | 141.6 |
| 1218.4 | 7.0 | 45.7 | 1172.7 | 7.5 | 4.2 | 203.1 |
| 1665.3 | 8.0 | 48.9 | 1616.4 | 8.5 | 5.2 | 277.5 |
| 2162.6 | 9.0 | 51.8 | 2110.7 | 9.5 | 6.2 | 360.4 |

**Table B.2.** Hydraulic properties for gate opening of 6 x 3 $m^2$ over a range of events

| Gate width: 6 m<br>Gate opening height: 3 m | | | gate area: 18 $m^2$ | | | |
|---|---|---|---|---|---|---|
| Q orifice + Q spill ($m^3/s$) | Head (m) | Q orifice ($m^3/s$) | Q spill (m3/s) | y from bed (m) | y from spill way (m) | Q/b |
| 90.1 | 2.0 | 73.3 | 16.8 | 3.5 | 0.2 | 15.0 |
| 266.6 | 3.0 | 89.8 | 176.9 | 4.5 | 1.2 | 44.4 |
| 392.7 | 3.5 | 97.0 | 295.7 | 5.0 | 1.7 | 65.4 |
| 721.0 | 4.5 | 109.9 | 611.1 | 6.0 | 2.7 | 120.2 |
| 1091.3 | 5.5 | 121.5 | 969.8 | 7.0 | 3.7 | 181.9 |
| 1520.3 | 6.5 | 132.1 | 1388.2 | 8.0 | 4.7 | 253.4 |
| 1999.2 | 7.5 | 141.9 | 1857.2 | 9.0 | 5.7 | 333.2 |
| 2523.4 | 8.0 | 146.6 | 2376.9 | 10.0 | 6.7 | 420.6 |

**Table B.3.** Hydraulic properties for gate opening of 6 x 7 $m^2$ over a range of events

| Gate width: 6 m<br>Gate opening height: 7 m | | | gate area: 42 $m^2$ | | | |
|---|---|---|---|---|---|---|
| Q orifice + Q spill ($m^3/s$) | Head (m) | Q orifice ($m^3/s$) | Q spill (m3/s) | y from bed (m) | y from spill way (m) | Q/b |
| 96.7 | -0.3 | 96.7 | 0.0 | 3.2 | -0.1 | 16.1 |
| 350.8 | 1.0 | 118.8 | 232.0 | 4.5 | 1.1 | 58.5 |
| 654.7 | 1.7 | 148.7 | 506.0 | 5.2 | 1.9 | 109.1 |
| 1015.9 | 2.4 | 179.2 | 836.7 | 5.9 | 2.6 | 169.3 |
| 1414.5 | 4.0 | 241.8 | 1172.7 | 7.5 | 4.2 | 235.8 |
| 1644.7 | 4.5 | 256.5 | 1388.2 | 8.0 | 4.7 | 274.1 |
| 2161.7 | 5.5 | 284.6 | 1877.1 | 9.0 | 5.7 | 360.3 |

**Table B.4.** Hydraulic properties for gate opening of 18 x 1 $m^2$ over a range of events

| Gate width: 18 m<br>Gate opening height: 1 m | | | gate area: 18 $m^2$ | | | |
|---|---|---|---|---|---|---|
| Q orifice + Q spill ($m^3/s$) | Head (m) | Q orifice ($m^3/s$) | Q spill (m3/s) | y from bed (m) | y from spill way (m) | Q/b |
| 104.3 | 3.0 | 89.8 | 14.6 | 3.5 | 0.2 | 5.8 |
| 205.4 | 3.7 | 100.1 | 105.3 | 4.2 | 0.9 | 11.4 |
| 356.2 | 4.5 | 109.9 | 246.3 | 5.0 | 1.7 | 19.8 |
| 623.4 | 5.5 | 121.5 | 501.9 | 6.0 | 2.7 | 34.6 |
| 938.6 | 6.5 | 132.1 | 806.5 | 7.0 | 3.7 | 52.1 |
| 1296.5 | 7.5 | 141.9 | 1154.6 | 8.0 | 4.7 | 72.0 |
| 1693.3 | 8.5 | 151.1 | 1542.2 | 9.0 | 5.7 | 94.1 |

**Table B.5.** Hydraulic properties for gate opening of 18 x 3 $m^2$ over a range of events

| Gate width: | 18 | m | gate area: | | | 54 $m^2$ |
|---|---|---|---|---|---|---|
| Gate opening height: | 3 | m | | | | |
| Q orifice + Q spill ($m^3/s$) | Head (m) | Q orifice ($m^3/s$) | Q spill (m3/s) | y from bed (m) | y from spill way (m) | Q/b |
| 55.8 | -0.4 | 55.8 | 0.0 | 1.1 | -2.2 | 3.1 |
| 234.4 | 2.0 | 219.9 | 14.6 | 3.5 | 0.2 | 13.0 |
| 537.2 | 3.5 | 290.9 | 246.3 | 5.0 | 1.7 | 29.8 |
| 831.7 | 4.5 | 329.8 | 501.9 | 6.0 | 2.7 | 46.2 |
| 1171.1 | 5.5 | 364.6 | 806.5 | 7.0 | 3.7 | 65.1 |
| 1551.0 | 6.5 | 396.4 | 1154.6 | 8.0 | 4.7 | 86.2 |
| 1968.0 | 7.5 | 425.8 | 1542.2 | 9.0 | 5.7 | 109.3 |
| 2409.2 | 8.0 | 439.7 | 1969.4 | 10.0 | 6.7 | 133.8 |

**Table B.6.** Hydraulic properties for gate opening of 18 x 7 $m^2$ over a range of events

| Gate width: | 18 | m | gate area: | | | 126 $m^2$ |
|---|---|---|---|---|---|---|
| Gate opening height: | 7 | m | | | | |
| Q orifice + Q spill ($m^3/s$) | Head (m) | Q orifice ($m^3/s$) | Q spill (m3/s) | y from bed (m) | y from spill way (m) | Q/b |
| 55.8 | -2.4 | 55.8 | 0.0 | 1.1 | -2.2 | 3.1 |
| 290.0 | -0.3 | 290.0 | 0.0 | 3.2 | -0.1 | 16.1 |
| 500.3 | 0.8 | 373.0 | 127.2 | 4.3 | 1.0 | 27.8 |
| 835.0 | 1.5 | 507.7 | 327.4 | 5.0 | 1.7 | 46.4 |
| 1022.6 | 1.9 | 573.2 | 449.4 | 5.4 | 2.1 | 56.8 |
| 1701.1 | 4.0 | 725.5 | 975.6 | 7.5 | 4.2 | 94.5 |
| 1924.1 | 4.5 | 769.6 | 1154.6 | 8.0 | 4.7 | 106.9 |
| 2353.4 | 5.0 | 811.2 | 1542.2 | 9.0 | 5.7 | 130.7 |

**Table B.7.** Hydraulic properties for gate opening of 30 x 1 $m^2$ over a range of events

| Gate width: 30 m<br>Gate opening height: 1 m | | | gate area: 30 $m^2$ | | | |
|---|---|---|---|---|---|---|
| Q orifice + Q spill ($m^3/s$) | Head (m) | Q orifice ($m^3/s$) | Q spill (m3/s) | y from bed (m) | y from spill way (m) | Q/b |
| 55.8 | 0.6 | 55.8 | 0.0 | 1.1 | -2.2 | 1.9 |
| 173.3 | 3.0 | 161.1 | 12.2 | 3.5 | 0.2 | 5.8 |
| 402.4 | 4.5 | 198.2 | 204.3 | 5.0 | 1.7 | 13.4 |
| 891.2 | 6.5 | 237.2 | 654.0 | 7.0 | 3.7 | 29.7 |
| 1175.7 | 7.5 | 254.7 | 921.0 | 8.0 | 4.7 | 39.2 |
| 1534.6 | 8.6 | 272.8 | 1261.8 | 9.1 | 5.8 | 51.2 |
| 1879.5 | 9.5 | 286.7 | 1592.8 | 10.1 | 6.8 | 62.6 |
| 2255.8 | 10.0 | 294.1 | 1961.7 | 11.1 | 7.8 | 75.2 |

**Table B.8**. Hydraulic properties for gate opening of 30 x 3 $m^2$ over a range of events

| Gate width: 30 m<br>Gate opening height: 3 m | | | gate area: 90 $m^2$ | | | |
|---|---|---|---|---|---|---|
| Q orifice + Q spill ($m^3/s$) | Head (m) | Q orifice ($m^3/s$) | Q spill (m3/s) | y from bed (m) | y from spill way (m) | Q/b |
| 55.8 | -0.4 | 55.8 | 0 | 1.08 | -2.2 | 2 |
| 290.0 | 1.7 | 290.0 | 0.0 | 3.2 | -0.1 | 9.7 |
| 500.3 | 2.5 | 441.2 | 59.1 | 4.0 | 0.7 | 16.7 |
| 719.8 | 3.5 | 522.1 | 197.7 | 5.0 | 1.7 | 24.0 |
| 988.0 | 4.5 | 592.0 | 396.0 | 6.0 | 2.7 | 32.9 |
| 1296.2 | 5.5 | 654.4 | 641.8 | 7.0 | 3.7 | 43.2 |
| 1632.4 | 6.5 | 711.5 | 921.0 | 8.0 | 4.7 | 54.4 |
| 1993.6 | 7.5 | 764.2 | 1229.3 | 9.0 | 5.7 | 66.5 |
| 2356.2 | 8.0 | 789.3 | 1566.9 | 10.0 | 6.7 | 78.5 |

**Table B.9.** Hydraulic properties for gate opening of 30 x 7 $m^2$ over a range of events

| Gate width: 30 m<br>Gate opening height: 7 m | | | gate area: 210 $m^2$ | | | |
|---|---|---|---|---|---|---|
| Q orifice + Q spill ($m^3/s$) | Head (m) | Q orifice ($m^3/s$) | Q spill (m3/s) | y from bed (m) | y from spill way (m) | Q/b |
| 55.8 | -2.4 | 55.8 | 0.0 | 1.1 | -2.2 | 1.9 |
| 290.0 | -0.3 | 290.0 | 0.0 | 3.2 | -0.1 | 9.7 |
| 500.3 | 0.8 | 373.0 | 0.0 | 4.3 | 1.0 | 16.7 |
| 835.0 | 1.5 | 507.7 | 327.4 | 5.0 | 1.7 | 27.8 |
| 1022.6 | 1.9 | 573.2 | 449.4 | 5.4 | 2.1 | 34.1 |
| 1222.5 | 2.3 | 639.2 | 583.3 | 5.8 | 2.4 | 40.8 |
| 1860.0 | 4.6 | 1297.0 | 563.0 | 8.1 | 4.8 | 62.0 |
| 2102.9 | 5.0 | 1352.0 | 750.9 | 9.1 | 5.8 | 70.1 |

### Appendix C: The system dynamic model framework

Yellow variables indicate the need for user input.

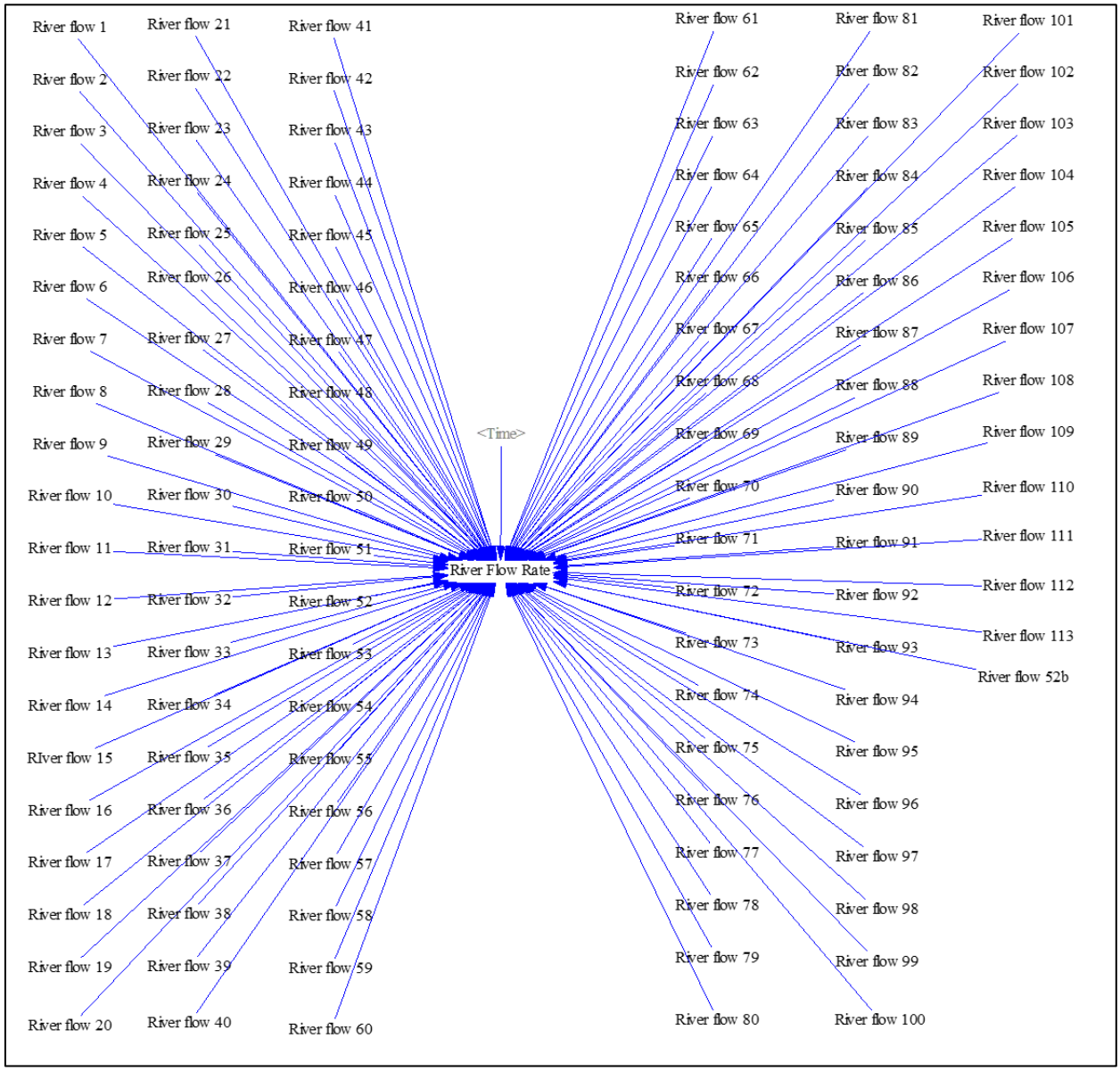



**Figure C.1.** Hourly hydrograph input

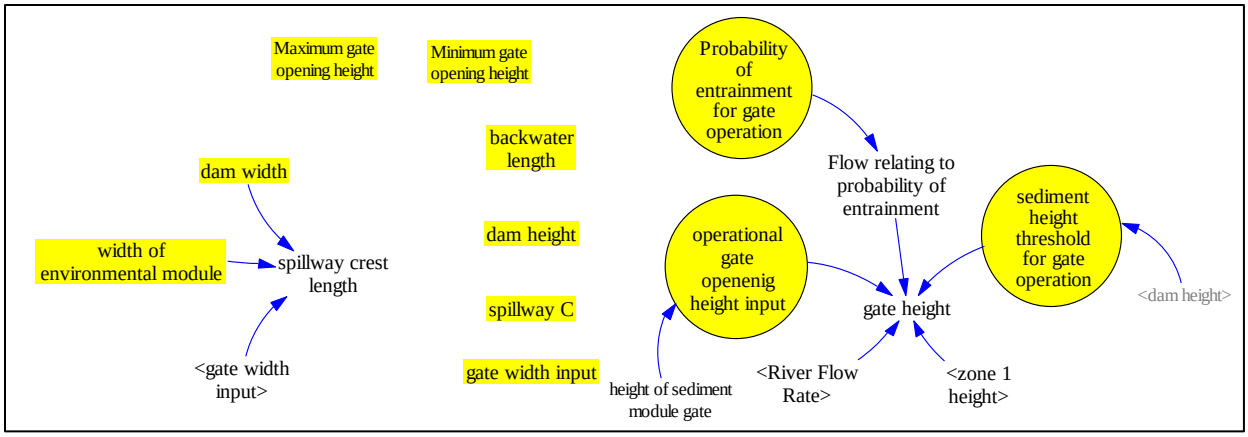



**Figure C.2.** Structural dimensions and sediment management parameters.

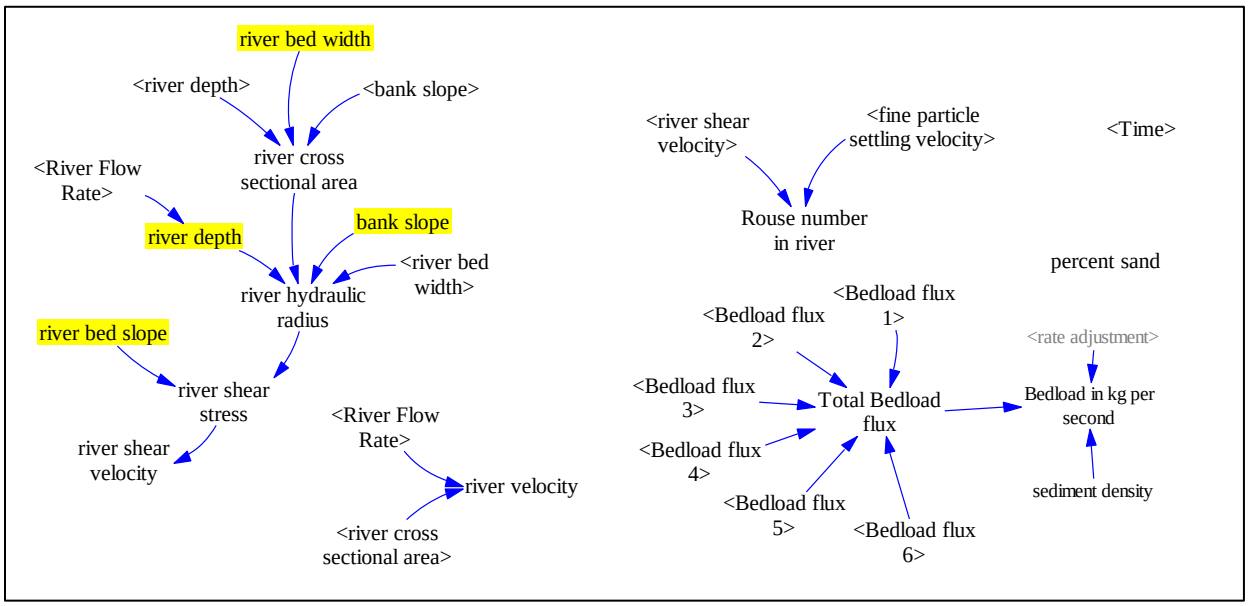



**Figure C.3.** Subsystem calculating river conditions upstream of backwater effects.

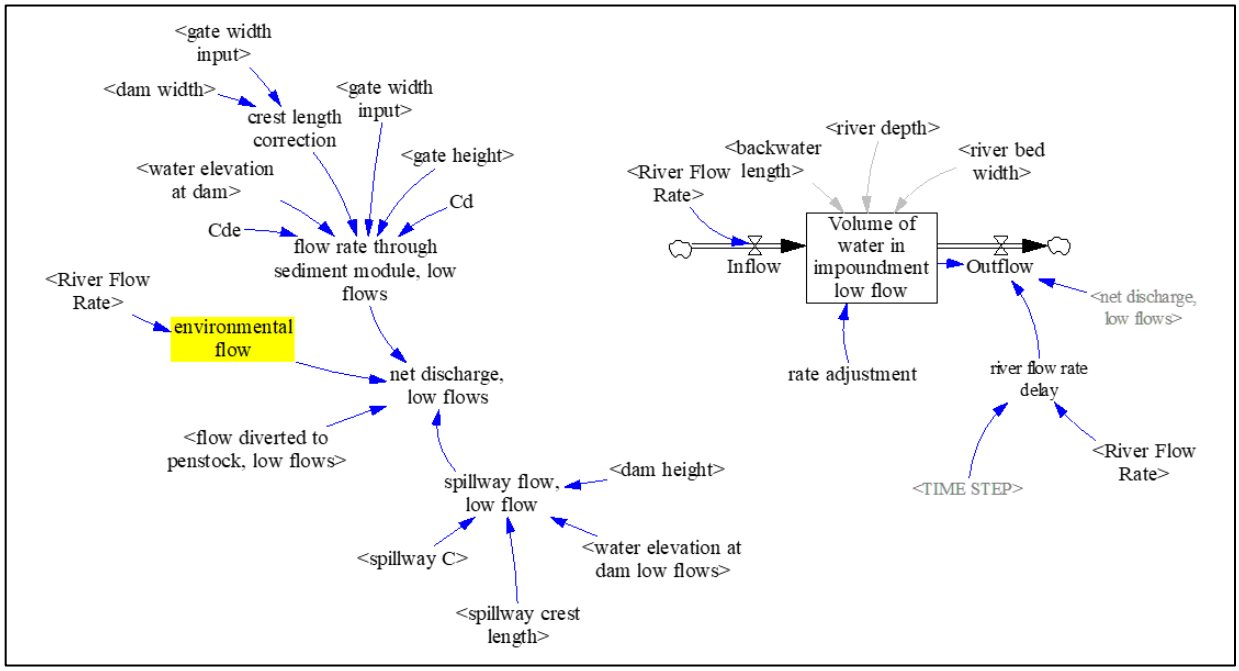



**Figure C.4.** Subsystem calculating water flow, storage, and depth in the impoundment when water depth < dam height.

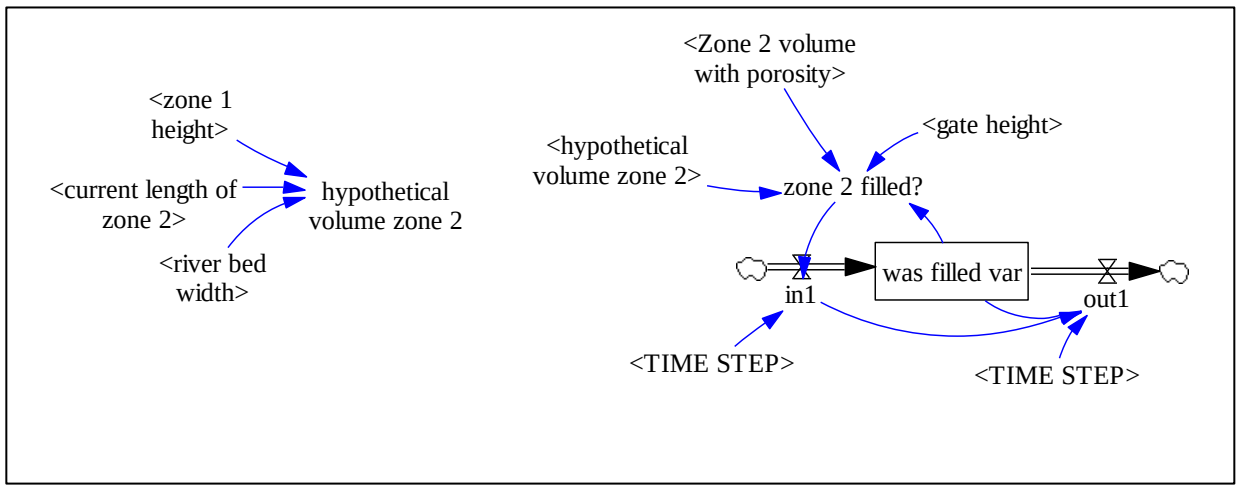



**Figure C.5.** Subsystem keeping track of the status of sediment in zone 1 as compared to the potential sediment that would be present if ramp were fully developed to dam face.

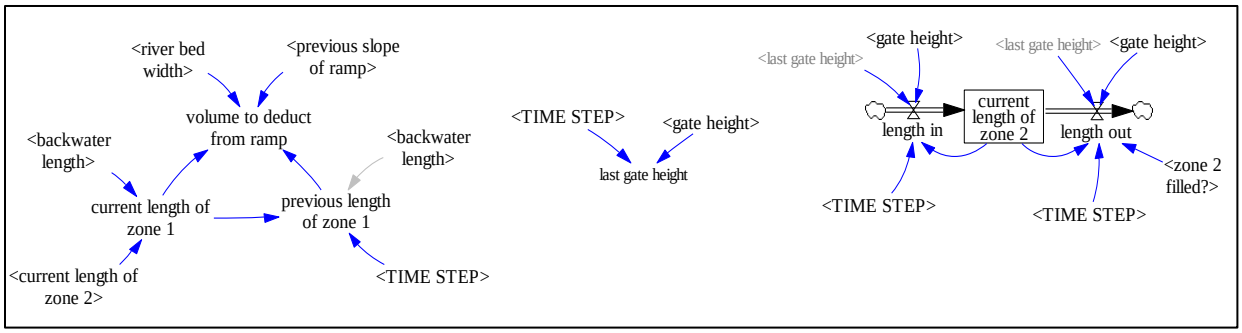



**Figure C.6.** Subsystem keeping track of the length of zone 1 and 2 depending on the most recent gate opening height.

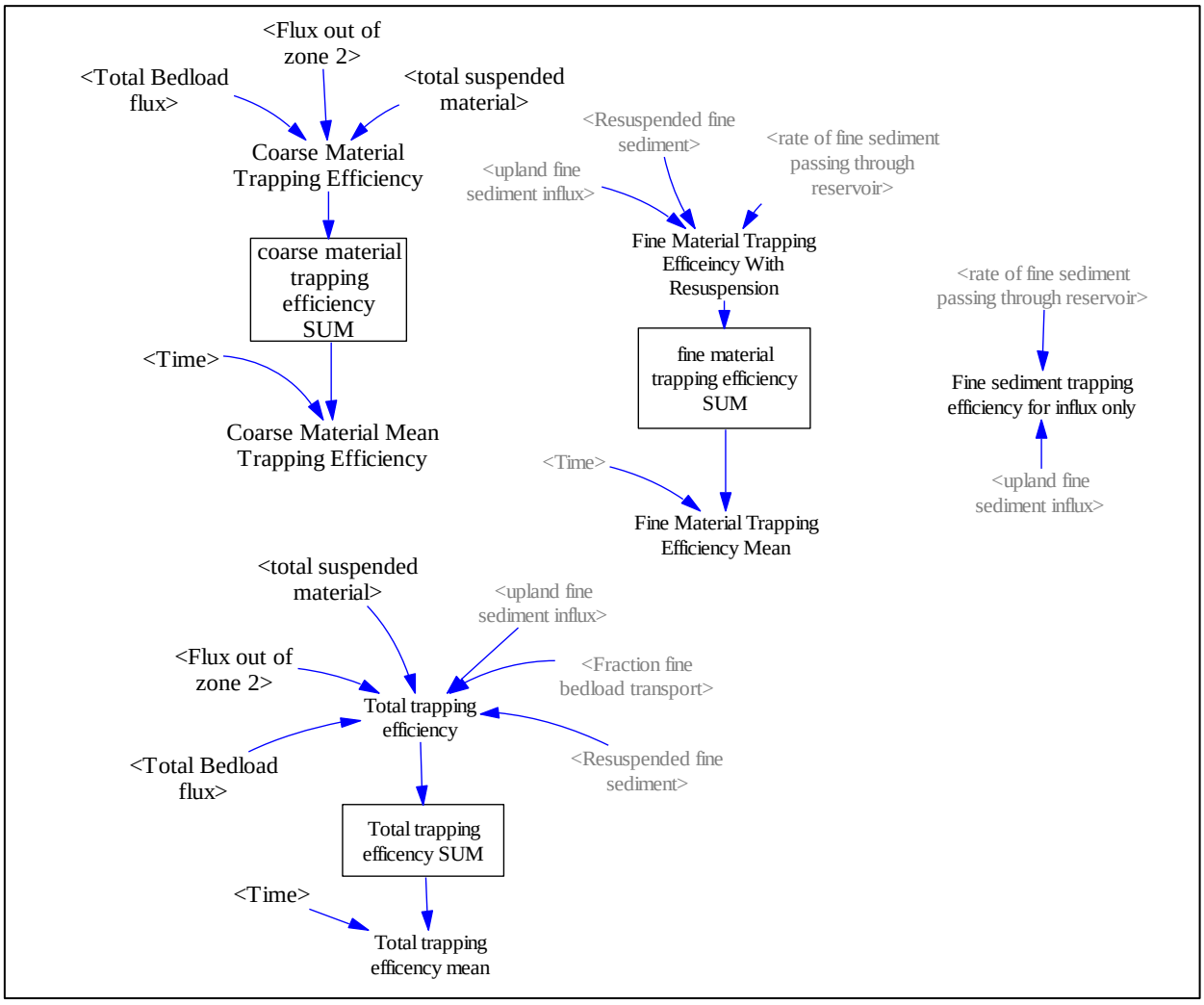



**Figure C.7.** Subsystem keeping track of sediment trapping efficiency of the dam.

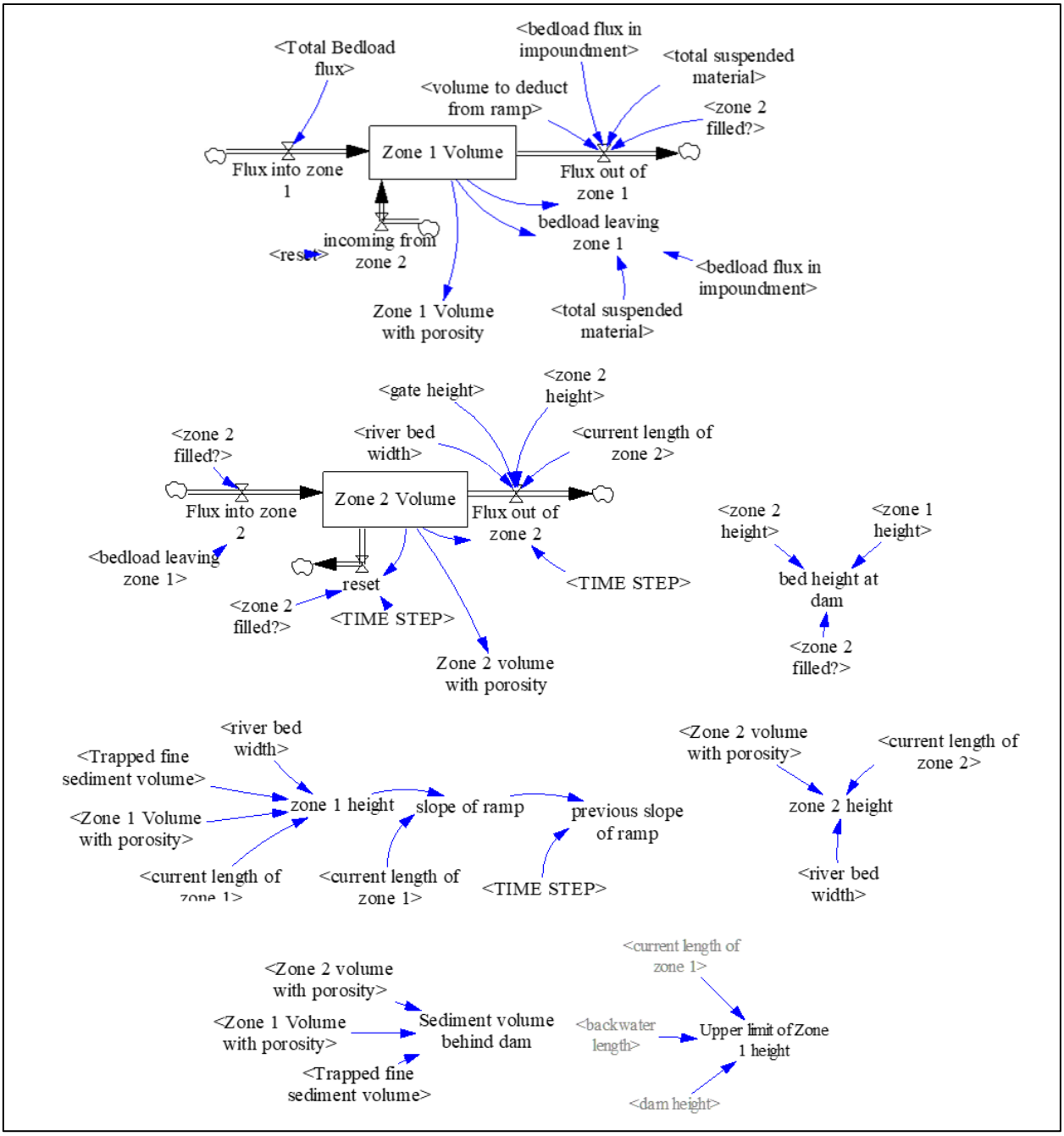



**Figure C.8.** Subsystem keeping track of the movement of sediment through the impoundment.

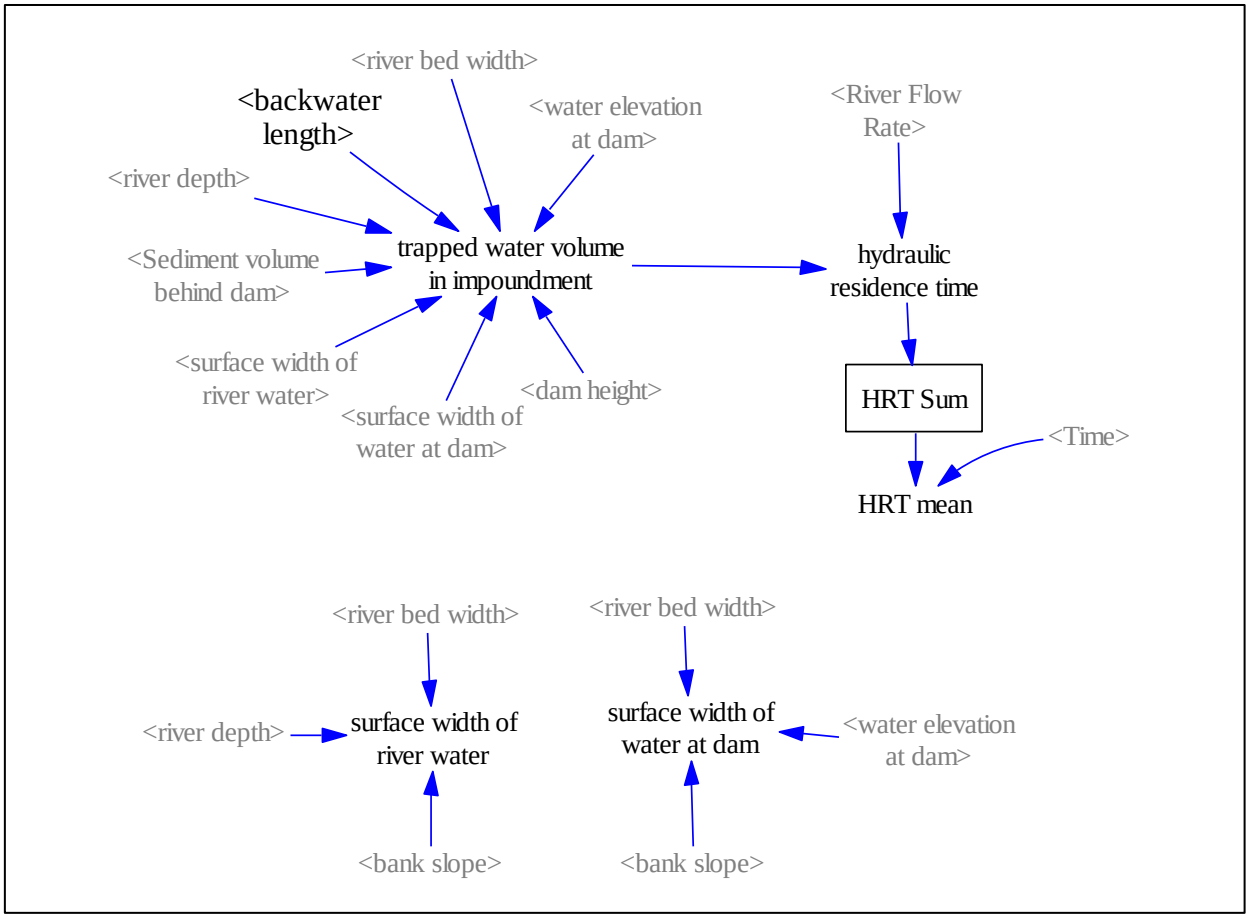



**Figure C.9.** System keeping track of the Hydraulic Residence Time (HRT) of the impoundment.

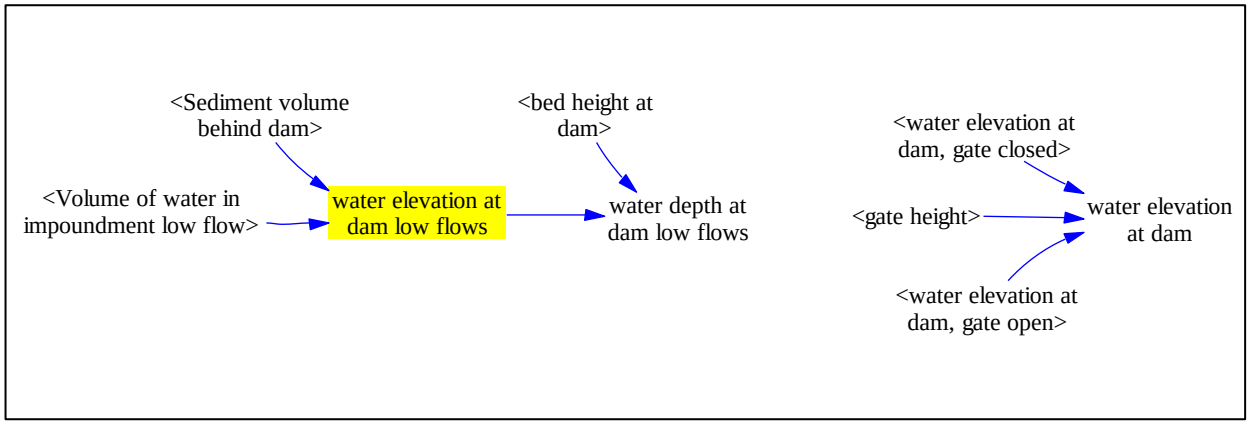



**Figure C.10.** Subsystem calculating water elevation at the dam.

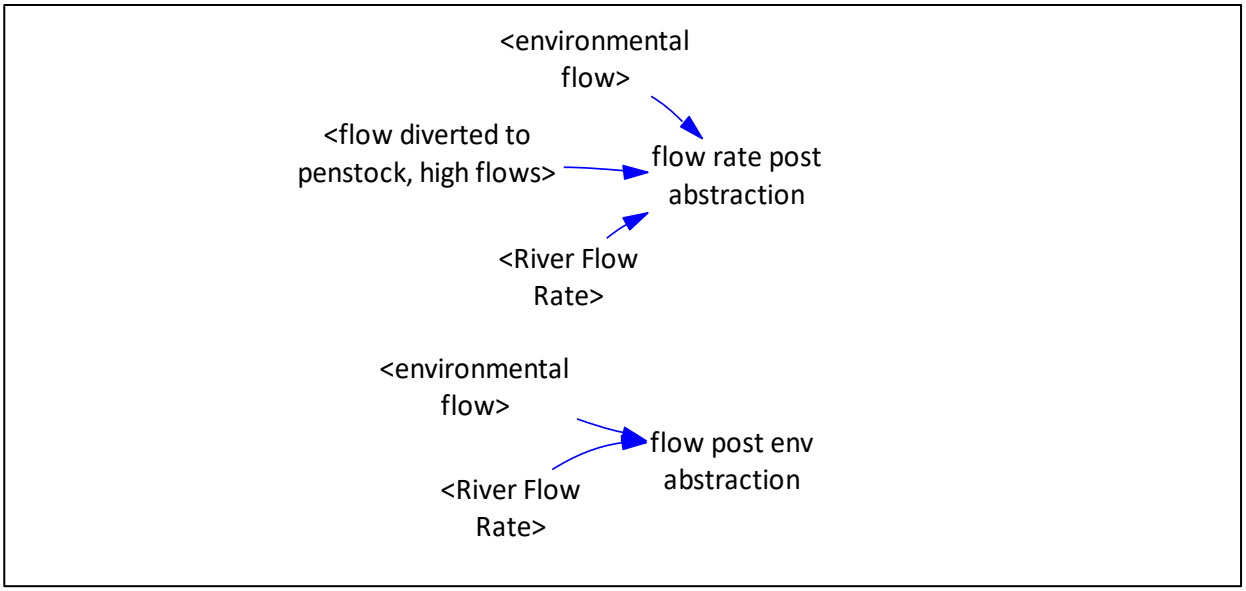



**Figure C.11.** System calculating track of water available to each module.

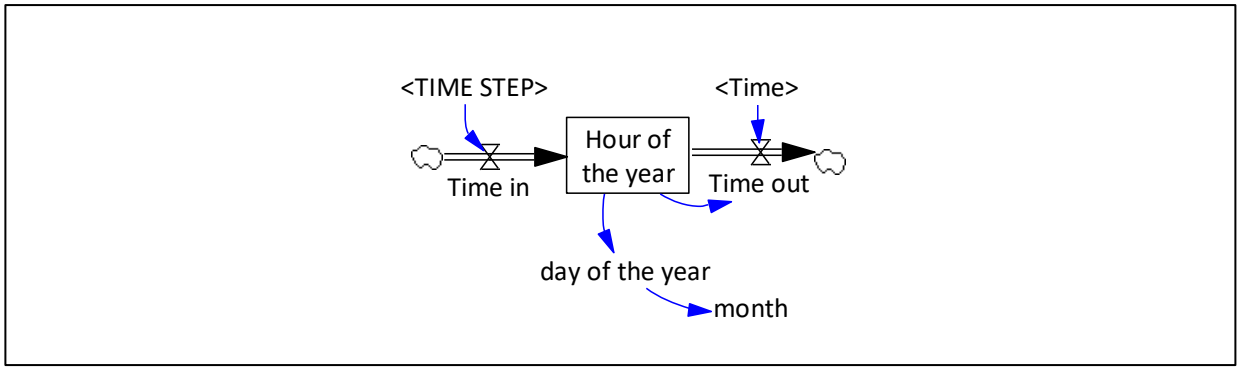



**Figure C.12.** Subsystem keeping track of how each time step relates to modeled time.

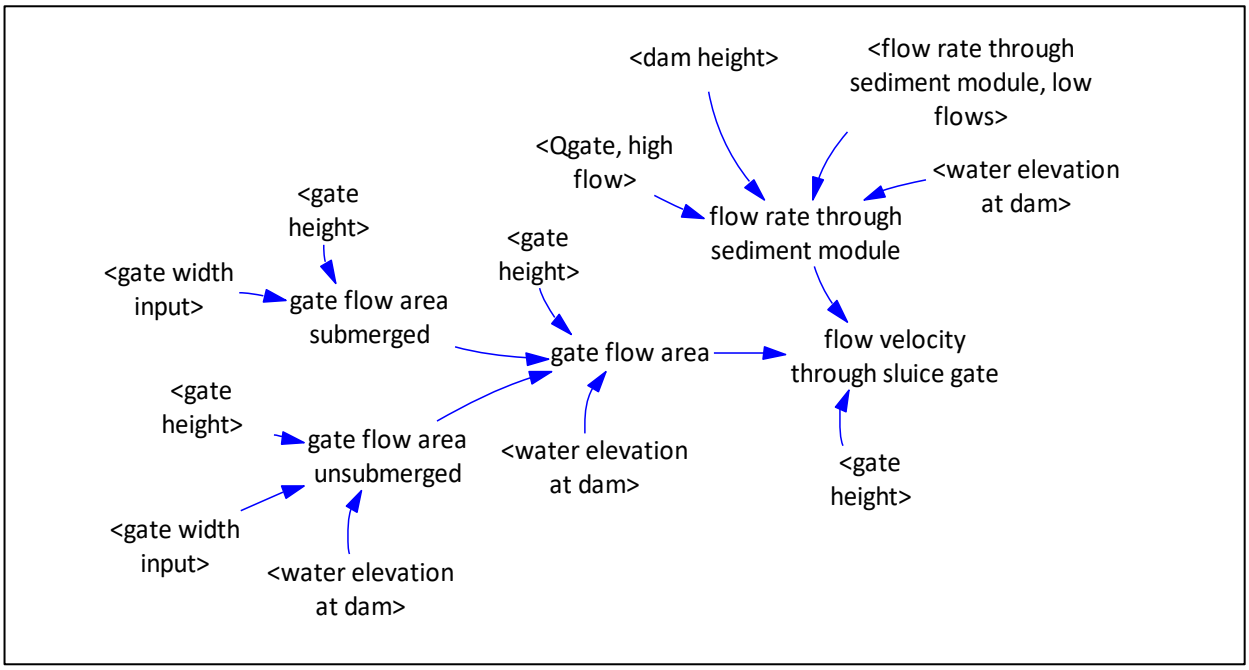



**Figure C.13.** Subsystem calculating the hydraulics of the sluice gate.

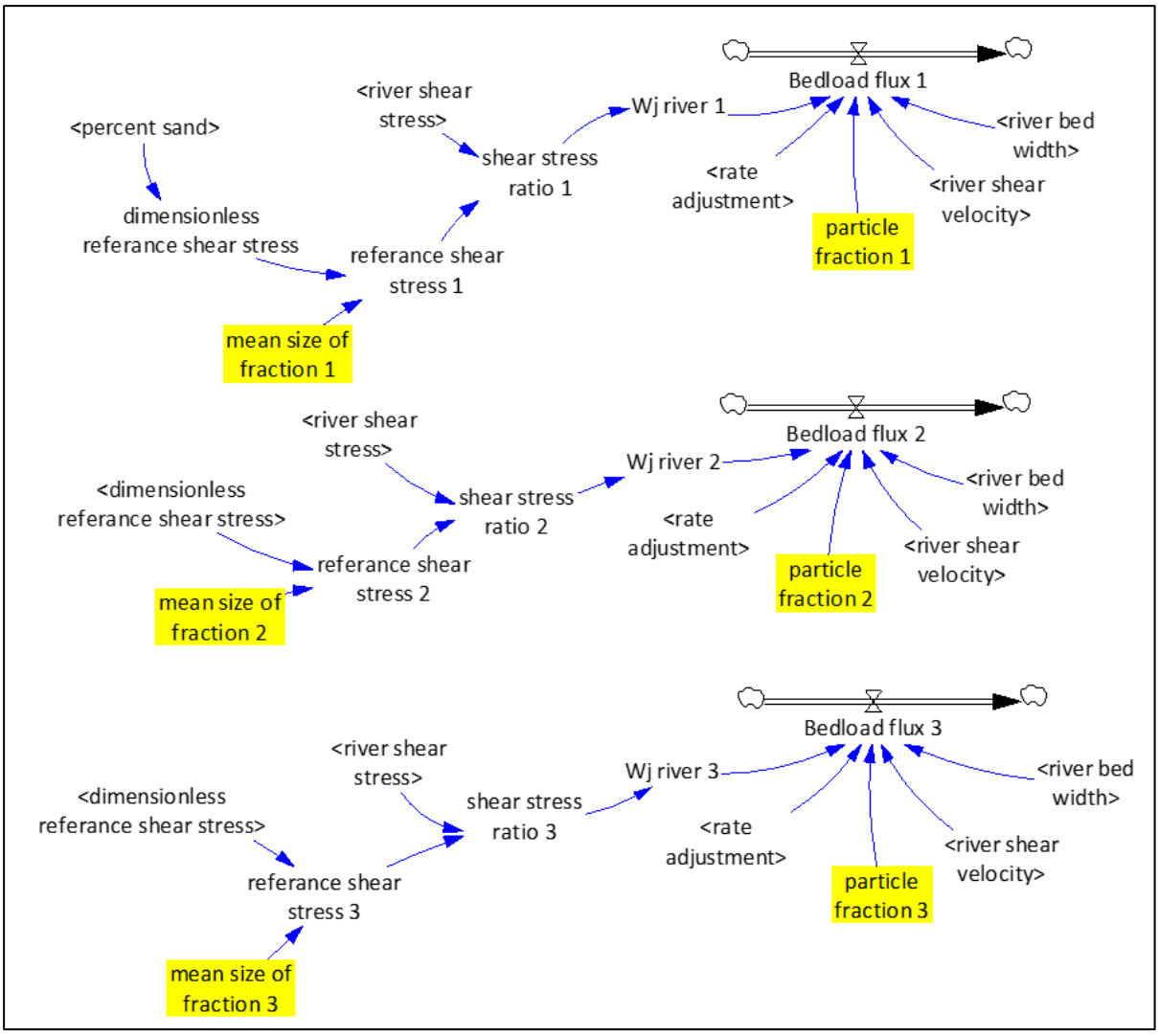



**Figure C.14.a.** Subsystem calculating bedload influx to the impoundment.

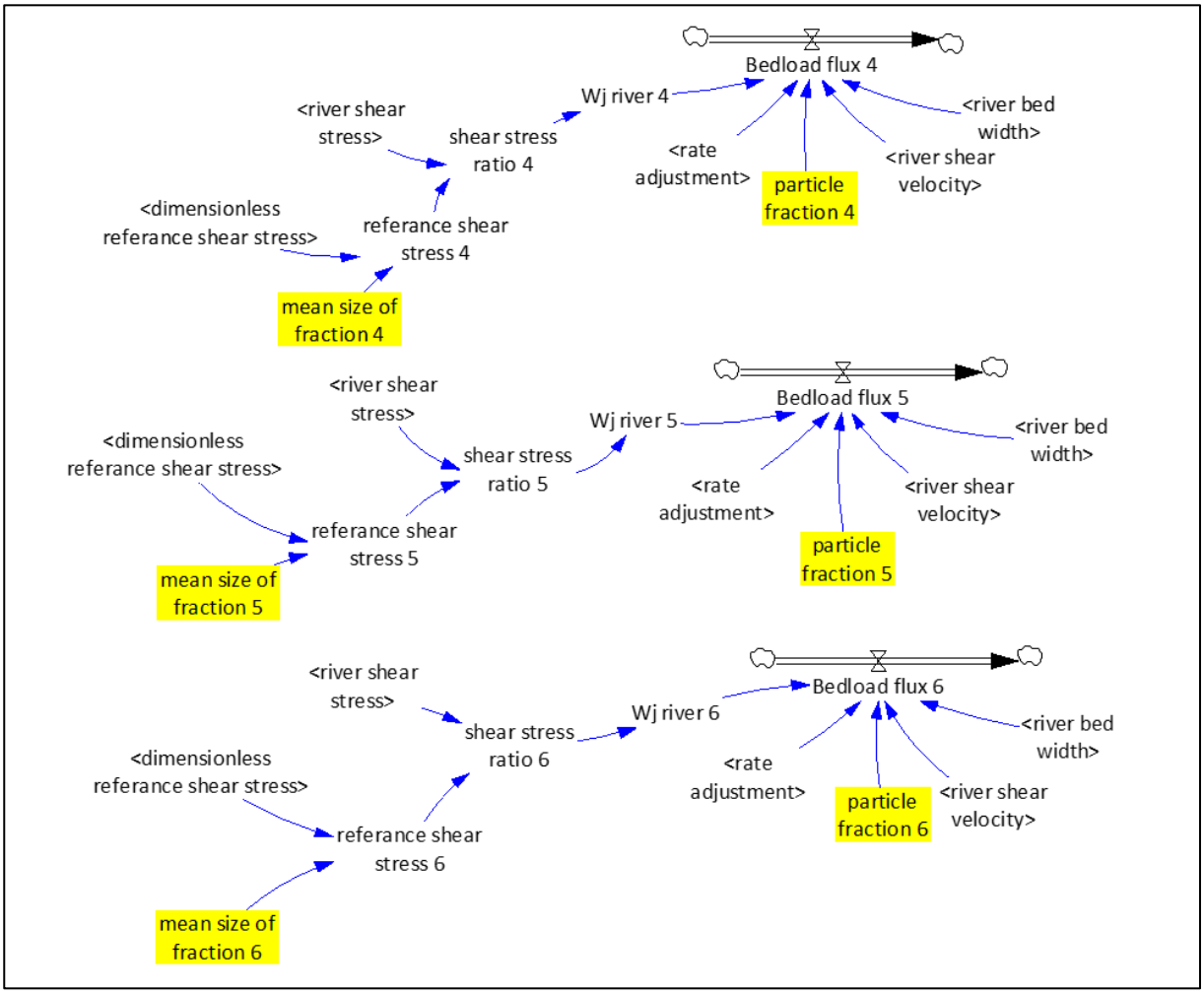



**Figure C.14.b.** Subsystem calculating bedload influx to the impoundment.

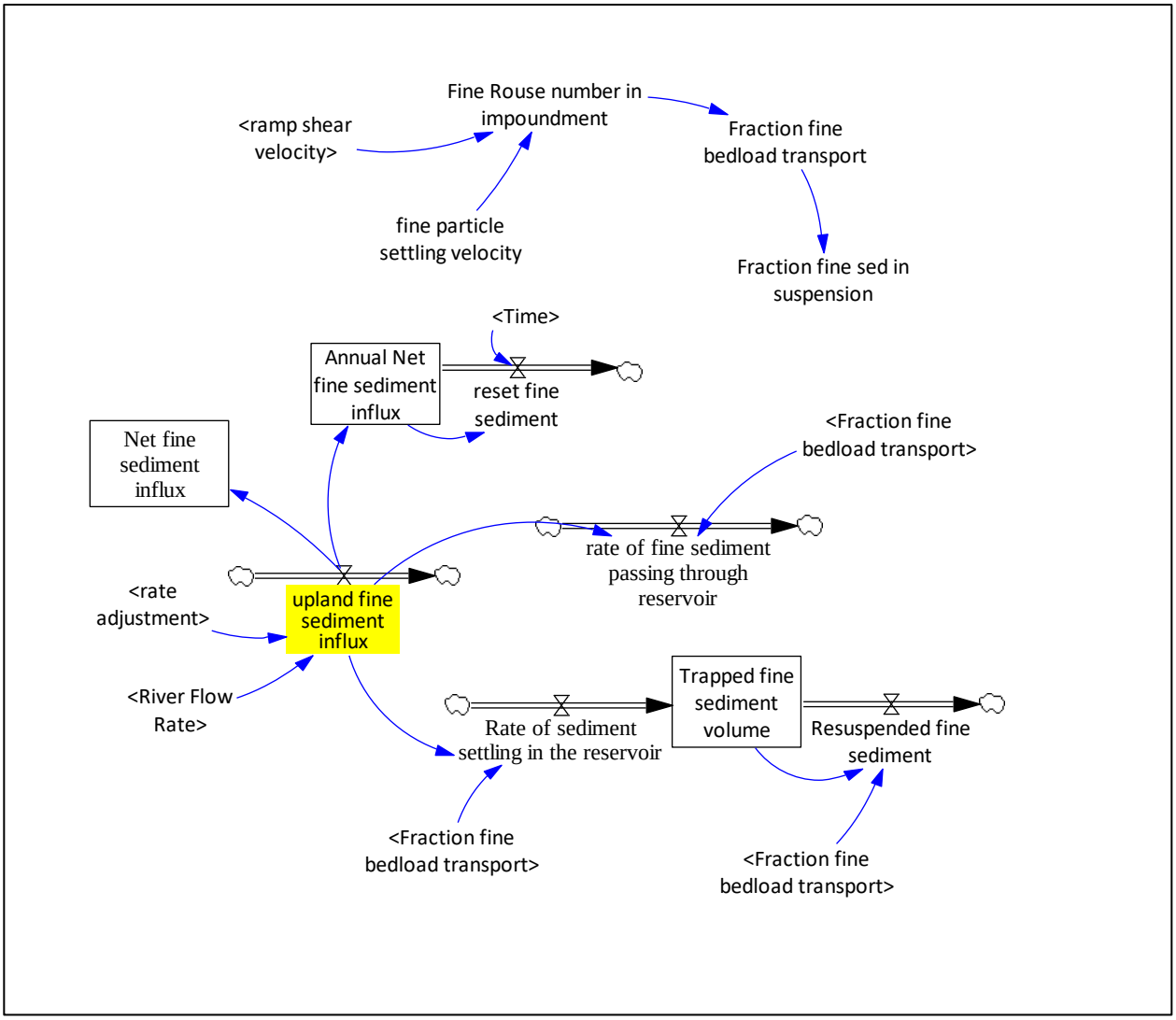



**Figure C.15.** Subsystem calculating suspended sediment flux into the impoundment.

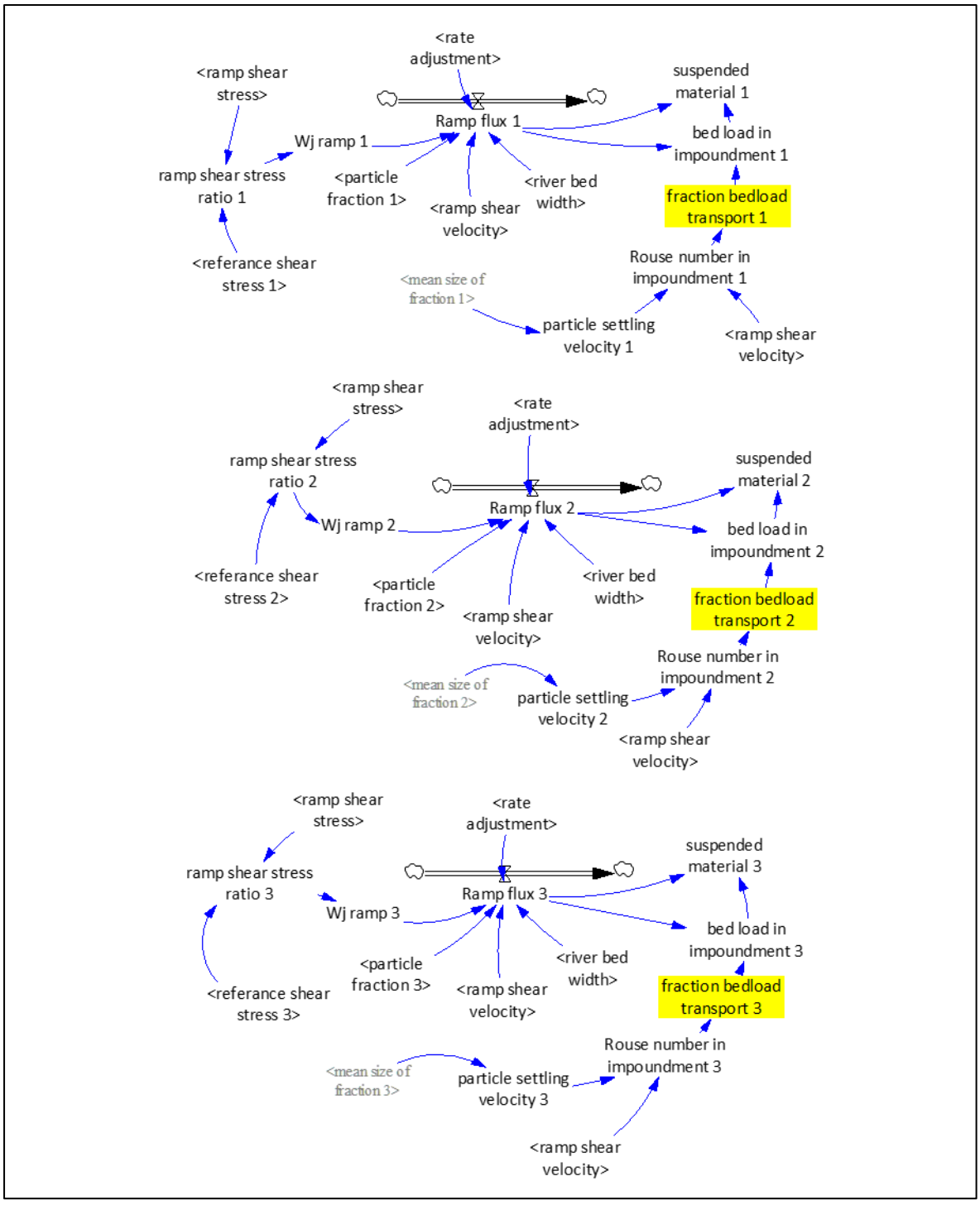



**Figure C.16.a.** Subsystem calculating resuspension of coarse sediment in impoundment.

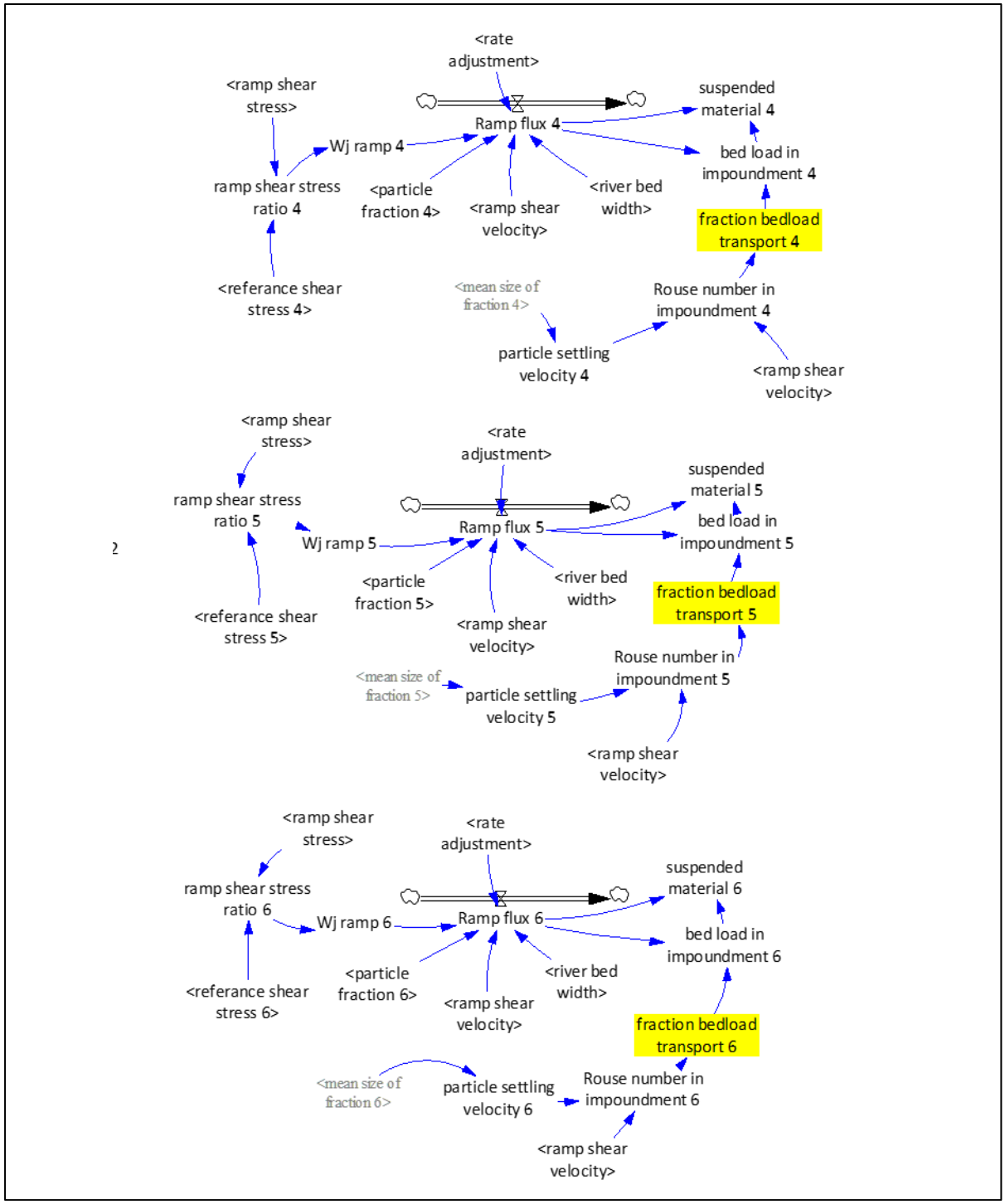



**Figure C.16.b.** Subsystem calculating resuspension of coarse sediment in impoundment.

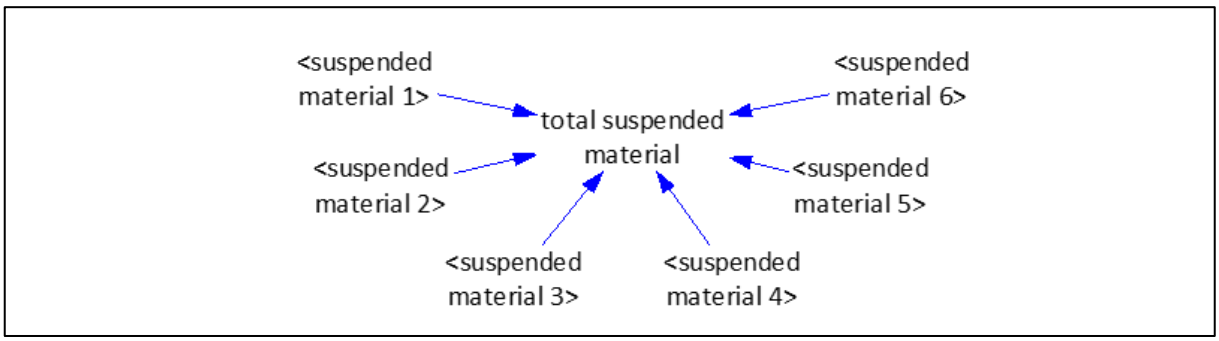



**Figure C.17.** Subsystem calculating net resuspended coarse sediment in impoundment for outflux.

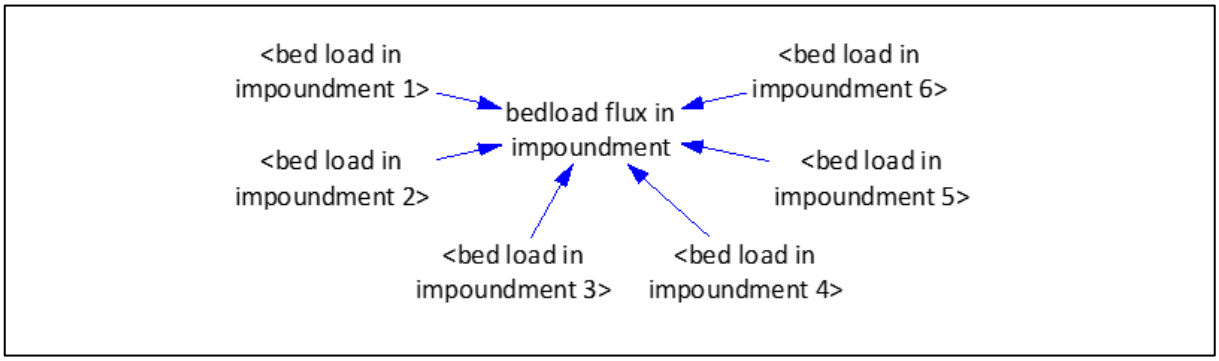



**Figure C.18.** Subsystem calculating transport potential of coarse sediment as bedload in the impoundment.

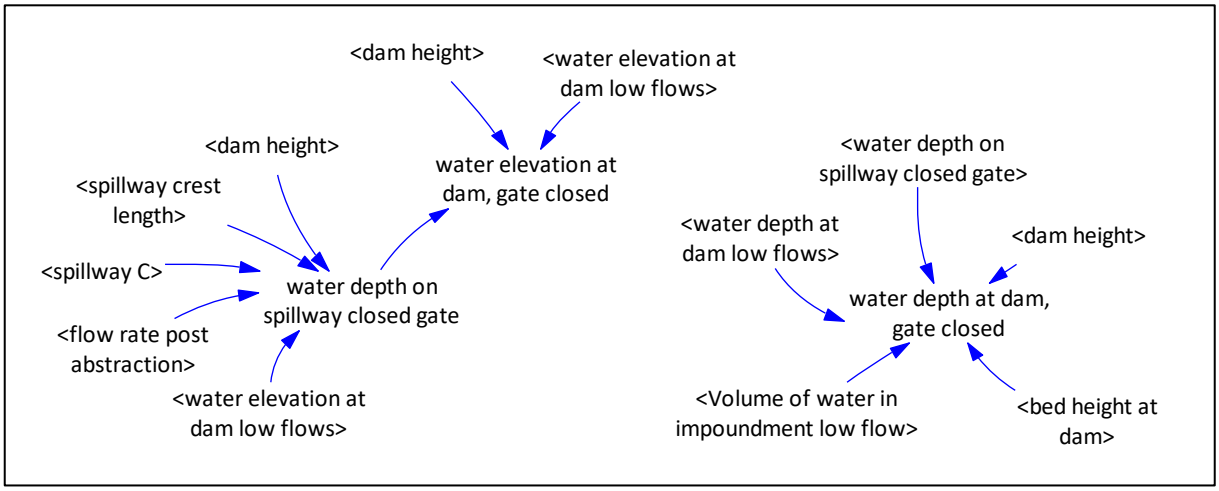



**Figure C.19.** Subsystem calculating depth of water at dam.

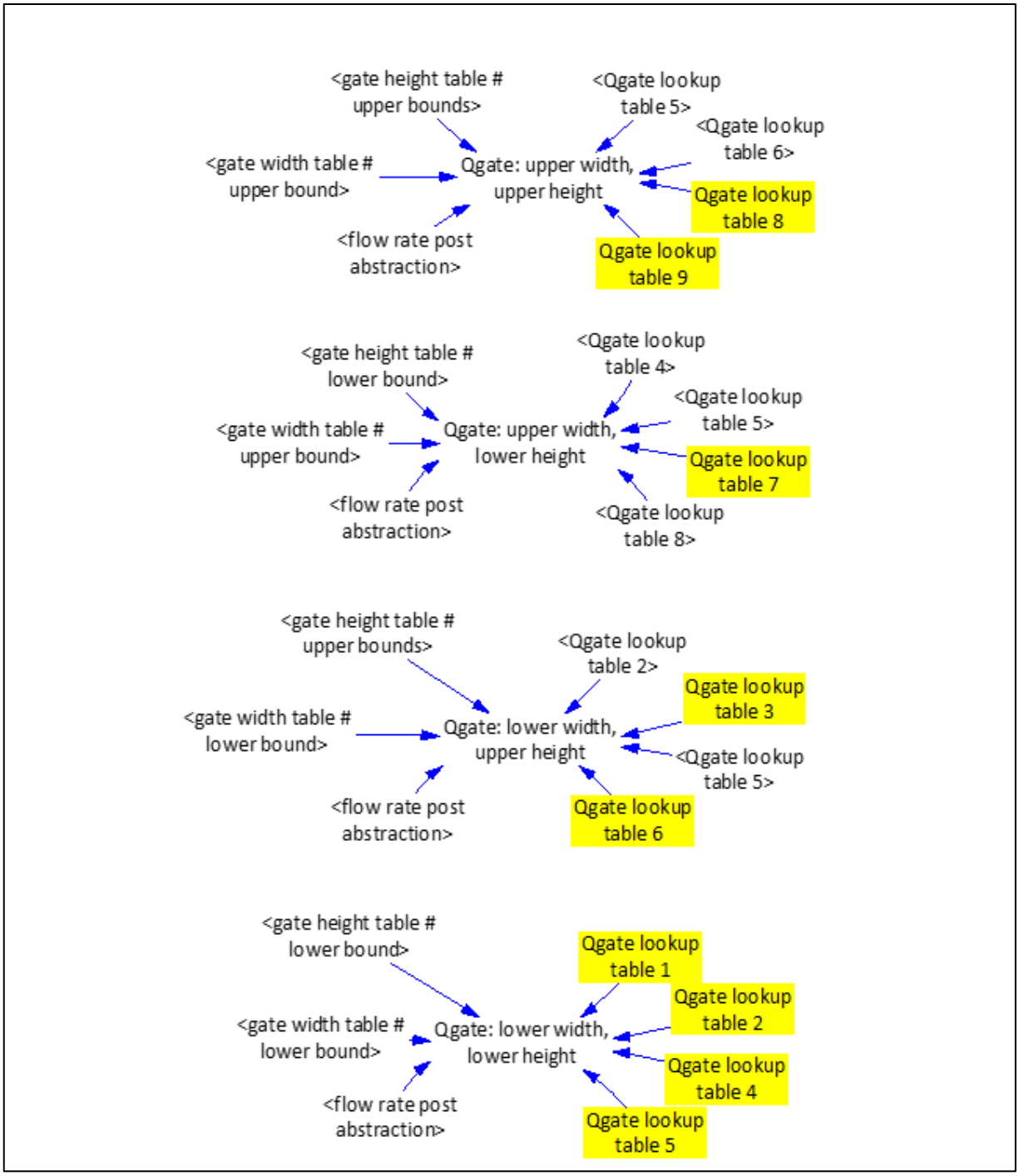



**Figure C.20.a** Subsystem interpolating the flow through the sluice gate.

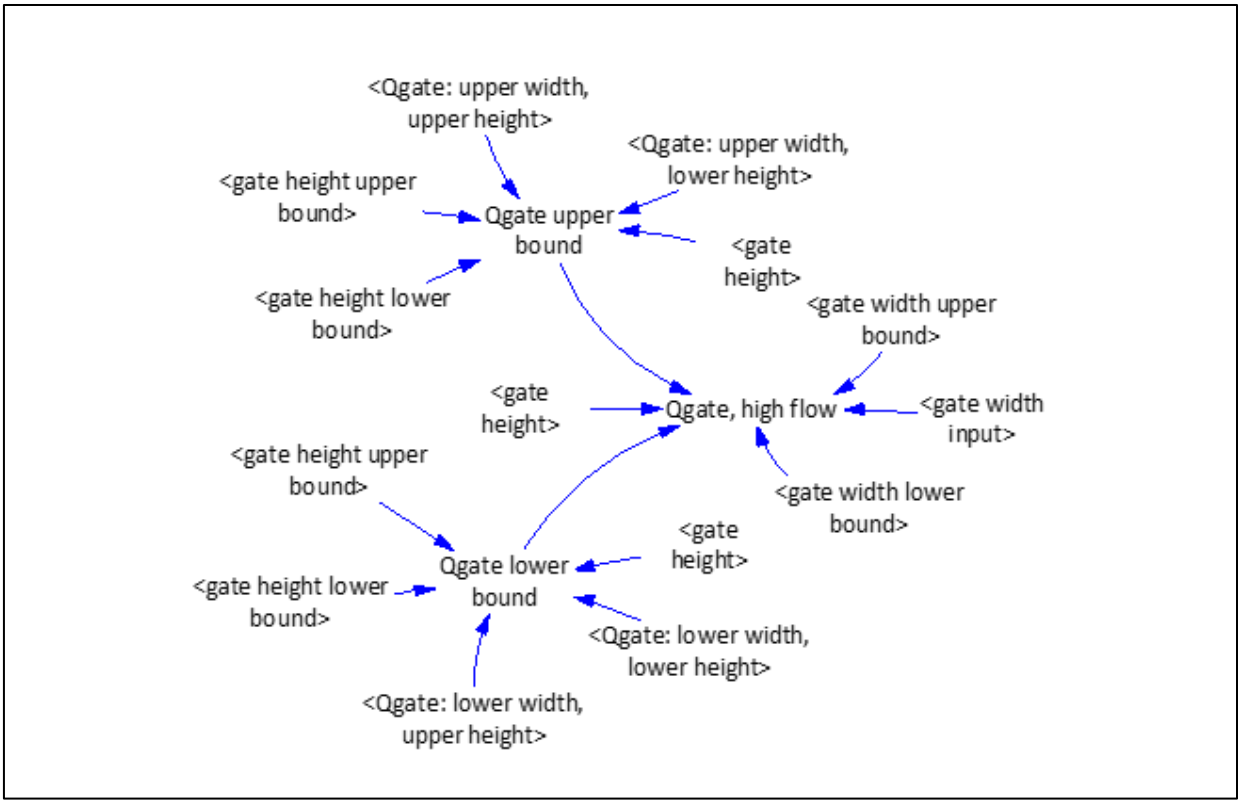



**Figure C.20.b** Subsystem interpolating the flow through the sluice gate.

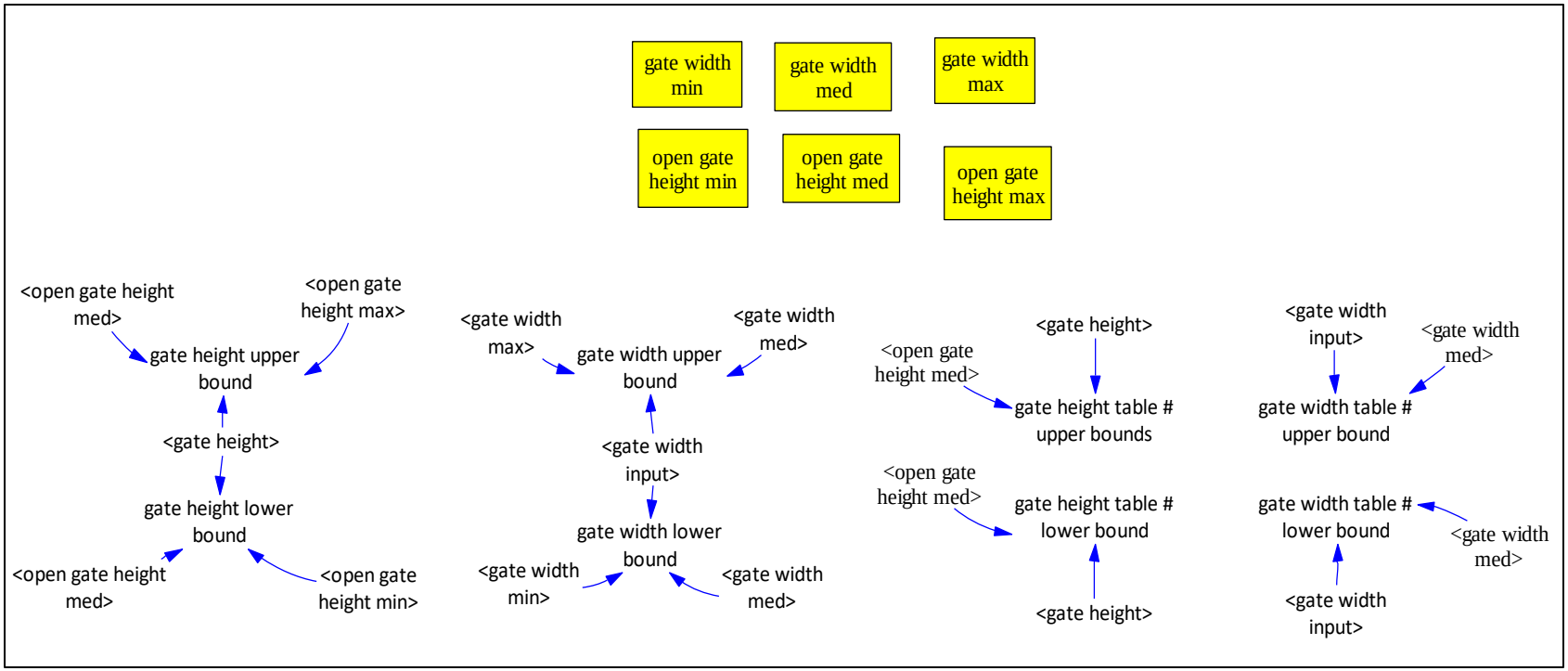



**Figure C.21.** Subsystem supporting interpolations for flow through the sluice gate by setting boundary conditions.

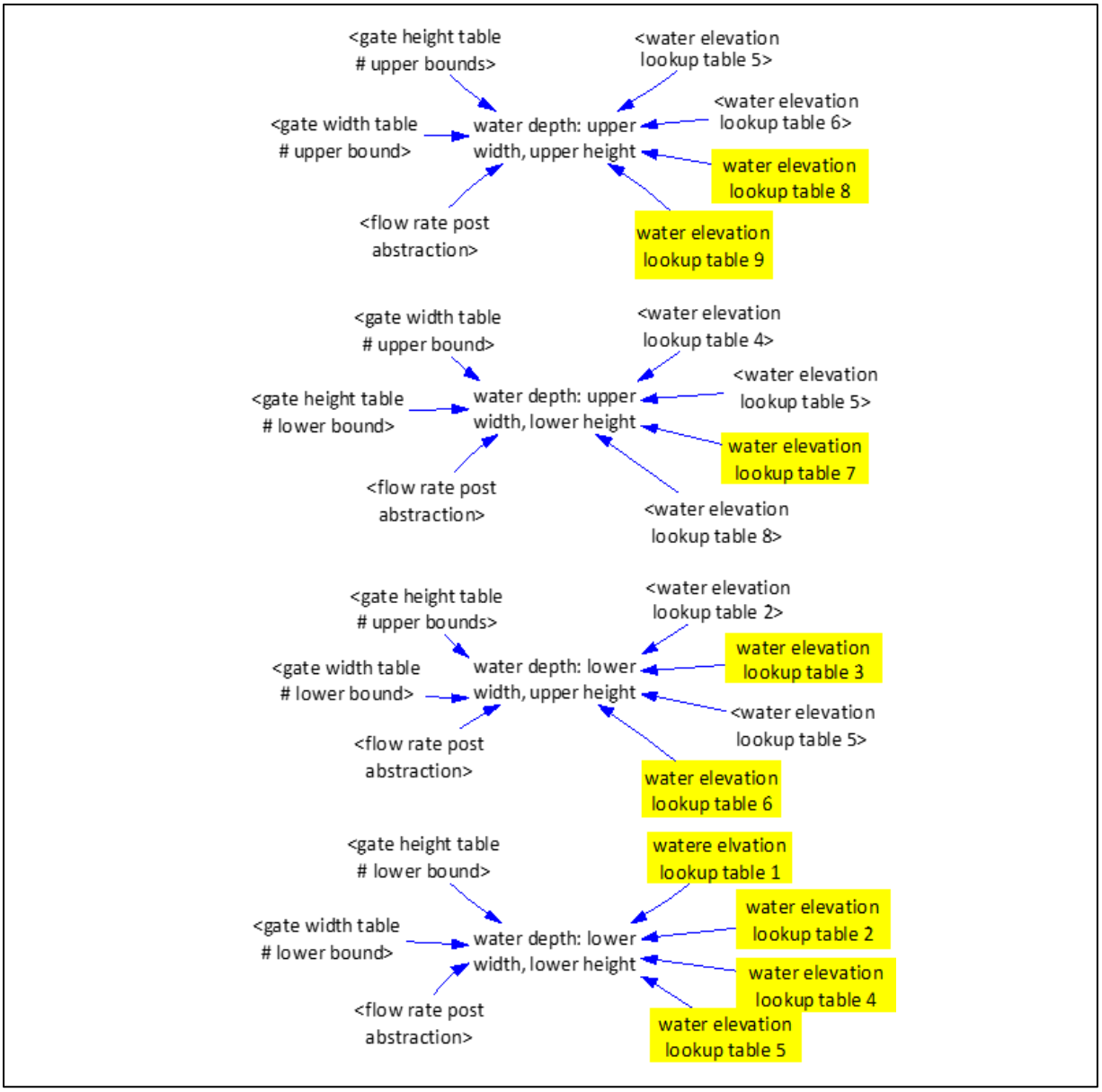



**Figure C.22.a** Subsystem interpolating water depth at dam when sluice gate is operational.

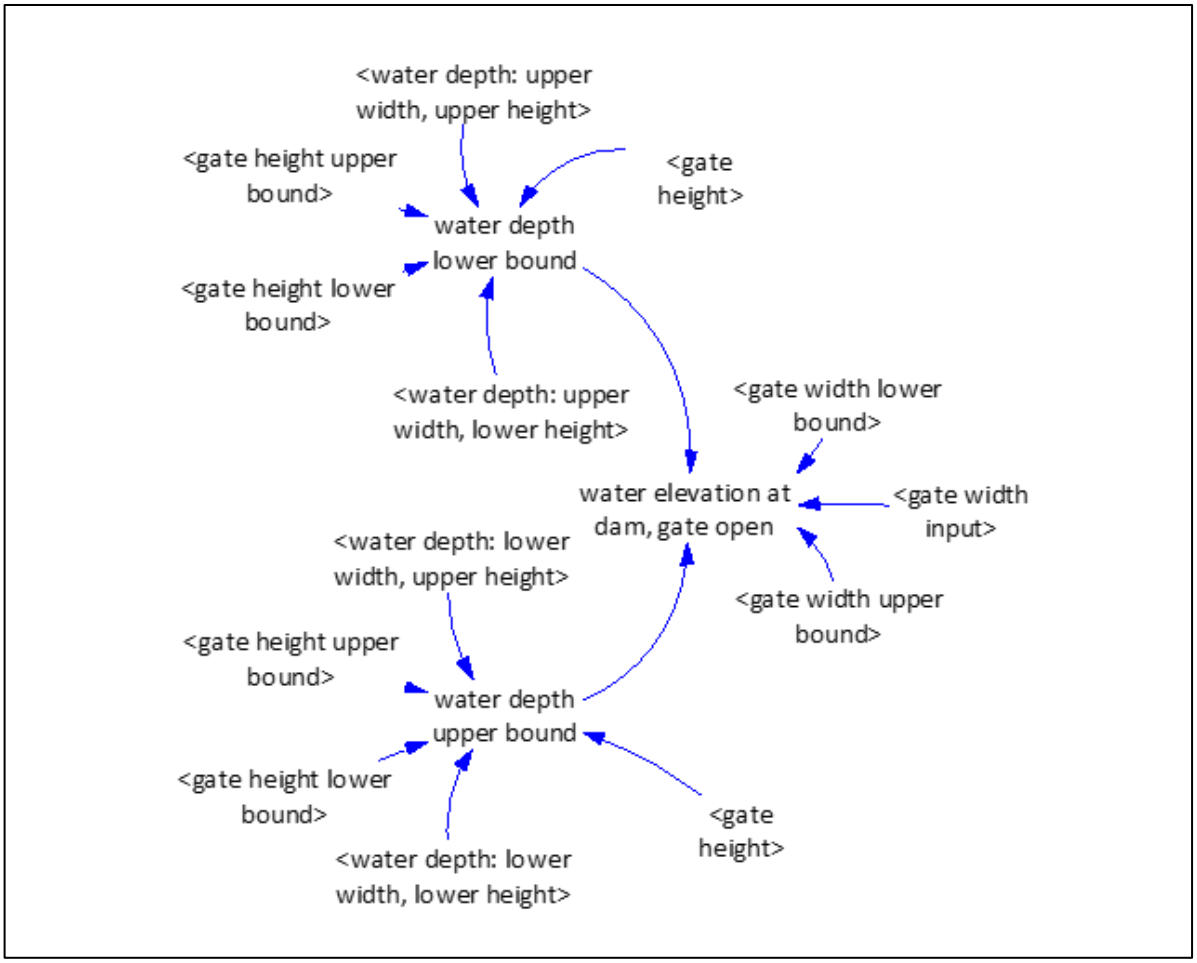



**Figure C.22.b** Subsystem interpolating water depth at dam when sluice gate is operational.

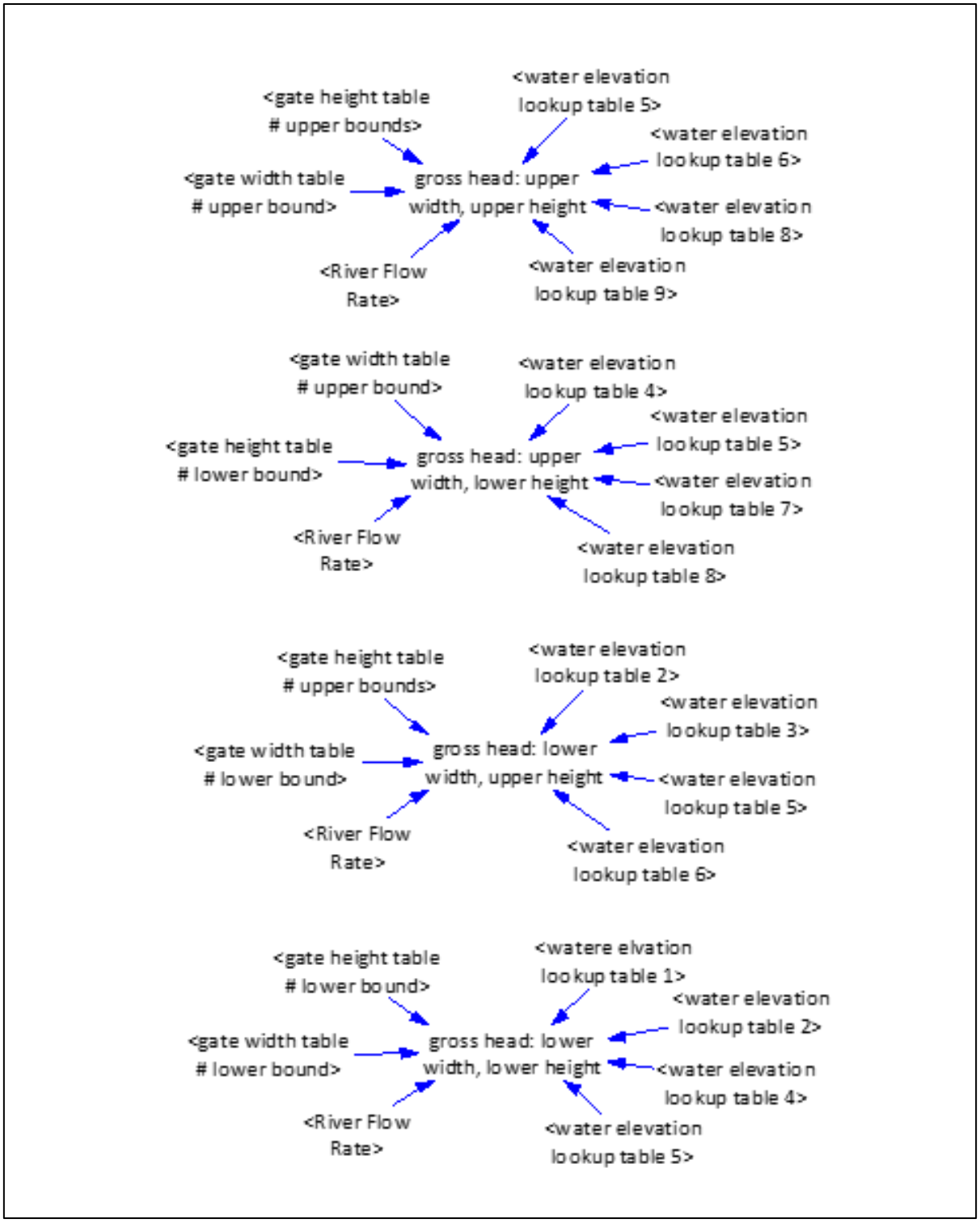



**Figure C.23.a** Subsystem interpolating water gross head at dam when sluice gate is operational.

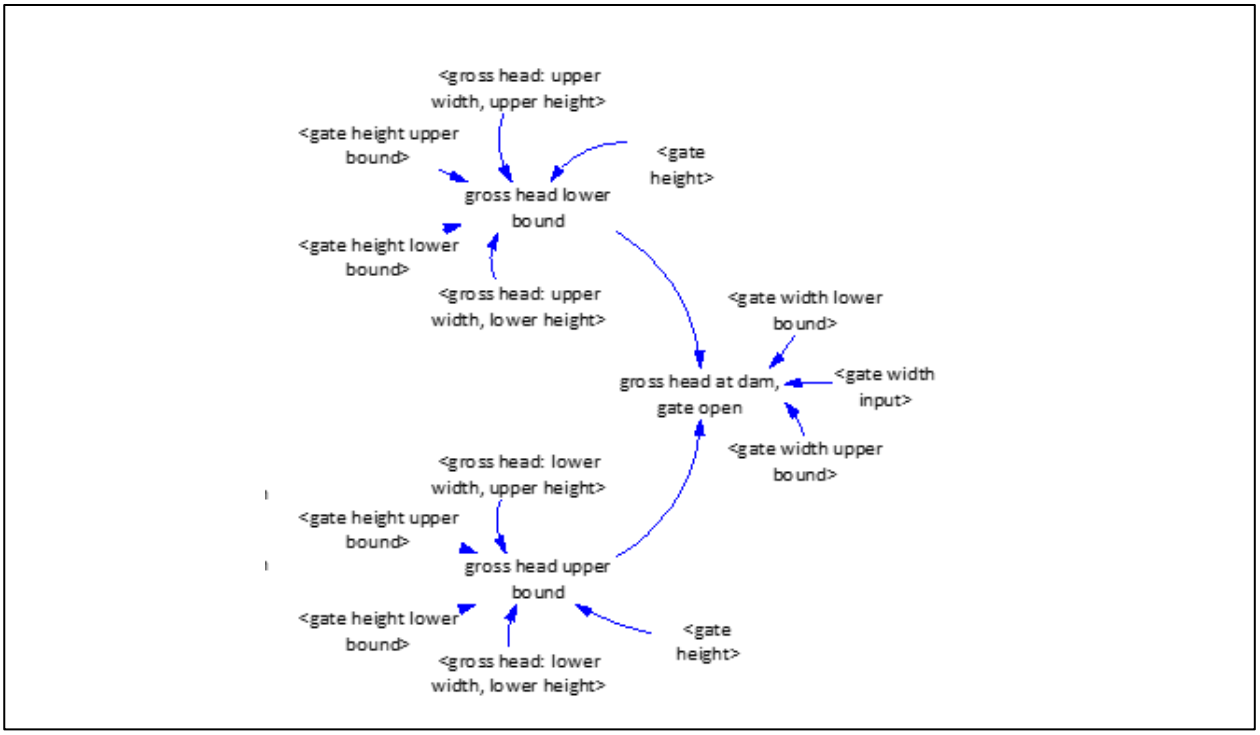



**Figure C.23.b** System interpolating water gross head at dam when sluice gate is operational.

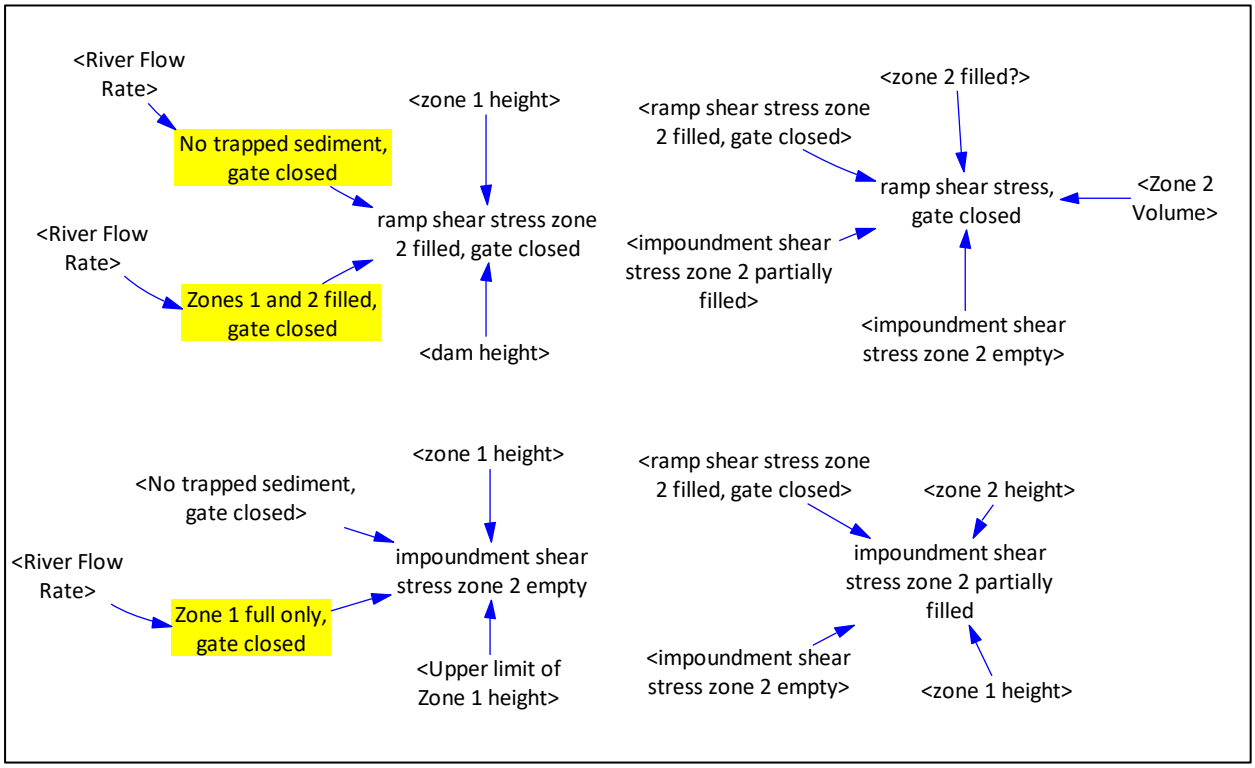



**Figure C.24.** Subsystem interpolating water gross head at dam when sluice gate is operational.

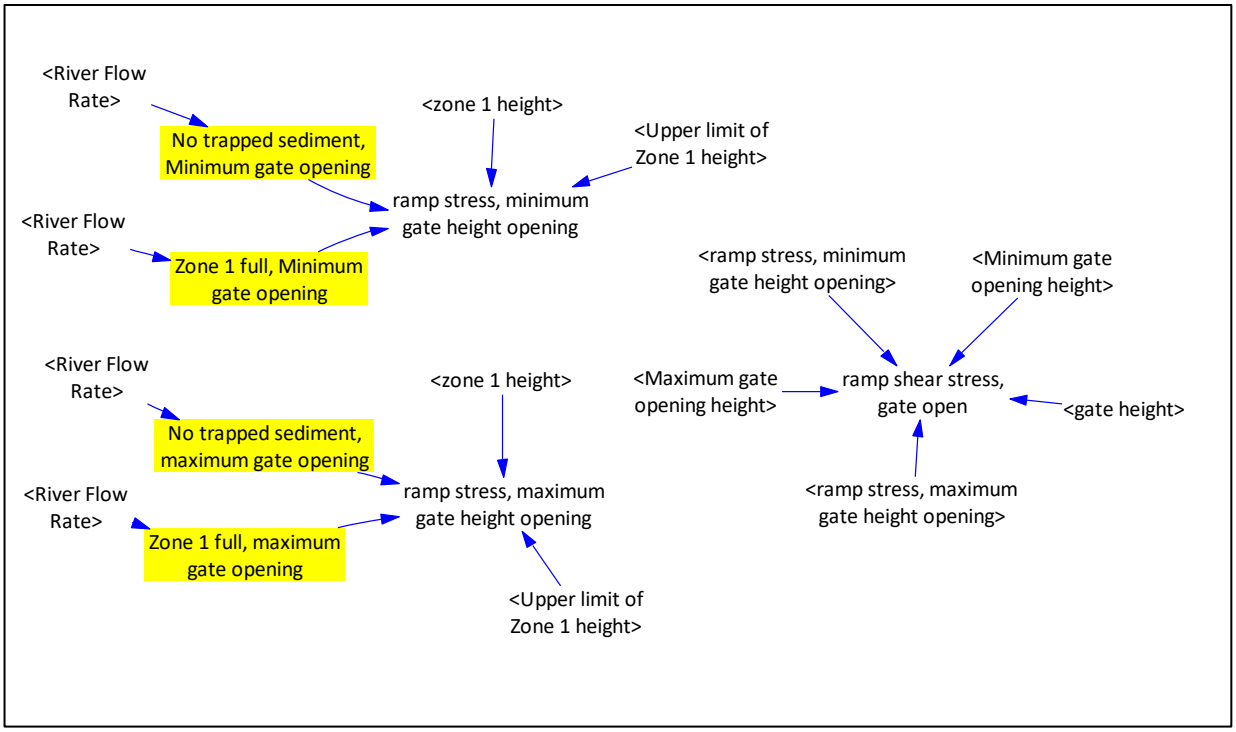



**Figure C.25.** Subsystem interpolating shear stress on sediment ramp when sluice gate is operational.

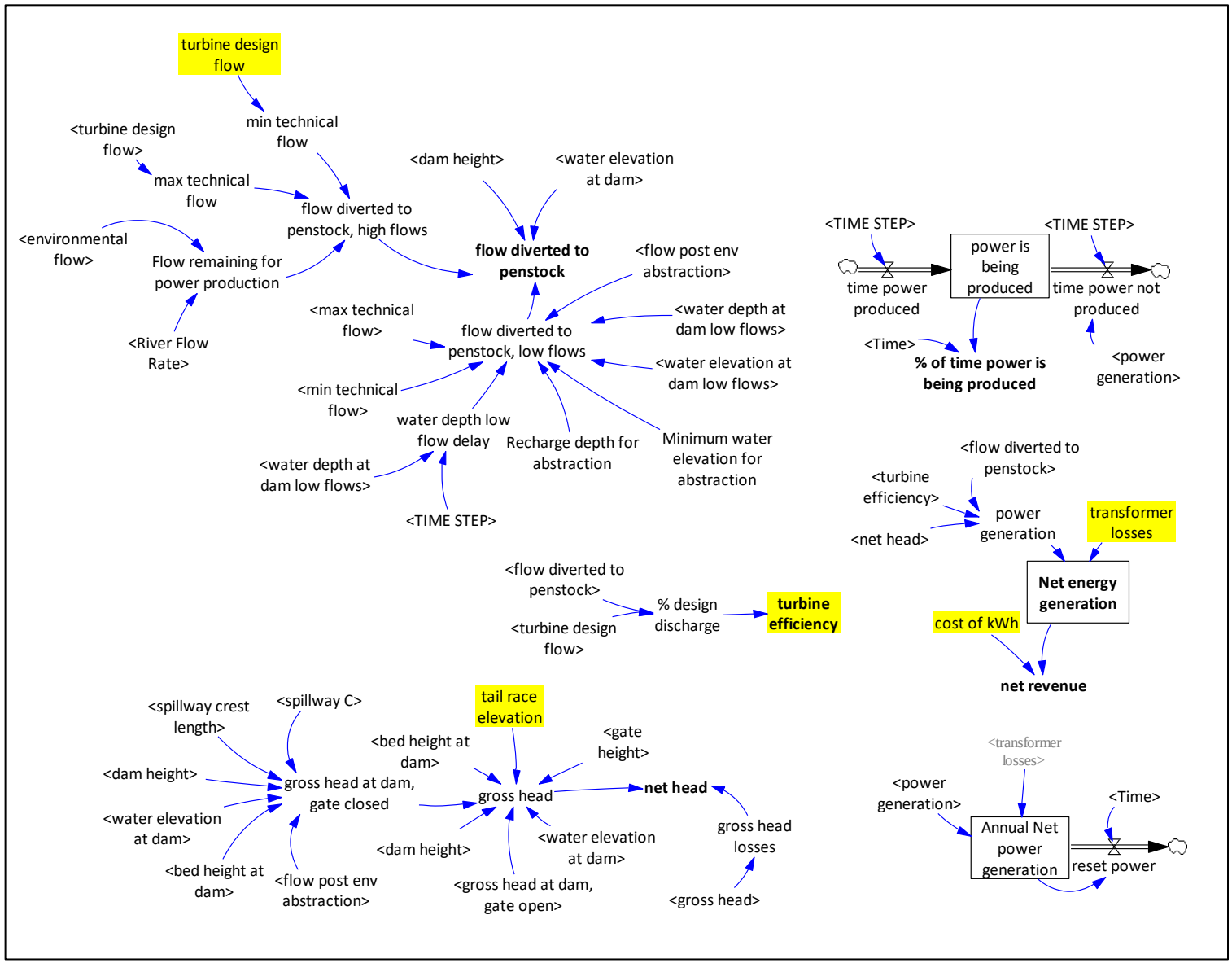



**Figure C.26.** Subsystem calculating power production.

# Vita

Sarah Dowda graduated with a bachelor's in biology in 2011 from the Evergreen State College located in her home state of Washington. After working as a horticulturalist for a number of years she returned to school at the University of Memphis for two years in order to complete perquisites for a master's program in environmental engineering. In 2018 she was accepted into the master's program for environmental engineering at the University of TN, Knoxville, where she worked as a research assistant funded by a grant from the Department of Energy's research facility at Oak Ridge National Laboratory. She anticipates graduating with a concentration in water resources engineering in May, 2020.